International Journal of Modern Physics C
Vol. 25, No. 8 (2014) 1430003 (66 pages)
© World Scientific Publishing Company
DOI: 10.1142/S0129183114300036

Event-based simulation of quantum physics experiments*

K. Michielsen

Institute for Advanced Simulation, Jülich Supercomputing Centre
Forschungszentrum Jülich, D-52425 Jülich, Germany
RWTH Aachen University, D-52056 Aachen, Germany
k.michielsen@fz-juelich.de

H. De Raedt

Department of Applied Physics, Zernike Institute for Advanced Materials
University of Groningen, Nijenborgh 4
NL-9747 AG Groningen, The Netherlands
h.a.de.raedt@rug.nl

Received 14 April 2014
Accepted 6 June 2014
Published 22 July 2014

We review an event-based simulation approach which reproduces the statistical distributions of wave theory not by requiring the knowledge of the solution of the wave equation of the whole system but by generating detection events one-by-one according to an unknown distribution. We illustrate its applicability to various single photon and single neutron interferometry experiments and to two Bell-test experiments, a single-photon Einstein–Podolsky–Rosen experiment employing post-selection for photon pair identification and a single-neutron Bell test interferometry experiment with nearly 100% detection efficiency.

Keywords: Computational techniques; discrete event simulation; quantum theory.

PACS Nos.: 02.70.−c, 03.65.−w, 03.65.Ud.

1. Introduction

The statistical properties of a vast number of laboratory experiments with individual entities such as electrons, atoms, molecules, photons, etc. can be extremely well described by quantum theory. The mathematical framework of quantum theory allows for a straightforward calculation of numbers which can be compared with experimental data as long as these numbers refer to statistical averages of measured quantities, such as for example an interference pattern, the specific heat and magnetic susceptibility.

*Lecture given at the "Advanced School on Quantum Foundations and Open Quantum Systems" held in João Pessoa, Brazil, from 16–28 July 2012.

However, as soon as an experiment records individual clicks of a detector which contribute to the statistical average of a quantity then a fundamental problem appears. Quantum theory provides a recipe to compute the frequencies for observing events but it does not account for the observation of the individual events themselves, a manifestation of the quantum measurement problem.[1,2] Examples of such experiments are single-particle interference experiments in which the interference pattern is built up by successive discrete detection events and Bell-test experiments in which two-particle correlations are computed as averages of pairs of individual detection events recorded at two different detectors and seen to take values which correspond to those of the singlet state in the quantum theoretical description.

An intriguing question to be answered is why individual entities which do not interact with each other can exhibit the collective behavior that gives rise to the observed interference pattern and why two particles, which only interacted in the past, after individual local manipulation and detection can show correlations corresponding to those of the singlet state. Since quantum theory postulates that it is fundamentally impossible to go beyond the description in terms of probability distributions, an answer in terms of a cause-and-effect description of the observed phenomena cannot be given within the framework of quantum theory.

We provide an answer by constructing an event-based simulation model that reproduces the statistical distributions of quantum (and Maxwell's) theory without solving a wave equation but by modeling physical phenomena as a chronological sequence of events whereby events can be actions of an experimenter, particle emissions by a source, signal generations by a detector, interactions of a particle with a material and so on.[3–5] The underlying assumption of the event-based simulation approach is that current scientific knowledge derives from the discrete events which are observed in laboratory experiments and from relations between those events. Hence, the event-based simulation approach concerns what we can say about these experiments but not what "really" happens in Nature. This underlying assumption strongly differs from the premise that the observed discrete events are signatures of an underlying objective reality which is mathematical in nature.

The general idea of the event-based simulation method is that simple rules define discrete-event processes which may lead to the behavior that is observed in experiments. The basic strategy in designing these rules is to carefully examine the experimental procedure and to devise rules such that they produce the same kind of data as those recorded in experiment, while avoiding the trap of simulating thought experiments that are difficult to realize in the laboratory. Evidently, mainly because of insufficient knowledge, the rules are not unique. Hence, the simplest rules can be used until a new experiment indicates otherwise. On the one hand one may consider the method being entirely classical since it only uses concepts of the macroscopic world, but on the other hand one could consider the method being nonclassical because some of the rules are not those of classical Newtonian dynamics.

Obviously, using trial and error to find discrete-event rules that reproduce experimental results is unlikely to be successful. Instead, we started our search for

useful rules by asking ourselves the question "by what kind of discrete-event rule should a beam splitter (BS) operate in order to mimic the build-up, event-by-event, of the interference pattern observed in the single-photon Mach–Zehnder experiments performed by Grangier *et al.*[6]?" The simplest rule (discussed below) that performs this task seems to be rather generic in the sense that it can be used to construct discrete-event processes that reproduce the results of many interference experiments. Of course, for some experiments, the simple rule is "too simple" and more sophisticated, backwards compatible variants are required. However, the guiding principle for designing the latter is the same as for the simple rule.

The event-based approach has successfully been used for discrete-event simulations of the single BS and Mach–Zehnder interferometer (MZI) experiments of Grangier *et al.*[6] (see Refs. 3, 7 and 8), Wheeler's delayed choice experiment of Jacques *et al.*[9] (see Refs. 3, 10 and 11), the quantum eraser experiment of Schwindt *et al.*[12] (see Refs. 3, 13 and 14), two-beam single-photon interference experiments and the single-photon interference experiment with a Fresnel biprism of Jacques *et al.*[15] (see Refs. 3, 4 and 16), quantum cryptography protocols (see Ref. 17), the Hanbury Brown–Twiss experiment of Agafonov *et al.*[18] (see Refs. 3, 19 and 20), universal quantum computation (see Refs. 21 and 22), Einstein–Podolsky–Rosen–Bohm (EPRB)-type of experiments of Aspect *et al.*[23,24] and Weihs *et al.*[25] (see Refs. 3, 4, 26–31), the propagation of electromagnetic plane waves through homogeneous thin films and stratified media (see Refs. 3 and 32) and neutron interferometry experiments (see Refs. 4 and 5).

In this paper, we review the applicability of the event-based simulation method to various single-photon and single-neutron interferometry experiments and to Bell-test experiments. The paper is organized as follows. Section 2 is devoted to the single-particle two-slit experiment, one of the most fundamental experiments in quantum physics. We first discuss Feynman's thought experiment, demonstrating single-electron interference, and briefly review its laboratory realizations. We then describe the two-beam experiment with single-photons, a variant of Young's double slit experiment. It is seen that for these single-particle interference experiments, quantum theory gives a recipe to compute the observed interference pattern after many detection events are registered, but quantum theory does not account for the one-by-one build-up process of the pattern in terms of the individual detection events. Hence, as formulated in Sec. 3, the challenge is to come up with a set of rules which allow to produce detection events with frequencies which agree with a given distribution (in this particular case a two-slit interference pattern) without these rules referring, in any way, to the distribution itself. The event-based simulation method solves this challenging problem by modeling various physical phenomena as a chronological sequence of different events, such as actions of the experimenter, particles emitted by a source, signals generated by a detector and so on. In Sec. 4, we explain the basis of the event-based simulation method by specifying rules which allow to reproduce the results of the quantum theoretical description of the idealized Stern–Gerlach experiment and of a single-photon experiment with a

linearly birefringent crystal demonstrating Malus' law, without making any use of quantum theoretical concepts. In this section, we also discuss the efficiency of two types of single-particle detectors used in the event-based simulation method. In Sec. 5, we show that a similar set of rules can be used to simulate single-particle interference. We demonstrate this on the basis of the single-photon two-beam experiment thereby also exactly simulating Feynman's thought experiment, the MZI experiment, Wheeler's delayed choice experiment and a single-neutron interferometry experiment with a Mach–Zehnder type of interferometer. We explain why the event-based simulation method can produce interference without solving a wave problem. Section 6 is devoted to the event-based simulation of EPRB-type of experiments with correlated photon pairs and with neutrons with correlated spatial and spin degrees of freedom. Since both experiments are Bell-test experiments testing whether or not a Bell-Clauser–Horne–Shimony–Holt (CHSH) inequality can be violated, we also elaborate on the conclusions that can be drawn from such a violation. For both experiments we explain why the event-based model, a classical causal model, can produce the results of quantum theory. A discussion is given in Sec. 7.

2. Two-Slit and Two-Beam Experiments

One of the most fundamental experiments in quantum physics is the single-particle double-slit experiment. Feynman stated that the phenomenon of electron diffraction by a double-slit structure is "impossible, *absolutely* impossible, to explain in any classical way, and has in it the heart of quantum mechanics. In reality it contains the only mystery."[33] While Young's original double-slit experiment helped to establish the wave theory of light,[34] variants of the experiment over the years with electrons (see below), single photons (see below), neutrons,[35,36] atoms[37,38] and molecules[39–41] helped the development of ideas on concepts such as wave-particle duality in quantum theory.[2]

Two prevailing variants of the double-slit experiments can be recognized, one consists of a source S and a screen with two apertures and another one consists of a source S and a biprism. The first one is a real two-slit experiment in which the two slits can be regarded as two virtual sources S_1 and S_2, the latter one is a two-beam experiment which can also be replaced by a system with two virtual sources S_1 and S_2.[42] In contrast to the two-slit experiment in which diffraction or scattering and interference phenomena play a role, the phenomenon of diffraction or scattering is absent in the two-beam experiment, except for the diffraction or scattering at the sources themselves.

A brief note on the difference in usage of the words diffraction, scattering and interference is here in place. Feynman mentioned in his lecture notes that "no-one has ever been able to define the difference between interference and diffraction satisfactorily. It is just a question of usage, and there is no specific, important physical difference between them."[43] In classical optics, diffraction is the effect of a wave bending as it passes through an opening or goes around an object. The amount of bending depends on the relative dimensions of the object or opening compared to the

wavelength of the wave. Interference is the superposition of two or more waves resulting in a new wave pattern. Therefore a double-slit, as well as a single-slit structure illuminated by (classical) light yields an interference (or diffraction) pattern due to diffraction and interference. In principle, diffraction and interference are phenomena observed only with waves. However, an interference pattern identical in form to that of classical optics can be observed by collecting many detector spots or clicks which are the result of electrons, photons, neutrons, atoms or molecules traveling one-by-one through a double-slit structure. In these experiments, the so-called interference pattern is the statistical distribution of the detection events (spots at or clicks of the detector). Hence in these particle-like experiments, only the correlations between detection events reveal interference. Misleadingly this interference pattern is often called a diffraction pattern in analogy with classical optics where both the phenomena of diffraction and interference are responsible for the resulting pattern. In the particle-like experiment it would be better to replace the word diffraction by scattering because scattering refers to the spreading of a beam of particles (or a beam of rays) over a range of directions as a result of collisions with other particles or objects. In what follows we use the term interference pattern for the statistical distribution of detection events.

2.1. *Two-slit experiment with electrons*

In 1964, Feynman described a thought experiment consisting of an electron gun emitting individual electrons in the direction of a thin metal plate with two slits in it behind which is placed a movable detector.[33] Feynman made the following observations:

- Sharp identical "clicks" which are distributed erratically, are heard from the detector.
- The probability $P_1(x)$ or $P_2(x)$ of arrival, through one slit with the other slit closed, at position x is a symmetric curve with its maximum located at the center position of the open slit.
- The probability $P_{12}(x)$ of arrival through both slits looks like the intensity of water waves which propagated through two holes thereby forming a so-called "interference pattern" and looks completely different from the curve $P_1(x) + P_2(x)$, a curve that would be obtained by repeating the experiment with bullets.

which lead him to the conclusions:

- Electrons arrive at the detector in identical "lumps", like particles.
- The probability of arrival of these lumps is distributed like the distribution of intensity of a wave propagating through both holes.
- It is in this sense that an electron behaves "sometimes like a particle and sometimes like a wave".

Note that Feynman made his reasoning with probabilities $P_1(x)$, $P_2(x)$, $P_{12}(x)$, which he said to be proportional to the average rate of clicks $N_1(x)$, $N_2(x)$, $N_{12}(x)$. However, one cannot simply add $P_1(x)$ and $P_2(x)$ and compare the result with $P_{12}(x)$ because these are probabilities for different conditions (different "contexts"), namely only slit 1 open, only slit 2 open and both slits 1 and 2 open, respectively.[2] Hence, no conclusions can be drawn from making the comparison between $P_{12}(x)$ and $P_1(x) + P_2(x)$.

Although Feynman wrote "you should not try to set up this experiment" because "the apparatus would have to be made on an impossibly small scale to show the effects we are interested in", advances in (nano)technology made possible various laboratory implementations of his fundamental thought experiment. The first electron interference pattern obtained with an electron-biprism, the analog of a Fresnel biprism in optics, was reported in 1955.[44,45] In 1961, Jönsson performed the first electron interference experiment with multiple (up to five) slits in the micrometer range.[46] However, these were not single-electron interference experiments since there was not just one electron in the apparatus at any one time. The first real single-electron interference experiments that were conducted were electron-biprism experiments (for a review see Refs. 47 and 48) in which single electrons either pass to the left or to the right of a conducting wire (there are no real slits in this type of experiments).[49–51] In these experiments, the interference pattern is built up from many independent detection events. Electron–electron interaction plays no role in the interference process since the electrons pass the wire one-by-one. More recently, single-electron interference experiments have been demonstrated with one, two, three and four slits fabricated by focused ion beam milling.[52–54] However, in these experiments only the final recorded electron intensity is shown. In a follow-up single-electron two-slit experiment a fast-readout pixel detector was used which allows the measurement of the distribution of the electron arrival times and the observation of the build-up of the interference pattern by individual detection events.[55] Hence, this experiment comes very close to Feynman's thought experiment except that the two electron distributions for one slit open and the other one closed are not measured. Note that one of these distributions was measured in Ref. 52 by a nonreversible process of closing one slit and without using the fast-readout pixel detector. Very recently, it has been reported that a full realization of Feynman's thought experiment has been performed.[56] In this experiment a movable mask is placed behind the double-slit structure to open/close the slits. Unfortunately, the mask is positioned behind the slits and not in front of them, so that all electrons always encounter a double-slit structure and are filtered afterwards by the mask. Hence, one could say that anno 2014 Feynman's thought experiment has yet to be performed.

2.2. *Two-beam experiment with photons*

Another interesting variant of Young's double slit experiment involves a very dim light source so that on average only one photon is emitted by the source at any time.

Inspired by Thomson's idea that light consists of indivisible units that are more widely separated when the intensity of light is reduced,[57] in 1909, Taylor conducted an experiment with a light source varying in strength and illuminating a needle thereby demonstrating that the diffraction pattern observed with a feeble light source (exposure time of three months) was as sharp as the one obtained with an intense source and a shorter exposure time.[58] In 1985, a double-slit experiment was performed with a low-pressure mercury lamp and neutral density filters to realize a very low-light level.[59] It was shown that at the start of the measurement bright dots appeared at random positions on the detection screen and that after a couple of minutes an interference pattern appeared. Demonstration versions of double-slit experiments illuminated by strongly attenuated lasers are reported in Refs. 60 and 61 and in Fig. 1 of Ref. 62. However, attenuated laser sources are imperfect single-photon sources. Light from these sources attenuated to the single-photon level never antibunches, which means that the anticorrelation parameter $\alpha \geq 1$. For a real single-photon source $0 < \alpha < 1$. In 2005, a variation of Young's experiment was performed with a Fresnel biprism and a single-photon source based on the pulsed, optically excited photoluminescence of a single N-V color center in a diamond nanocrystal.[15] In this two-beam experiment there is always only one photon between the source and the detection plane. It was observed that the interference pattern gradually builds up starting from a couple of dots spread over the screen for small exposure times. A time-resolved two-beam experiment has been reported in Refs. 63 and 64. Recently, a temporally and spatially resolved two-beam experiment has been performed with entangled photons, providing insight in the dynamics of the build-up process of the interference pattern.[65]

2.3. *The experimental observations and their quantum theoretical description*

The common observation in these single-particle interference experiments, where "single particle" can be read as electron, photon, neutron, atom or molecule, is that individual detection events gradually build up an interference pattern and that the final interference pattern can be described by wave theory. In trying to give a pictorial (cause-and-effect) view of what is going on in these experiments, it is commonly assumed that there is a one-to-one correspondence between an emission event, "the departure of a single particle from the source" and a detection event, "the arrival of the single particle at the detector". This assumption might be wrong. The only conclusion that can be drawn from the experiments is that there is some relation between the emission and detection events.

In view of the quantum measurement problem,[1,2,66] a cause-and-effect description of the observed phenomena is unlikely to be found in the framework of quantum theory. Quantum theory provides a recipe to compute the frequencies for observing events and thus to compute the final interference pattern which is observed after the experiment is finished. However, it does not account for the observation of the

individual detection events building up the interference pattern. In fact quantum theory postulates that it is fundamentally impossible to go beyond the description in terms of probability distributions. Of course, one could simply use pseudo-random numbers to generate events according to the probability distribution that is obtained by solving the time-dependent Schrödinger equation. However, that is not the problem one has to solve as it assumes that the probability distribution of the quantum mechanical problem is known, which is exactly the knowledge that one has to generate without making reference to quantum theory. If we would like to produce, event-by-event, the interference pattern from Maxwell's theory and do not want to generate events according to the known intensity function we would face a similar problem.

3. Theoretical Challenge and Paradigm Shift

In general, the challenge is the following. Given a probability distribution of observing events, construct an algorithm which runs on a digital computer and produces events with frequencies which agree with the given distribution without referring the algorithm, in any way, to the probability distribution itself. Traditionally, the behavior of systems is described in terms of mathematics, making use of differential or integral equations, probability theory and so on. Although that this traditional modeling approach has been proven to be very successful it does not seem capable of tackling this challenge. This challenge requires something as disruptive as a paradigm shift. In scientific fields different from (quantum) optics or quantum mechanics in general, a paradigm shift has been realized in terms of a discrete-event approach to describe the often very complex collective behavior of systems with a set of very simple rules. Examples of this approach are the lattice Boltzmann model to describe the flow of (complex) fluids and the cellular automata of Wolfram.[67]

We have developed a discrete-event simulation method to solve the above mentioned challenging problem by modeling physical phenomena as a chronological sequence of events whereby events can be actions of the experimenter, particles emitted by a source, signals generated by a detector, particles impinging on material and so on. The basic idea of the simulation method is to try to invent an algorithm which uses the same kind of events (data) as in experiment and reproduces the statistical results of quantum or wave theory without making use of this theory. An overview of the method and its applications can be found in Refs. 3–5. The method provides an "explanation" and "understanding" of what is going on in terms of elementary events, logic and arithmetic. Note that a cause-and-effect simulation on a digital computer is a "controlled experiment" on a macroscopic device which is logically equivalent to a mechanical device. Hence, an event-by-event simulation that reproduces results of quantum theory shows that there exists a macroscopic, mechanical model that mimics the underlying physical phenomena. This is completely in agreement with Bohr's answer "There is no quantum world. There is only an abstract quantum mechanical description. It is wrong to think that the task of

physics is to find out how nature is. Physics concerns what we can say about nature." to the question whether the algorithm of quantum mechanics could be considered as somehow mirroring an underlying quantum world.[68] Although widely circulated, these sentences are reported by Petersen[68] and there is doubt that Bohr actually used this wording.[69]

4. Event-by-Event Simulation Method

4.1. *Stern–Gerlach experiment*

We explain the basics of the event-by-event simulation method using the observations made in the Stern–Gerlach experiment.[70] The experiment shows that a beam of silver atoms directed through an inhomogeneous magnetic field splits into two components. The conclusion drawn by Gerlach and Stern is that, independent of any theory, it can be stated, as a pure result of the experiment, and as far as the exactitude of their experiments allows them to say so, that silver atoms in a magnetic field have only two discrete values of the component of the magnetic moment in the direction of the field strength; both have the same absolute value with each half of the atoms having a positive and a negative sign, respectively.[71]

In quantum theory, the stationary state of the two-state system, which is the representation of the statistical experiment, is described by the density matrix $\rho = (1 + \mathbf{S} \cdot \sigma)/2$, where $\sigma = (\sigma^x, \sigma^y, \sigma^z)$ denotes the Pauli vector and $\mathbf{S}$ denotes the average direction of magnetic moments. The average measured magnetic moment in the direction $\mathbf{a}$ is given by $\mathbf{S} \cdot \mathbf{a} = \mathrm{Tr}\rho\sigma \cdot \mathbf{a}$.

The fundamental question is how to go from the averages to the events observed in the experiment. Application of Born's rule gives the probability to observe an atom in the beam (anti-)parallel to the direction $\mathbf{a}$

$$P(w \,|\, \mathbf{S} \cdot \mathbf{a}) = \frac{1 + w\mathbf{S} \cdot \mathbf{a}}{2}, \tag{1}$$

where $w = +1$ ($w = -1$) refers to the beam parallel (anti-parallel) to $\mathbf{a}$.

Given the probability in Eq. (1) the question is how to generate a sequence of "true" random numbers $w_1, w_2, \ldots, w_N$, each taking values ± 1, such that $\sum_{n=1}^{N} w_n/N \approx \mathbf{S} \cdot \mathbf{a}$. Probability theory postulates that such a procedure exists but is silent about how the procedure should look like. In practice one could use a probabilistic processor, a device which responds to and processes input in a probabilistic way, employing pseudo-random number generators to generate a uniformly distributed pseudo-random number $0 < r_n < 1$ to produce $w_n = +1$ if $r_n < (1 + \mathbf{S} \cdot \mathbf{a})/2$ and $w_n = -1$ otherwise. Repeating this procedure N times gives $\sum_{n=1}^{N} w_n/N \approx \mathbf{S} \cdot \mathbf{a}$. However, the form of $P(w \,|\, \mathbf{S} \cdot \mathbf{a}) = (1 + w\mathbf{S} \cdot \mathbf{a})/2$ with $w = \pm 1$ is postulated and the procedure is deterministic thereby only giving the illusion of randomness to everyone who does not know the details of the algorithm and the initial state of the pseudo-random generator. Hence, we accomplished nothing

and the question is whether we can do better than by using this probabilistic processor.

Let us consider a deterministic processor, a deterministic learning machine (DLM),[8,72] that receives input in the form of identical numbers

$$0 \leq u_n \equiv u = (1 + \mathbf{S} \cdot \mathbf{a})/2 \leq 1, \tag{2}$$

for $n = 1, \ldots, N$. The processor has an internal state represented by a variable $0 \leq v_n \leq 1$ which adapts to the received input u in a manner such that the difference with the input is minimal, namely

$$v_n = \gamma v_{n-1} + (1 - \gamma)\Delta_n, \tag{3}$$

where $\Delta_n = \Theta(|\gamma v_{n-1} + (1 - \gamma) - u| - |\gamma v_{n-1} - u|)$ with $\Theta(\cdot)$ denoting the unit step function taking only the value 0 or 1 and $0 \leq \gamma < 1$ is a learning parameter controlling both the speed and accuracy with which the processor learns the input value u. The initial value v_0 of the internal state is chosen at random. The output numbers generated by the processor are

$$w_n = 2\Delta_n - 1 = \pm 1. \tag{4}$$

In general the behavior of the deterministic processor defined by Eq. (3) is difficult to analyze without a computer. However, the operation of the processor can be easily translated in simple computer code

```
u1 = gamma * y
u2 = u1 + 1 - gamma
if (abs(v - u1) < abs(v - u2)) then
w = -1
u = u1
else
w = +1
u = u2
end if
```
(5)

Also without computer, this code allows getting a quick notion on how the internal state of the processor adapts to the input. Taking as an example $u = 5/8$, $\gamma = 0.5$ and $v_n = 4/8$ gives $v_{n+1} = 6/8$, $v_{n+2} = 7/8$, $v_{n+3} = 7/16, \ldots$ From this step-by-step analysis it can be seen how v_n comes closer to u, goes further away from it to come closer again in a next step and how v_n keeps oscillating around u in the stationary regime. A detailed mathematical analysis of the dynamics of the processor defined by the rule Eq. (3) is given in Ref. 73. For $\gamma \to 1^-$ we find that $\sum_{n=1}^{N} w_n/N \approx 2u - 1 = \mathbf{S} \cdot \mathbf{a}$.

In conclusion, we designed an event-by-event process which can reproduce the results of the quantum theoretical description of the idealized Stern–Gerlach

experiment without making use of any quantum theoretical concepts. The strategy employed by the processor is to minimize the distance between two numbers thereby "learning" the input number. Hence, at least one of the results of quantum theory seems to emerge from an event-based process, a dramatic change in the paradigm of the quantum science community.

4.2. *Malus' law*

The important question is whether this event-based approach can also be applied to other experiments which up to now are exclusively described in terms of wave or quantum theory. To scrutinize this question, we consider a basic optics experiment with a linearly birefringent crystal, such as calcite acting as a polarizer. A beam of linearly polarized monochromatic light impinging on a calcite crystal along a direction not parallel to the optical axis of the crystal is split into two beams travelling in different directions and having orthogonal polarizations. The two beams are referred to as the ordinary and extraordinary beam, respectively.[42] The intensity of the beams is given by Malus' law, which has experimentally been established in 1810,

$$I_o = I\,\sin^2(\psi - \phi), \quad I_e = I\,\cos^2(\psi - \phi), \tag{6}$$

where I, I_o and I_e are the intensities of the incident, ordinary and extraordinary beam, respectively, ψ is the polarization of the incident light and ϕ specifies the orientation of the crystal.[42] Observations in single-photon experiments show that Malus' law is also obeyed at the single-photon level.

In the quantum theoretical description of these single-photon experiments in which the photons are detected one-by-one in either the ordinary beam (represented by a detection event $w = 0$) or in the extraordinary beam (represented by a detection event $w = 1$) it is postulated that the polarizer sends a photon to the extraordinary direction with probability $\cos^2(\psi - \phi)$ and to the ordinary direction with probability $\sin^2(\psi - \phi)$. Hence, quantum theory postulates that $\lim_{N\to\infty} \sum_{n=1}^{N} w_n/N \to \cos^2(\psi - \phi)$.

Following a procedure similar to that of the Stern–Gerlach experiment it is obvious that we can construct a simple probabilistic processor employing pseudo-random numbers to generate a uniform random number $0 < r_n < 1$ and send out a $w_n = 0$ ($w_n = 1$) event if $\cos^2(\psi - \phi) \leq r_n$ ($\cos^2(\psi - \phi) > r_n$) so that after repeating this procedure N times we indeed have $\lim_{N\to\infty} \sum_{n=1}^{N} w_n/N \to \cos^2(\psi - \phi)$. However, again, by doing this we accomplished nothing because Malus' law has been postulated from the start in the form $P(w\,|\,\psi - \phi) = w\cos^2(\psi - \phi) + (1 - w)\sin^2(\psi - \phi)$ with $w = 0, 1$. Moreover, this probabilistic processor has a relatively poor performance[73] and therefore in what follows we design and analyze a much more efficient DLM that generates events according to Malus' law.

The DLM mimicking the operation of a polarizer has one input channel, two output channels and one internal vector with two real entries. The DLM receives as

input, a sequence of angles ψ_n for $n = 1, \ldots, N$ and knows about the orientation of the polarizer through the angle ϕ. Using rotational invariance, we represent these input messages by unit vectors

$$\mathbf{u}_n = (u_{0,n}, u_{1,n}) = (\cos(\psi_n - \phi), \sin(\psi_n - \phi)). \tag{7}$$

Instead of the random number generator that is part of the probabilistic processor, the DLM has an internal degree of freedom represented by the unit vector $\mathbf{v}_n = (v_{0,n}, v_{1,n})$. The direction of the initial internal vector $\mathbf{v}_0$ is chosen at random. As the DLM receives input data, it updates its internal state. The update rules are defined by

$$v_{0,n} = \pm\sqrt{1 + \gamma^2(v_{0,n-1}^2 - 1)}, \quad v_{1,n} = \gamma v_{1,n-1}, \tag{8}$$

corresponding to the output event $w_n = 0$ and

$$v_{0,n} = \gamma v_{0,n-1}, \quad v_{1,n} = \pm\sqrt{1 + \gamma^2(v_{1,n-1}^2 - 1)}, \tag{9}$$

corresponding to the output event $w_n = 1$. The parameter $0 < \gamma < 1$ controls the learning process of the DLM. The $\pm$-sign takes care of the fact that the DLM has to decide between two quadrants. The DLM selects one of the four possible outcomes for $\mathbf{v}_n = (v_{0,n}, v_{1,n})$ by minimizing the cost function defined by

$$C = -\mathbf{v}_n \cdot \mathbf{u}_n = -(v_{0,n}u_{0,n} + v_{1,n}u_{1,n}). \tag{10}$$

Obviously, the cost C is small (close to -1), if the vectors $\mathbf{u}_n$ and $\mathbf{v}_n$ are close to each other. In conclusion, the DLM generates output events $w_n = 0, 1$ by minimizing the distance between the input vector and its internal vector by means of a simple, deterministic decision process.

In general, the behavior of the DLM defined by the rules Eqs. (8)–(10) is difficult to analyze without using a computer. However, for a fixed input vector $\mathbf{u}_n = (u_0, u_1)$ for $n = 1, \ldots, N$, the DLM will minimize the cost Eq. (10) by rotating its internal vector $\mathbf{v}_n$ toward $\mathbf{u}_n$ but $\mathbf{v}_n$ will not converge to the input vector $\mathbf{u}_n$ and will keep oscillating about $\mathbf{u}_n$. This is the stationary state of the machine. An example of a simulation is given in Fig. 1. Once the DLM has reached the stationary state the number of $w_n = 0$ output events divided by the total number of output events is $\cos^2(\psi_n - \phi)$ and thus in agreement with Malus' law if we interpret the $w_n = 0$ output events as corresponding to the extraordinary beam. Note that the details of the approach to the stationary state depend on the initial value of the internal vector $\mathbf{v}_0$, but the properties of the stationary state do not. A detailed stationary-state analysis is given in Ref. 72.

4.3. *Single particle detection*

In the event-based simulation of the Stern–Gerlach experiment and of the experiment demonstrating Malus' law the two-valued output events w_n $(n = 1, \ldots, N)$ can

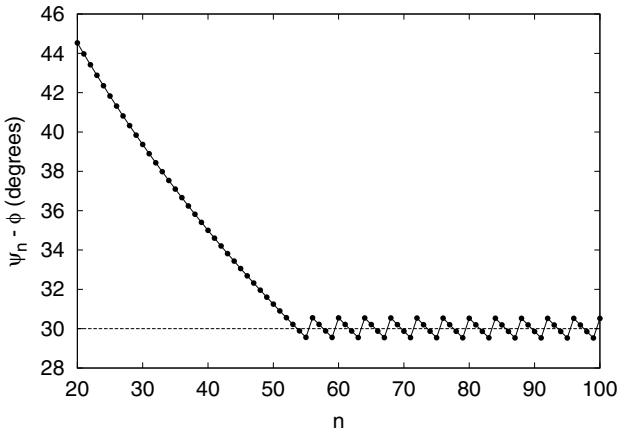

Fig. 1. The angle $\psi_n - \phi$ representing the internal vector $\mathbf{v}_n$ of the DLM defined by Eqs. (8) and (10) as a function of the number of events n. The input events are vectors $\mathbf{u}_n = (\cos 30°, \sin 30°)$. The direction of the initial internal vector $\mathbf{v}_0$ is chosen at random. In this simulation $\gamma = 0.99$. For $n > 60$ the ratio of the number of 0 events to 1 events is 1/3, which is $(\sin 30°/\cos 30°)^2$. Data for $1 \leq n < 20$ lie on the decaying line but have been omitted to show the oscillating behavior more clearly. Lines are guides to the eye.

be processed by two detectors placed behind the DLM modeling the Stern–Gerlach magnet and the calcite crystal, respectively. It can be easily seen that in these two experiments the only operation the detectors have to perform is to simply count every incoming output event w_n. However, real single-particle detectors are often more complex devices with diverse properties. In our event-based simulation approach we model the main characteristics of these devices by rules as simple as possible to obtain similar results as those observed in a laboratory experiment. So far, we have designed two types of detectors, simple particle counters and adaptive threshold devices.[3] The adaptive threshold detector can be employed in the simulation of all single-photon experiments we have considered so far[3] but is absolutely essential in the simulation of, for example, the two-beam single photon experiment (see Sec. 5.1).

The efficiency, defined as the ratio of detected to emitted particles, of our model detectors is measured in an experiment with one single-particle point source placed far away from the detector. If the detector is a simple particle counter then the efficiency is 100%, if it is an adaptive threshold detector then the efficiency is nearly 100%. Since no absorption effects, dead times, dark counts, timing jitter or other effects causing particle miscounts are simulated, these model detectors are highly idealized versions of real single-photon detectors.

Evidently, the efficiency of a detector plays an important role in the overall detection efficiency in an experiment, but it is not the only determining factor. Also the experimental configuration, as well in the laboratory experiment as in the event-based simulation approach, in which the detector is used to play an important role. Although the adaptive threshold detectors are ideal and have a detection efficiency of

nearly 100%, the overall detection efficiency can be much less than 100% depending on the experimental configuration. For example, using adaptive threshold detectors in a Mach–Zehnder interferometry experiment leads to an overall detection efficiency of nearly 100% (see Sec. 5.2.1), while using the same detectors in a single-photon two-beam experiment (see Sec. 5.1.1) leads to an overall detection efficiency of about 15%.[3,16] For the simple particle counters the configuration has no influence on the overall detection efficiency. Apart from the configuration, also the data processing procedure which is applied after the data has been collected may have an influence on the final detection efficiency. An example is the postselection procedure with a time-coincidence window which is employed to group photons, detected in two different stations, into pairs.[25] Even if in the event-based simulation approach simple particle counters with a 100% detection efficiency are used and thus all emitted photons are accounted for during the data collection process, the final detection efficiency is less than 100% because some detection events are omitted in the post-selection data procedure using a time-coincidence window.

In conclusion, even if ideal detectors with a detection efficiency of 100% would be commercially available, then the overall detection efficiency in a single-particle experiment could still be much less than 100% depending on (i) the experimental configuration in which the detectors are employed and (ii) the data analysis procedure that is used after all data has been collected.

5. Single Particle Interference

The particle-like behavior of photons has been shown in an experiment composed of a single 50/50 BS, of which only one input port is used, and a source emitting single photons and pairs of photons.[6] The wave mechanical character of the collection of photons has been demonstrated in single-particle interference experiments such as the single-photon two-beam experiment[15] (see Sec. 5.1), an experiment which shows, with minimal equipment, interference in its purest form (without diffraction), and the single-photon MZI experiment[6] (see Sec. 5.2).

The three experiments have in common that, if one analyzes the data after collecting N detection events, long after the experiment has finished, the averages of the detection events agree with the results obtained from wave theory, that is with the classical theory of electrodynamics (Maxwell theory). In the first experiment one obtains a constant intensity of 0.5 at both detectors placed at the output ports of the BS, in the other two experiments one obtains an interference pattern. However, since the source is not emitting waves but so-called single photons[6,15] the question arises how to interpret the output which seems to show particle or wave character depending on the circumstances of the experiment. This question is not limited to photons. Already in 1924, de Broglie introduced the idea that also matter can exhibit wave-like properties.[74]

To resolve the apparent behavioral contradiction, quantum theory introduces the concept of particle-wave duality.[1] As a result, these single-particle experiments are

often considered to be quantum experiments. However, the pictorial description using concepts from quantum theory, when applied to individual detection events (not to the averages) leads to conclusions that defy common sense: The photon (electron, neutron, atom, molecules, etc.) seems to change its representation from a particle to a wave while traveling from the source to the detector in the single-photon interference experiments.

In 1978, Wheeler proposed a gedanken experiment,[75] a variation on Young's double slit experiment, in which the decision to observe wave or particle behavior is postponed until the photon has passed the slits. An experimental realization of Wheeler's delayed choice experiment with single-photons traveling in an open or closed configuration of an MZI has been reported in Refs. 9 and 76. The outcome, that is the average result of many detection events, is in agreement with wave theory (Maxwell or quantum theory). However, the pictorial description using concepts of quantum theory to explain the experimental facts[9] is even more strange than in the above mentioned experiments: The decision to observe particle or wave behavior influences the behavior of the photon in the past and changes the representation of the photon from a particle to a wave.

A more sensical description of the observation of individual detection events and of an interference pattern after many single detection events have been collected in single-particle interference experiments, can be given in terms of the event-based simulation approach. This finding is not in contradiction with Feynman's statement that electron (single particle) diffraction by a double-slit structure is "impossible, *absolutely* impossible, to explain in any classical way, and has in it the heart of quantum mechanics".[33] Reading "any classical way" as "any classical Hamiltonian mechanics way", Feynman's statement is difficult to dispute. However, taking a broader view by allowing for dynamical systems that are outside the realm of classical Hamiltonian dynamics, it becomes possible to model the gradual appearance of interference patterns through the event-by-event simulation method.

5.1. *Two-beam experiment*

We consider the experiment sketched in Fig. 2. Single particles coming from two coherent beams gradually build up an interference pattern when the particles arrive one-by-one at a detector screen. This two-beam experiment can be viewed as a simplification of Young's double-slit experiment in which the slits are regarded as the virtual sources S_1 and S_2 (see Ref. 42) and can be used to perform Feynman's thought experiment in which both slits are open or one is open and the other one closed. In the event-based model of this experiment particles are created one at a time at one of the sources and are detected by one of the detectors forming the screen. We assume that all these detectors are identical and cannot communicate among each other. We also do not allow for direct communication between the particles. This implies that this event-by-event model is locally causal by

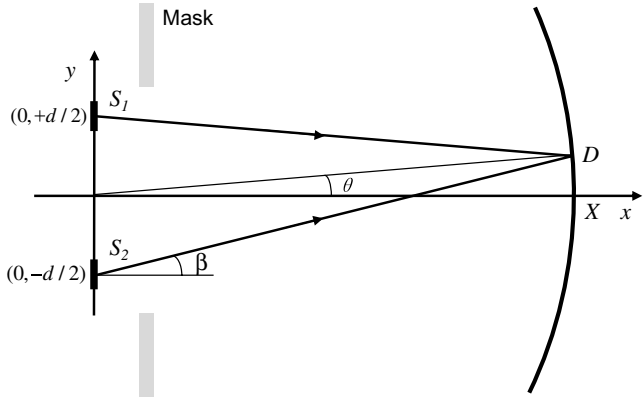

Fig. 2. Schematic diagram of a two-beam experiment with single-particle sources S_1 and S_2 of width a, separated by a center-to-center distance d. In a first experiment, which can be seen as a variant of Young's double slit experiment, N single particles leave the sources S_1 and S_2 one-by-one, at positions y drawn randomly from a uniform distribution over the interval $[-d/2 - a/2, -d/2 + a/2] \cup [+d/2 - a/2, +d/2 + a/2]$ and travel in the direction given by the angle β, a uniform pseudo-random number between $-\pi/2$ and $\pi/2$. In a second experiment, a movable mask is placed behind the sources which can block either S_1 or S_2. The sources S_1 and S_2 alternately emit M particles one-by-one, until a total of N particles has been emitted ($M \leq N/2$ and $kM = N$ with k an integer number). In both experiments, particles are emitted one-by-one either from S_1 or from S_2 and at any time there is only one particle traveling from source to detector. The particles are recorded by detectors D positioned on a semi-circle with radius X and center $(0, 0)$. The angular position of a detector is denoted by θ.

construction. Then, if it is indeed true that individual particles build up the interference pattern one-by-one, just looking at Fig. 2 leads to the logically unescapable conclusion that the interference pattern can only be due to the internal operation of the detector.[77] Detectors which simply count the incoming particles are not sufficient to explain the appearance of an interference pattern and apart from the detectors there is nothing else that can cause the interference pattern to appear. Making use of the statistical property of quantum theory one could assume that if a detector is replaced by another one as soon as it has detected one particle, one obtains similar interference patterns if the detection events of all these different detectors are combined or if only one detector detects all the particles. However, since there is no experimental evidence confirming this assumption and since our event-based approach is based on laboratory experimental setups and observations we do not consider this being a realistic option. Thus, logic dictates that a minimal event-based model for the two-beam experiment requires an algorithm for the detector that does a little more than just counting particles.

5.1.1. *Event-based model*

In what follows we specify the event-by-event model for the single-photon two-beam experiment (see Fig. 2) in sufficient detail such that the reader who is interested can reproduce the simulation results (a Mathematica implementation of a slightly more

sophisticated algorithm[16] can be downloaded from the Wolfram Demonstration Project web site[78]).

— *Source and particles*: In the first experiment described in Fig. 2, N photons leave the sources one-by-one, at positions y drawn randomly from a uniform distribution over the interval $[-d/2-a/2,-d/2+a/2]\cup[+d/2-a/2,+d/2+a/2]$. In the second experiment the sources alternately emit M photons one-by-one until a total of N photons has been emitted. Here, $M \leq N/2$ and $kM = N$, where k denotes an integer number. The photons are regarded as messengers, traveling in the direction specified by the angle β, being a uniform pseudo-random number between $-\pi/2$ and $\pi/2$. Each messenger carries a message

$$\mathbf{u}(t) = (\cos(2\pi ft), \sin(2\pi ft)), \tag{11}$$

represented by a harmonic oscillator which vibrates with frequency f (representing the "color" of the light). The internal oscillator operates as a clock to encode the time of flight t, which is set to zero when a messenger is created, thereby modeling the coherence of the two single-particle beams.

This pictorial model of a "photon" was used by Feynman to explain quantum electrodynamics.[79] The event-based approach goes one step further in that it specifies in detail, in terms of a mechanical procedure, how the "amplitudes" which appear in the quantum formalism get added together. In Feynman's path integral formulation of light propagation, which is essentially quantum mechanical, the amplitude was obtained by summing over all possible paths.[79]

The time of flight of the particles depends on the source-detector distance. Here, we discuss as an example, the experimental setup with a semi-circular detection screen (see Fig. 2) but in principle any other geometry for the detection screen can be considered. The messenger leaving the source at $(0, y)$ under an angle β will hit the detector screen of radius X at a position determined by the angle θ given by $\sin\theta = (y\cos^2\beta + \sin\beta\sqrt{X^2 - y^2\cos^2\beta})/X$, where $|y/X| < 1$. The time of flight is then given by $t = \sqrt{X^2 - 2yX\sin\theta + y^2}/c$, where c is the velocity of the messenger. The messages $\mathbf{u}(t)$ together with the explicit expression for the time of flight are the only input to the event-based algorithm.

— *Detector*: Here, we describe the model for one of the many identical detectors building up the detection screen. Microscopically, the detection of a particle involves very intricate dynamical processes.[66] In its simplest form, a light detector consists of a material that can be ionized by light. This signal is then amplified, usually electronically, or in the case of a photographic plate by chemical processes. In Maxwell's theory, the interaction between the incident electric field $\mathbf{E}$ and the material takes the form $\mathbf{P}\cdot\mathbf{E}$, where $\mathbf{P}$ is the polarization vector of the material.[42] Assuming a linear response, $\mathbf{P}(\omega) = \chi(\omega)\mathbf{E}(\omega)$ for a monochromatic wave with frequency ω, it is clear that in the time domain, this relation expresses the fact that the material retains some memory about the incident field, $\chi(\omega)$ representing the memory kernel that is characteristic for the material used.

In line with the idea that an event-based approach should use the simplest rules possible, we reason as follows. In the event-based model, the nth message $\mathbf{u}_n = (\cos 2\pi f t_n, \sin 2\pi f t_n)$ is taken to represent the elementary unit of electric field $\mathbf{E}(t)$. Likewise, the electric polarization $\mathbf{P}(t)$ of the material is represented by the vector $\mathbf{v}_n = (v_{0,n}, v_{1,n})$. Upon receipt of the nth message this vector is updated according to the rule

$$\mathbf{v}_n = \gamma \mathbf{v}_{n-1} + (1-\gamma)\mathbf{u}_n, \tag{12}$$

where $0 < \gamma < 1$ and $n > 0$. Obviously, if $\gamma > 0$, a message processor that operates according to the update rule Eq. (12) has memory, as required by Maxwell's theory. It is not difficult to prove that as $\gamma \to 1^-$, the internal vector $\mathbf{v}_n$ converges to the average of the time-series $\{\mathbf{u}_1, \mathbf{u}_2, \ldots\}$.[3,16] By reducing γ, the number of messages needed to adapt decreases but also the accuracy of the DLM decreases. In the limit that $\gamma = 0$, the DLM learns nothing, it simply echoes the last message that it received.[7,8] The parameter γ controls the precision with which the DLM defined by Eq. (12) learns the average of the sequence of messages $\mathbf{u}_1, \mathbf{u}_2, \ldots$ and also controls the pace at which new messages affect the internal state $\mathbf{v}$ of the machine.[7] Moreover, in the continuum limit (meaning many events per unit of time), the rule given in Eq. (12) translates into the constitutive equation of the Debye model of a dielectric,[16,80] a model used in many applications of Maxwell's theory.[81]

After updating the vector $\mathbf{v}_n$, the DLM uses the information stored in $\mathbf{v}_n$ to decide whether or not to generate a click. As a highly simplified model for the bistable character of the real photodetector or photographic plate, we let the machine generate a binary output signal w_n according to

$$w_n = \Theta(\mathbf{v}_k^2 - r_n), \tag{13}$$

where $\Theta(\cdot)$ is the unit step function and $0 \le r_n < 1$ is a uniform pseudo-random number. Note that the use of pseudo-random numbers is convenient but not essential.[3] Since in experiment it cannot be known whether a photon has gone undetected, we discard the information about the $w_n = 0$ detection events and define the total detector count as $N' = \sum_{j=1}^{n'} w_j$, where n' is the number of messages received. N' is the number of clicks (one's) generated by the processor.

The efficiency of the detector model is determined by simulating an experiment that measures the detector efficiency, which for a single-photon detector is defined as the overall probability of registering a count if a photon arrives at the detector.[82] In such an experiment a point source emitting single particles is placed far away from a single detector. As all particles that reach the detector have the same time of flight (to a good approximation), all the particles that arrive at the detector will carry the same message which is encoding the time of flight. As a result $\mathbf{v}_n$ (see Eq. (12)) rapidly converges to the vector corresponding to this message, so that the detector clicks every time a photon arrives. Thus, the detection efficiency, as defined for real detectors,[82] for our detector model is very close to 100%. Hence,

the model is a highly simplified and idealized version of a single-photon detector. However, although the detection efficiency of the detector itself may be very close to 100%, the overall detection efficiency, which is the ratio of detected to emitted photons in the simulation of an experiment, can be much less than one. This ratio depends on the experimental setup.

— *Simulation procedure*: Each of the detectors of the circular screen has a predefined spatial window within which it accepts messages. As a messenger hits a detector, this detector updates its internal state $\mathbf{v}$, (the internal states of all other detectors do not change) using the message $\mathbf{u}_n$ and then generates the event w_n. In the case $w_n = 1$ ($w_n = 0$), the total count of the particular detector that was hit by the nth messenger is (not) incremented by one and the messenger itself is destroyed. Only after the messenger has been destroyed, the source is allowed to send a new messenger. This rule ensures that the whole simulation complies with Einstein's criterion of local causality. This process of creating and destroying messengers is repeated many times, building up the interference pattern event-by-event. Note that the number of emitted photons N is larger than the sum of the number of clicks generated by all the detectors forming the detection screen although no photons are lost during their travel from source to detector.

5.1.2. *Simulation results*

In Fig. 3(a), we present simulation results for the first experiment for a representative case for which the analytical solution from wave theory is known. Namely, in the Fraunhofer regime ($d \ll X$), the analytical expression for the light intensity at the detector on a circular screen with radius X is given by[42]

$$I(\theta) = A\,\sin^2\left(\frac{qa\sin\theta}{2}\right)\cos^2\left(\frac{qd\sin\theta}{2}\right)\Big/\left(\frac{qa\sin\theta}{2}\right)^2, \tag{14}$$

where A is a constant, $q = 2\pi f/c$ denotes the wavenumber with f and c being the frequency and velocity of the light, respectively, and θ denotes the angular position of the detector D on the circular screen, see Fig. 2. Note that Eq. (14) is only used for comparison with the simulation data and is by no means input to the model. From Fig. 3(a) it is clear that the event-based model reproduces the results of wave theory and this without taking recourse of the solution of a wave equation.

As the detection efficiency of the event-based detector model is very close to 100%, the interference patterns generated by the event-based model cannot be attributed to inefficient detectors. It is therefore of interest to take a look at the ratio of detected to emitted photons, the overall detection efficiency, and compare the detection counts, observed in the event-by-event simulation of the two-beam interference experiment, with those observed in a real experiment with single photons.[15] In the simulation that yields the results of Fig. 3(a), each of the 181 detectors making up the detection area is hit on average by 55×10^3 photons and the total number of clicks generated by the detectors is 0.16×10^7. Hence, the ratio of the total number of

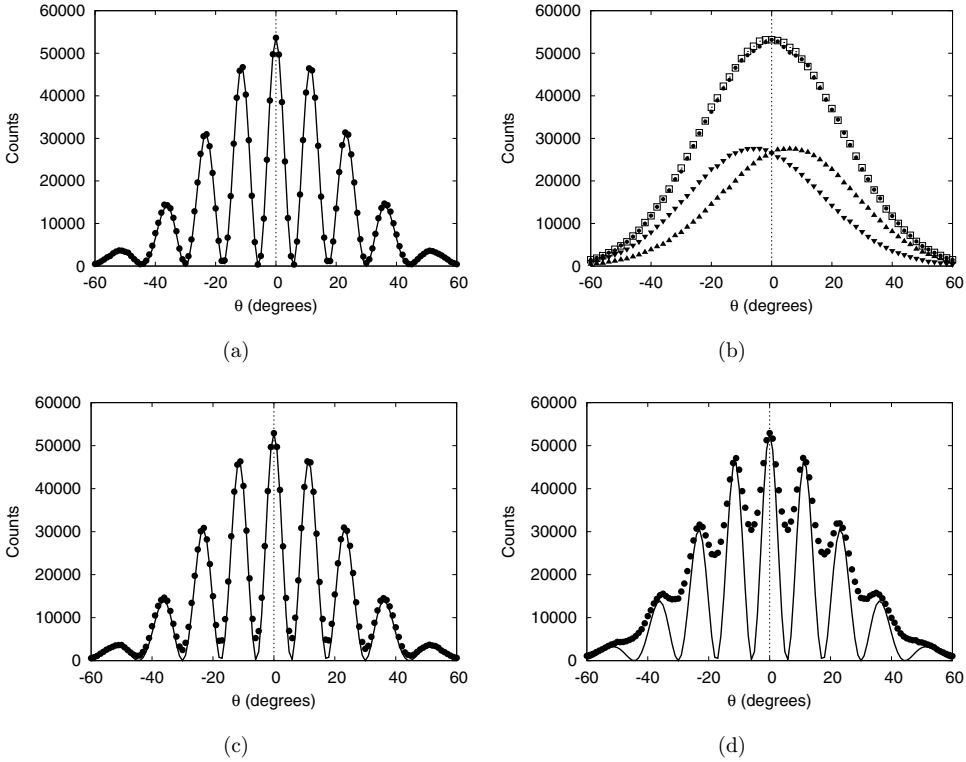

Fig. 3. Detector counts (markers) as a function of θ as obtained from the event-based simulation of the two-beam interference experiments described in Fig. 2. Simulation parameters: $N = 10^7$ so that on average, each of the 181 detectors, positioned on the semi-circular screen with an angular spacing of 1° in the interval $[-90^\circ, 90^\circ]$, receives about 55×10^3 particles, $\gamma = 0.999$, $a = c/f$, $d = 5c/f$, $X = 75c/f$, where c denotes the velocity and f the frequency of the particles ($c/f = 670\,\text{nm}$ in our simulations). (a): First experiment in which sources S_1 and S_2 in random order emit in total N particles one-by-one. This experiment resembles Young's (and Feynman's) two-slit experiment. (b): First experiment in which only source S_1 or S_2 emits $N = 5 \times 10^6$ particles one-by-one (downward and upward triangles, respectively). The open squares are the sum of the detector counts of the two experiments with one source emitting and the other one blocked. This experiment resembles Feynman's two-slit experiment with first slit S_2 blocked and then slit S_1 blocked. The closed circles are the result of the second experiment in which first S_1 and then S_2 emit a group of $M = 5 \times 10^6$ particles one-by-one. (c): Second experiment with $M = 10^6$. (d): Second experiment with $M = 25 \times 10^5$. The solid line in (a), (c) and (d) is a least-square fit of the simulation data of (a) to the prediction of wave theory, Eq. (14), with only one fitting parameter.

detected to emitted photons is of the order of 0.16, two orders of magnitude larger than the ratio 0.5×10^{-3} observed in single-photon interference experiments.[15]

In Fig. 3(b), we show simulation results for the experiment in which first only source S_1 emits $N = 5 \times 10^6$ photons (downward triangles) while S_2 is blocked by the mask. Then in a new experiment (all detectors are reset) S_2 emits $N = 5 \times 10^6$ photons while S_1 is blocked (upward triangles). The sum of the two resulting detection curves is given by the curve with open squares. It is clear that this curve is completely different from the curve depicted in Fig. 3(a), as is also described in

Feynman's thought experiment (see Sec. 2.1). Also in Fig. 3(b), we present the simulation results for the experiment in which first the source S_1 emits a group of $M = 5 \times 10^6$ particles one-by-one and then the source S_2 emits $M = 5 \times 10^6$ particles one-by-one (no resetting of the detectors). The resulting detection curve is drawn with closed circles. For small values of θ there is a difference between the curves with open squares and closed circles. This difference is due to the memory effect which is present in the detector model. Obviously this difference depends on γ and the detector model that is used. For more complicated detector models than the one given by Eq. (12) this small difference disappears (results not shown).

Figures 3(c) and 3(d) depict simulation results of the experiment in which sources S_1 and S_2 alternately emit M particles one-by-one with $M = 10^6$ and $M = 25 \times 10^5$, respectively. It is seen that except for very large values of M ($M \gtrsim 10^6$), the interference pattern is the same as the one shown in Fig. 3(a). Nevertheless, for these large values of M interference can still be observed. This is a result of the memory effects built in the detector model. However, for any value of M, a simple quantum theoretical calculation would predict no interference pattern but an intensity pattern which is the sum of two single slit patterns, as the particles pass through one or the other slit, and never through both. Hence, for this type of experiment the predictions of quantum theory and of the event-based model differ.

Although we are not aware of any experiment that precisely tests the above described scenario, one experimental study in which only one slit was available to each photon[83] produced intriguing results. In that study, an opaque barrier, all the way from the laser source to the obstacle between the two slits, was used to make sure that photons had one or the other slit available to them. The interference pattern observed was nevertheless essentially unchanged despite the presence of the barrier. We are, however, not aware of any follow-up work on that study.

5.1.3. *Why is interference produced without solving a wave problem?*

As mentioned earlier, using simple particle counters as detectors would not result in an interference pattern. Essential to produce an interference pattern is to account for the information about the differences in the times of flight (or phase differences) of the particles which encode the distance the particles travelled from one of the two sources to one of the detectors constituting the circular detection screen. Simple particle counters do nothing with the information which is encoded in the messages carried by the particles and produce a click for each incoming particle. Since, in the single-photon two-beam experiment the detectors are the only apparatuses available that can process these phase differences (there are no other apparatuses present except for the source) we necessarily need to employ an algorithm for the detector that exploits this information in order to produce the clicks that gradually build up the interference pattern. A collection of about 200 independent adaptive threshold detectors defined by Eqs. (12) and (13) and each with a detection efficiency of nearly 100% is capable of doing this. As pointed out earlier, the reason why, in this

particular experiment, this is possible is that not every particle that impinges on the detector yields a click.

5.2. *MZI experiment*

5.2.1. *Event-based model*

The DLM network that simulates a single-photon MZI experiment (see Fig. 4(a)) consists of a source, two identical BSs two phase shifters and two detectors. The network of processing units is a one-to-one image of the experimental setup.[6] Note that the two mirrors in the MZI simply bend the paths of the photons by $\pi/2$ without introducing a phase change or loss of particles and therefore they do not need to be considered in the event-based simulation network. In what follows we specify the processing units in sufficient detail such that the reader who is interested can reproduce the simulation results. We require that the processing units for identical optical components should be reusable within the same and within different experiments. Demonstration programs, including source codes, are available for download.[84,a]

— *Source and particles*: In a pictorial description of the experiment depicted in Fig. 4(a) the photons, leaving the source S one-by-one, can be regarded as particles playing the role of messengers. Each messenger carries a message

$$\mathbf{u}_{k,n} = (\cos(2\pi f t_{k,n}), \sin(2\pi f t_{k,n})), \tag{15}$$

where f denotes the frequency of the light source and $t_{k,n}$ the time that particles need to travel a given path. The subscript $n > 0$ numbers the consecutive messengers and k labels the channel of the BS at which the messenger arrives (see below). Note that in this experiment no explicit information about distances and frequencies is required since we can always work with relative phases.

When a messenger is created its internal clock time is set to zero ($t_{k,n} = 0$) and since the source is connected to the $k = 0$ input channel of the first BS the messenger gets the label $k = 0$ (see Fig. 4(a)).

— BS: A BS is an optical component that partially transmits and partially reflects an incident light beam. Dielectric plate BSs are often used as 50/50 BSs. From classical electrodynamics we know that if an electric field is applied to a dielectric material the material becomes polarized.[42] Assuming a linear response, the polarization vector of the material is given by $\mathbf{P}(\omega) = \chi(\omega)\mathbf{E}(\omega)$ for a monochromatic wave with frequency ω. In the time domain, this relation expresses the fact that the material retains some memory about the incident field, $\chi(\omega)$ representing the memory kernel that is characteristic for the material used. We use this kind of memory effect in our algorithm to model the BS.

A BS has two input and two output channels labeled by 0 and 1 (see Fig 4(a)). Note that in case of the MZI experiment, for beam splitter BS1 only entrance port

[a] Sample Fortran and Java programs and interactive programs that perform event-based simulations of a beam splitter, one Mach–Zehnder interferometer, and two chained Mach–Zehnder interferometers can be found at http://www.compphys.net/.

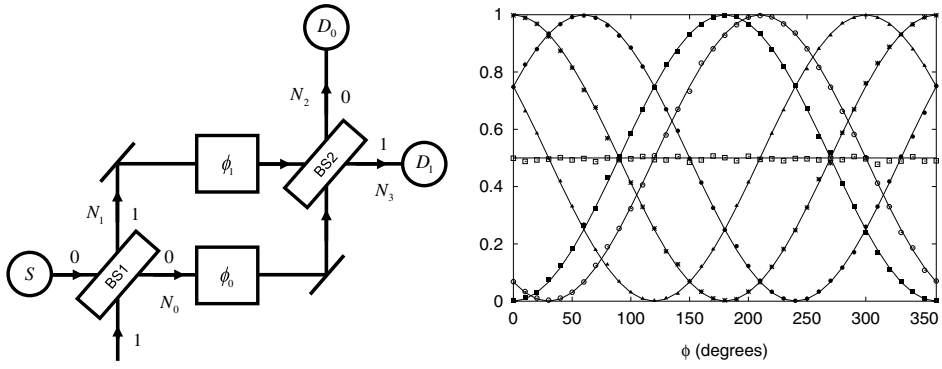

(a) (b)

Fig. 4. (a) Schematic diagram of a MZI with a single-photon source S. The MZI consists of two BSs, BS1 and BS2, two phase shifters ϕ_0 and ϕ_1 and two mirrors. N_0 (N_2) and N_1 (N_3) count the number of events in the output channel 0 of BS1 (BS2) and in the output channel 1 of BS1 (BS2), respectively. Dividing N_i for $i = 0, \ldots, 3$ by the total count N yields the relative frequency of finding a photon in the corresponding arm of the interferometer. Since photon detectors operate by absorbing photons, in a real laboratory experiment only N_2 and N_3 can be measured by detectors D_0 and D_1, respectively. (b) Simulation results for the normalized detector counts (markers) as a function of $\phi = \phi_0 - \phi_1$. Input channel 0 receives $(\cos\psi_0, \sin\psi_0)$ with probability one. One uniform random number in the range $[0, 360]$ is used to choose the angle ψ_0. Input channel 1 receives no events. The parameter $\gamma = 0.98$. Each data point represents 10 000 events ($N = N_0 + N_1 = N_2 + N_3 = 10\,000$). Initially the rotation angle $\phi_0 = 0$ and after each set of 10 000 events, ϕ_0 is increased by $10°$. Open squares: N_0/N; solid squares: N_2/N for $\phi_1 = 0$; open circles: N_2/N for $\phi_1 = 30°$; solid circles: N_2/N for $\phi_1 = 240°$; asterisks: N_3/N for $\phi_1 = 0$; solid triangles: N_3/N for $\phi_1 = 300°$. Lines represent the results of quantum theory.[b]

$k = 0$ is used. In the event-based model, the BS has two internal registers $\mathbf{R}_{k,n} = (R_{0,k,n}, R_{1,k,n})$ (one for each input channel) and an internal vector $\mathbf{v}_n = (v_{0,n}, v_{1,n})$ with the additional constraints that $v_{i,n} \geq 0$ for $i = 0, 1$ and that $v_{0,n} + v_{1,n} = 1$. As we only have two input channels, the latter constraint can be used to recover $v_{1,n}$ from the value of $v_{0,n}$. We prefer to work with internal vectors that have as many elements as there are input channels. These three two-dimensional vectors $\mathbf{v}_n$, $\mathbf{R}_{0,n}$ and $\mathbf{R}_{1,n}$ are labeled by the message number n because their content is updated every time the BS receives a message. Before the simulation starts we set $\mathbf{v}_0 = (v_{0,0}, v_{1,0}) = (r, 1 - r)$, where r is a uniform pseudo-random number. In a similar way, we use pseudo-random numbers to set $\mathbf{R}_{0,0}$ and $\mathbf{R}_{1,0}$.

When the nth messenger carrying the message $\mathbf{u}_{k,n}$ arrives at entrance port $k = 0$ or $k = 1$ of the BS, the BS first stores the message in the corresponding register $\mathbf{R}_{k,n}$ and updates its internal vector according to the rule

$$\mathbf{v}_n = \gamma \mathbf{v}_{n-1} + (1 - \gamma)\mathbf{q}_n, \tag{16}$$

[b]We make a distinction between quantum theory and quantum physics. We use the term *quantum theory* when we refer to the mathematical formalism, i.e. the postulates of quantum mechanics (with or without the wave function collapse postulate)[2] and the rules (algorithms) to compute the wave function. The term *quantum physics* is used for microscopic, experimentally observable phenomena that do not find an explanation within the mathematical framework of classical mechanics.

where $0 < \gamma < 1$ is a parameter that controls the learning process and $\mathbf{q}_n = (1, 0)$ ($\mathbf{q}_n = (0, 1)$) if the nth event occurred on channel $k = 0$ ($k = 1$). By construction $v_{i,n} \geq 0$ for $i = 0, 1$ and $v_{0,n} + v_{1,n} = 1$. Hence the update rule Eq. (16) preserves the constraints on the internal vector. Obviously, these constraints are necessary if we want to interpret the $v_{k,n}$ as (an estimate of) the frequency for the occurrence of an event of type k. Note that the BS stores information about the last message only. The information carried by earlier messages is overwritten by updating the internal registers. From Eq. (16), one could say that the internal vector $\mathbf{v}$ (corresponding to the material polarization $\mathbf{P}$) is the response of the BS to the incoming messages (photons) represented by the vectors $\mathbf{q}$ (corresponding to the elementary unit of electric field $\mathbf{E}$). Therefore, the BS "learns" so to speak from the information carried by the photons. The characteristics of the learning process depend on the parameter γ (corresponding to the response function χ).

Next, in case of a 50/50 BS, the BS uses the six numbers stored in $\mathbf{R}_{0,n}$, $\mathbf{R}_{1,n}$ and $\mathbf{v}_n$ to calculate four numbers $g_{0,n} = (R_{0,0,n}\sqrt{v_{0,n}} - R_{1,1,n}\sqrt{v_{1,n}})/\sqrt{2}$, $g_{1,n} = (R_{0,1,n}\sqrt{v_{1,n}} + R_{1,0,n}\sqrt{v_{0,n}})/\sqrt{2}$, $g_{2,n} = (R_{0,1,n}\sqrt{v_{1,n}} - R_{1,0,n}\sqrt{v_{0,n}})/\sqrt{2}$ and $g_{3,n} = (R_{0,0,n}\sqrt{v_{0,n}} + R_{1,1,n}\sqrt{v_{1,n}})/\sqrt{2}$. These four real-valued numbers can be considered to represent the real and imaginary part of two complex numbers $g_{0,n} + ig_{1,n}$ and $g_{2,n} + ig_{3,n}$ which are obtained by the following matrix-vector multiplication

$$\begin{aligned}\begin{pmatrix} g_{0,n} + ig_{1,n} \\ g_{2,n} + ig_{3,n} \end{pmatrix} &= \frac{1}{\sqrt{2}} \begin{pmatrix} \sqrt{v_{0,n}}(R_{0,0,n} + iR_{1,0,n}) + i\sqrt{v_{1,n}}(R_{0,1,n} + iR_{1,1,n}) \\ i\sqrt{v_{0,n}}(R_{0,0,n} + iR_{1,0,n}) + \sqrt{v_{1,n}}(R_{0,1,n} + iR_{1,1,n}) \end{pmatrix} \\ &= \frac{1}{\sqrt{2}} \begin{pmatrix} 1 & i \\ i & 1 \end{pmatrix} \begin{pmatrix} \sqrt{v_{0,n}} & 0 \\ 0 & \sqrt{v_{1,n}} \end{pmatrix} \begin{pmatrix} R_{0,0,n} + iR_{1,0,n} \\ R_{0,1,n} + iR_{1,1,n} \end{pmatrix}. \end{aligned} \tag{17}$$

Identifying a_0 with $\sqrt{v_{0,n}}(R_{0,0,n} + iR_{1,0,n})$ and a_1 with $\sqrt{v_{1,n}}(R_{0,1,n} + iR_{1,1,n})$ it is clear that the computation of the four numbers $g_{i,n}$ for $i = 0, \ldots, 3$ plays the role of the matrix-vector multiplication in the quantum theoretical description of a BS

$$\begin{pmatrix} b_0 \\ b_1 \end{pmatrix} = \frac{1}{\sqrt{2}} \begin{pmatrix} a_0 + ia_1 \\ a_1 + ia_0 \end{pmatrix} = \frac{1}{\sqrt{2}} \begin{pmatrix} 1 & i \\ i & 1 \end{pmatrix} \begin{pmatrix} a_0 \\ a_1 \end{pmatrix}, \tag{18}$$

where (a_0, a_1) and (b_0, b_1) denote the input and output amplitudes, respectively. Note however that the DLM for the BS computes the four numbers $g_{i,n}$ for $i = 0, \ldots, 3$ for each incoming event thereby always updating $\mathbf{v}_n$ and $\mathbf{R}_{0,n}$ or $\mathbf{R}_{1,n}$. Hence, a_0 and a_1, and thus also b_0 and b_1, are constructed event-by-event and only under certain conditions ($\gamma \to 1^-$, sufficiently large number of input events N, stationary sequence of input events) they correspond to their quantum theoretical counterparts $a_0 = \sqrt{p_0}e^{i\psi_0}$, $a_1 = \sqrt{p_1}e^{i\psi_1}$ with $p_1 = 1 - p_0$ $(0 \leq p_0, p_1 \leq 1)$ and $b_0 = a_0 + ia_1$, $b_1 = a_1 + ia_0$ (see Eq. (18)).

In a final step the BS uses $g_{i,n}$ for $i = 0, \ldots, 3$ to create an output event. Therefore it generates a uniform random number r_n between zero and one. If

$g_{0,n}^2 + g_{1,n}^2 > r_n$, the BS sends a message

$$\mathbf{w}_{0,n} = (g_{0,n}, g_{1,n})/\sqrt{g_{0,n}^2 + g_{1,n}^2}, \tag{19}$$

through output channel 0. Otherwise it sends a message

$$\mathbf{w}_{1,n} = (g_{2,n}, g_{3,n})/\sqrt{g_{2,n}^2 + g_{3,n}^2}, \tag{20}$$

through output channel 1.

— *Phase shifters*: These devices perform a plane rotation on the vectors (messages) carried by the particles. As a result the phase of the particles is changed by ϕ_0 or ϕ_1 depending on the route followed.

— *Detector*: Detector D_0 (D_1) registers the output events at channel 0 (1). The detectors are ideal particle counters, meaning that they produce a click for each incoming particle. Hence, we assume that the detectors have 100% detection efficiency. Note that also adaptive threshold detectors can be used (see Sec. 5.1.1) equally well.[3]

— *Simulation procedure*: When a messenger is created we wait until its message has been processed by one of the detectors before creating the next messenger. This ensures that there can be no direct communication between the messengers and that our simulation model (trivially) satisfies Einsteins criterion of local causality. We assume that no messengers are lost. Since the detectors are ideal particle counters the number of clicks generated by the detectors is equal to the number of messengers created by the source. For fixed $\phi = \phi_0 - \phi_1$, a simulation run of N events generates the data set $\Gamma(\phi) = \{w_n | n = 1, \ldots, N\}$. Here $w_n = 0, 1$ indicates which detector fired (D_0 or D_1). Given the data set $\Gamma(\phi)$, we can easily compute the number of 0 (1) output events N_2 (N_3).

5.2.2. *Simulation results*

In Fig. 4(b), we present a few simulation results for the MZI and compare them to the quantum theoretical result. According to quantum theory, the amplitudes (b_0, b_1) in the output modes 0 and 1 of the MZI are given by[85]

$$\begin{pmatrix} b_0 \\ b_1 \end{pmatrix} = \frac{1}{2}\begin{pmatrix} 1 & i \\ i & 1 \end{pmatrix}\begin{pmatrix} e^{i\phi_0} & 0 \\ 0 & e^{i\phi_1} \end{pmatrix}\begin{pmatrix} 1 & i \\ i & 1 \end{pmatrix}\begin{pmatrix} a_0 \\ a_1 \end{pmatrix}, \tag{21}$$

where a_0 and a_1 denote the input amplitudes. For the particular choice $a_0 = 1$ and $a_1 = 0$, in which case there are no particles entering BS1 via channel 1, it follows from Eq. (21) that

$$|b_0|^2 = \sin^2\left(\frac{\phi_0 - \phi_1}{2}\right), \quad |b_1|^2 = \cos^2\left(\frac{\phi_0 - \phi_1}{2}\right). \tag{22}$$

For the results presented in Fig. 4(b) we assume that input channel 0 receives $(\cos\psi_0, \sin\psi_0)$ with probability one and that input channel 1 receives no events. This

corresponds to $(a_0, a_1) = (\cos\psi_0 + i\sin\psi_0, 0)$. We use a uniform random number to determine ψ_0. Note that this random number is used to generate all input events. The data points are the simulation results for the normalized intensity N_i/N for $i = 0, 2, 3$ as a function of $\phi = \phi_0 - \phi_1$. Note that in an experimental setting it is impossible to simultaneously measure $(N_0/N,\ N_1/N)$ and $(N_2/N,\ N_3/N)$ because photon detectors operate by absorbing photons. In the event-based simulation there is no such problem. From Fig. 4(b) it is clear that the event-based processing by the DLM network reproduces the probability distribution of quantum theory, see Eq. (22) with $|b_0|^2$ ($|b_1|^2$) corresponding to N_2/N (N_3/N).

5.2.3. *Why is interference produced without solving a wave problem?*

We consider BS2 of the MZI depicted in Fig. 4(a), the BS at which, in a wave picture, the two beams join to produce interference. The DLM simulating a BS requires two pieces of information to send out particles such that their distribution matches the wave-mechanical description of the BS. First, it needs an estimate of the ratio of particle currents in the input channels 0 and 1 (paths 0 and 1 of the MZI), respectively. Second, it needs to have information about the time of flight (phase difference) along the two different paths of the MZI. The first piece of information is provided for by the internal vector $\mathbf{v} = (v_0, v_1)$. Through the update rule Eq. (16), for a stationary sequence of input events, v_0 and v_1 converge to the average of the number of events on input channels 0 and 1, respectively. Thus, the ratio of the particles (corresponding to the intensities of the waves) in the two input beams are encoded in the vector $\mathbf{v}$. Note that this information is accurate only if the sequence of input events is stationary. After one particle arrived at port 0 and another one arrived at port 1, the second piece of information is available in the registers $\mathbf{R}_0$ and $\mathbf{R}_1$. This information plays the role of the phase of the waves in the two input beams. Hence, all the information (intensity and phase) is available to compute the probability for sending out particles. This is done by calculating the numbers g_i for $i = 0, \ldots, 3$ which, in the stationary state, are identical to the wave amplitudes obtained from the wave theory of a BS.[42]

5.3. *Wheeler's delayed choice experiment*

In a recent experimental realization of Wheeler's delayed-choice experiment by Jacques *et al.*[76] linearly polarized single photons are sent through a polarizing BS (PBS) that together with a second, movable, variable output PBS with adjustable reflectivity $\mathcal{R}$ forms an interferometer (see Fig. 5). In the first realization[9] two 50/50 BSs were used.

Tilting the PBS of the variable output BS induces a time-delay in one of the arms of the MZI, symbolically represented by the variable phase $\phi_1(x)$ in Fig. 5, and thus varies the phase shift $\phi(x) = \phi_0 - \phi_1(x)$ between the two arms of the MZI. A voltage applied to an electro-optic modulator (EOM) controls the reflectivity $\mathcal{R}$ of the variable beam splitter $\mathrm{BS}_{\mathrm{output}}$. If no voltage is applied to the EOM then $\mathcal{R} = 0$.

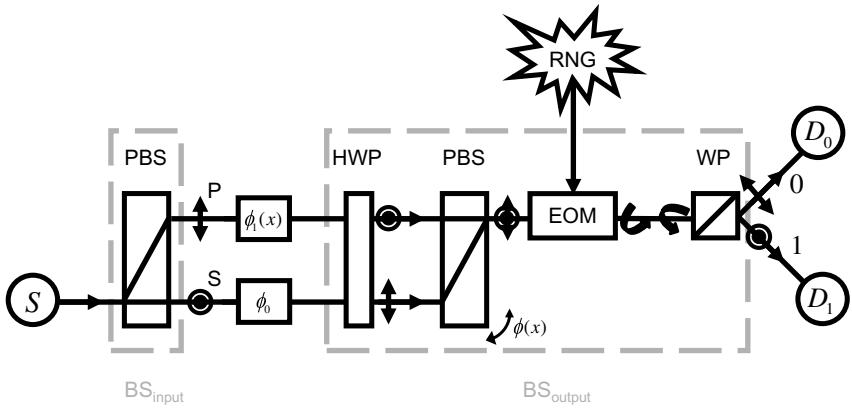

Fig. 5. Schematic diagram of the experimental setup of Wheeler's delayed-choice experiment with single photons.[9,76] S: single-photon source; PBS: polarizing beam splitter; HWP: half-wave plate; EOM: electro-optic modulator; RNG: random number generator; WP: Wollaston prism (= PBS); D_0 and D_1: detectors; P, S: polarization state of the photons; $\phi(x) = \phi_0 - \phi_1(x)$: phase shift between paths 0 and 1. The diagram is that of a MZI composed of a 50/50 input BS (BS_{input}) and a variable output BS (BS_{output}) with adjustable reflectivity $\mathcal{R}$.

Otherwise, $\mathcal{R} \neq 0$ (see Eq. (2) in Ref. 76) and the EOM acts as a wave plate which rotates the polarization of the incoming photon by an angle depending on the value of $\mathcal{R}$. The voltage applied to the EOM is controlled by a set of pseudo-random numbers generated by the random number generator RNG. The key point in this experiment is that the decision to apply a voltage to the EOM is made after the photon has passed BS_{input}.

For $0 \leq \mathcal{R} \leq 0.5$ measured values of the interference visibility[86] V and the path distinguishability[76] D, a parameter that quantifies the which-path information (WPI), were found to fulfill the complementary relation $V^2 + D^2 \leq 1$.[76] For $(V = 0, D = 1)$ and $(V = 1, D = 0)$, obtained for $\mathcal{R} = 0$ and $\mathcal{R} = 0.5$, respectively, full and no WPI was found, associated with particle-like and wave-like behavior, respectively. For $0 \leq \mathcal{R} \leq 0.5$ partial WPI was obtained while keeping interference with limited visibility.[76]

Although the detection events (detector "clicks") are the only experimental facts and logically speaking one cannot say anything about what happens with the photons traveling through the setup, Jacques *et al.*[9,76] gave the following pictorial description: Linearly polarized single photons are sent through a 50/50 PBS (BS_{input}), spatially separating photons with S polarization (path 0) and P polarization (path 1) with equal frequencies. After the photon has passed BS_{input}, but before the photon enters the variable BS_{output} the decision to apply a voltage to the EOM is made. The PBS of BS_{output} merges the paths of the orthogonally polarized photons travelling paths 0 and 1 of the MZI, but afterwards the photons can still be unambiguously identified by their polarizations. If no voltage is applied to the EOM then $\mathcal{R} = 0$ and the EOM does nothing to the photons. Because the polarization eigenstates of the Wollaston prism correspond to the P and S polarization of the photons travelling

path 0 and 1 of the MZI, each detection event registered by one of the two detectors D_0 or D_1 is associated with a specific path (path 0 or 1, respectively). Both detectors register an equal amount of detection events, independent of the phase shift $\phi(x)$ in the MZI. This experimental setting clearly gives full WPI about the photon within the interferometer (particle behavior), characterized by $D = 1$. In this case no interference effects are observed and thus $V = 0$. When a voltage is applied to the EOM, then $\mathcal{R} \neq 0$ and the EOM rotates the polarization of the incoming photon by an angle depending on $\mathcal{R}$. The Wollaston prism partially recombines the polarization of the photons that have travelled along different optical paths with phase difference $\phi(x)$ and interference appears ($V \neq 0$), a result expected for a wave. The WPI is partially washed out, up to be totally erased when $\mathcal{R} = 0.5$. Hence, the decision to apply a voltage to the EOM after the photon left $\mathrm{BS}_{\mathrm{input}}$ but before it passes $\mathrm{BS}_{\mathrm{output}}$, influences the behavior of the photon in the past and changes the representation of the photon from a particle to a wave.[9]

5.3.1. *Event-based model*

We construct a model for the messengers representing the linearly polarized photons and for the processing units representing the optical components in the experimental setup (see Fig. 5) thereby fulfilling the requirements that the processing units for identical optical components should be reusable within the same and within different experiments and that the network of processing units is a one-to-one image of the experimental setup. Although, in contrast to the experiments we have considered so far, in this experiment it is necessary to include the polarization in the model for the messengers representing the photons. These more general messengers can also be used in a simulation of the experiments discussed previously. In the event-based simulation of these experiments the polarization component of the message is simply not used in the DLMs modeling the optical components of their experimental setup. In what follows we describe the elements of the model in more detail.

— *Source and particles*: The polarization can be included in the model for the messengers representing the photons by adding to the message a second harmonic oscillator which also vibrates with frequency f. There are many different but equivalent ways to define the message. As in Maxwell's and quantum theory, it is convenient (though) not essential to work with complex valued vectors, that is with messages represented by two-dimensional unit vectors

$$\mathbf{u} = (e^{i\psi^{(1)}} \sin\xi, e^{i\psi^{(2)}} \cos\xi), \tag{23}$$

where $\psi^{(i)} = 2\pi f t + \delta_i$, for $i = 1, 2$. The angle ξ determines the relative magnitude of the two components and $\delta = \delta_1 - \delta_2 = \psi^{(1)} - \psi^{(2)}$, denotes the phase difference between the two components. Both ξ and δ determine the polarization of the photon. Hence, the photon can be considered to have a polarization vector $\mathbf{P} = (\cos\delta \sin 2\xi, \sin\delta \sin 2\xi, \cos 2\xi)$. The third degree of freedom in Eq. (23) is used to account for the time of flight of the photon. Within the present model, it is

thus postulated that the state of the photon is fully determined by the angles $\psi^{(1)}$, $\psi^{(2)}$ and ξ and by rules (to be specified), by which these angles change as the photon travels through the network.

A messenger with message $\mathbf{u}$ at time t and position $\mathbf{r}$ that travels with velocity $v = c/n$, where c denotes the velocity of light and n is the index of refraction of the material, along the direction $\mathbf{q}$ during a time interval $t' - t$, changes its message according to $\psi^{(i)} \to \psi^{(i)} + \phi$ for $i = 1, 2$, where $\phi = 2\pi f(t' - t)$. This suggests that we may view the two-component vectors $\mathbf{u}$ as the coordinates of two local oscillators, carried along by the messengers and that the messenger encodes its time of flight in these two oscillators.

It is evident that the representation used here maps one-to-one to the plane-wave description of a classical electromagnetic field,[42] except that we assign these properties to each individual photon, not to a wave. As there is no communication/interaction between the messengers there can be no wave equation (partial differential equation) that enforces a relation between the messages carried by different messages.

When the source creates a messenger, its message needs to be initialized. This means that the three angles $\psi^{(1)}$, $\psi^{(2)}$ and ξ need to be specified. The specification depends on the type of light source that has to be simulated. For a coherent light source, the three angles are different but the same for all the messengers being created. Hence, three random numbers are used to specify $\psi^{(1)}$, $\psi^{(2)}$ and ξ for all messengers.

In this section, we will demonstrate explicitly that in the event-based model (in general, not only for this experiment) photons always have full WPI even if interference is observed by giving the messengers one extra label, the path label having the value 0 or 1. The information contained in this label is not accessible in the experiment.[76] We only use it to track the photons in the network of processing units. The path label is set in the input BS and remains unchanged until detection. Therefore, we do not consider this label in the description of the processing units but take it into account when we detect the photons.

— PBS: A PBS is used to redirect photons depending on their polarization. For simplicity, we assume that the coordinate system used to define the incoming messages coincides with the coordinate system defined by two orthogonal directions of polarization of the PBS.

In general, a PBS has two input and two output channels labeled by 0 and 1, just like an ordinary BS (see Sec. 5.2.1). Note that in case of Wheeler's delayed choice experiment, the first PBS has only one input channel labeled by $k = 0$ and therefore the second PBS has only one output channel labeled by $k = 0$. In the event-based model, the PBS has a similar structure as the BS. Therefore, in what follows we only mention the main ingredients to construct the processing unit for the PBS. For more details we refer to Sec. 5.2.1.

The PBS has two internal registers $\mathbf{R}_{k,n} = (R_{0,k,n}, R_{1,k,n})$ with $R_{i,k,n}$ for $i = 0, 1$ representing a complex number, and an internal vector $\mathbf{v}_n = (v_{0,n}, v_{1,n})$, where

$v_{i,n} \geq 0$ for $i = 0, 1$, $v_{0,n} + v_{1,n} = 1$ and n denotes the message number. Before the simulation starts uniform pseudo-random numbers are used to set $\mathbf{v}_0$, $\mathbf{R}_{0,0}$ and $\mathbf{R}_{1,0}$.

When the nth messenger carrying the message $\mathbf{u}_{k,n}$ arrives at entrance port $k = 0$ or $k = 1$ of the PBS, the PBS first copies the message in the corresponding register $\mathbf{R}_{k,n}$ and updates its internal vector according to

$$\mathbf{v}_n = \gamma \mathbf{v}_{n-1} + (1 - \gamma)\mathbf{q}_n, \tag{24}$$

where $0 < \gamma < 1$ and $\mathbf{q}_n = (1, 0)$ ($\mathbf{q}_n = (0, 1)$) represents the arrival of the nth messenger on channel $k = 0$ ($k = 1$). Note that the DLM has storage for exactly 10 real-valued numbers.

Next the PBS uses the information stored in $\mathbf{R}_{0,n}$, $\mathbf{R}_{1,n}$ and $\mathbf{v}_n$ to calculate four complex numbers

$$\begin{pmatrix} h_{0,n} \\ h_{1,n} \\ h_{2,n} \\ h_{3,n} \end{pmatrix} = \begin{pmatrix} 1 & 0 & 0 & 0 \\ 0 & 1 & 0 & 0 \\ 0 & 0 & 0 & i \\ 0 & 0 & i & 0 \end{pmatrix} \begin{pmatrix} \sqrt{v_{0,n}} & 0 & 0 & 0 \\ 0 & \sqrt{v_{1,n}} & 0 & 0 \\ 0 & 0 & \sqrt{v_{0,n}} & 0 \\ 0 & 0 & 0 & \sqrt{v_{1,n}} \end{pmatrix} \begin{pmatrix} R_{0,0,n} \\ R_{0,1,n} \\ R_{1,0,n} \\ R_{1,1,n} \end{pmatrix}$$

$$= \begin{pmatrix} \sqrt{v_{0,n}} R_{0,0,n} \\ \sqrt{v_{1,n}} R_{0,1,n} \\ i\sqrt{v_{1,n}} R_{1,1,n} \\ i\sqrt{v_{0,n}} R_{1,0,n} \end{pmatrix} \tag{25}$$

and generates a uniform random number r_n between zero and one. If $|h_{0,n}|^2 + |h_{2,n}|^2 > r_n$, the PBS sends a message

$$\mathbf{w}_{0,n} = (h_{0,n}, h_{2,n}) / \sqrt{|h_{0,n}|^2 + |h_{2,n}|^2}, \tag{26}$$

through output channel 1. Otherwise it sends a message

$$\mathbf{w}_{1,n} = (h_{1,n}, h_{3,n}) / \sqrt{|h_{1,n}|^2 + |h_{3,n}|^2}, \tag{27}$$

through output channel 0.

— HWP: A HWP not only changes the polarization of the light but also its phase. In optics, a HWP is often used as a retarder. In the event-based model, the retardation of the wave corresponds to a change in the time of flight (and thus the phase) of the messenger. In contrast to the BS and PBS, a HWP may be simulated without DLM. The device has only one input and one output port (see Fig. 5). A HWP transforms the nth input message $\mathbf{u}_n$ into an output message

$$\mathbf{w}_n = -i(u_{0,n} \cos 2\theta + u_{1,n} \sin 2\theta, u_{0,n} \sin 2\theta - u_{1,n} \cos 2\theta), \tag{28}$$

where θ denotes the angle of the optical axis with respect to the laboratory frame. Hence, in order to change S polarization into P polarization, or vice versa, a HWP

is used with its optical axis oriented at $\pi/4$. This changes the phase of the photon by $-\pi/2$.

— EOM: An EOM rotates the polarization of the photon by an angle depending on the voltage applied to the modulator. In the laboratory experiment, the EOM is operated such that when a voltage is applied it acts as a HWP that rotates the input polarizations by $\pi/4$. We use a pseudo-random number to mimic the experimental procedure to control the EOM, but any other (systematic) sequence to control the EOM can be used as well.

— WP: The WP is a PBS with one input channel and two output channels and is simulated as the PBS described earlier.

— *Detector*: Detector D_0 (D_1) counts the output events at channel 0 (1) of the Wollaston prism. The detectors are ideal particle counters, meaning that they produce a click for each incoming particle. Hence, we assume that the detectors have 100% detection efficiency. Note that in this experimental configuration adaptive threshold detectors (see Sec. 5.1.1) can be used equally well because their detection efficiency is 100%.[3]

— *Simulation procedure*: When a messenger is created we wait until its message has been processed by one of the detectors before creating the next messenger (Einstein's criterion of local causality). During a simulation run of N events the data set $\Gamma(\phi(x)) = \{w_n, d_n, r_n | n = 1, \ldots, N; \phi(x) = \phi_0 - \phi_1(x)\}$ is generated, where $w_n = 0, 1$ indicates which detector fired (D_0 or D_1), $d_n = 0, 1$ indicates through which arm of the MZI the messenger (photon) came that generated the detection event (note that d_n is only measured in the simulation, not in the experiment), and r_n is a pseudo-random number that is chosen after the nth message has passed the first PBS, determining which voltage is applied to the EOM. Note that in one run of N events a choice is made between no voltage (open MZI configuration) or a particular voltage (closed MZI configuration) corresponding to a certain reflectivity $\mathcal{R}$ of the output BS (see Eq. (2) in Ref. 76). These choices are made such that on average the MZI configuration is as many times open as it is closed. The angle $\phi(x)$ denotes the phase shift between the two interferometer arms. This phase shift is varied by applying a plane rotation on the phase of the particles entering channel 0 of the second PBS. This corresponds to tilting the second PBS in the laboratory experiment.[76] For each $\phi(x)$ and MZI configuration the number of 0 (1) output events N_0 (N_1) is calculated.

5.3.2. *Simulation results*

We first demonstrate that our model yields full WPI of the photons. Figure 6(a) shows the number of detection events at D_0 as a function of ϕ (($\phi \equiv \phi(x)$ for a given fixed position of the PBS in $\mathrm{BS}_{\mathrm{output}}$) for $\mathcal{R} = 0.5$. The events generated by photons following paths 0 and 1 of the MZI are counted separately. It is clear that the number of photons that followed paths 0 (squares) and 1 (triangles) is equal and that the total intensity in output channel 0 (open circles) shows a sinusoidal function of ϕ.

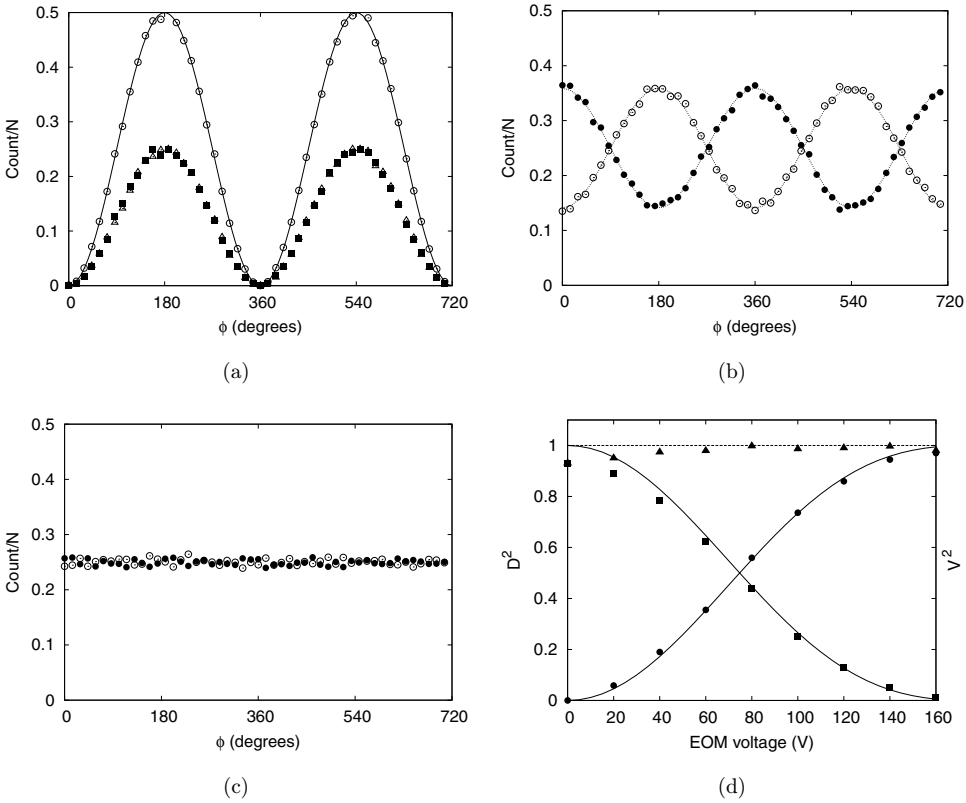

Fig. 6. Event-by-event simulation results of the normalized detector counts for different values of $\mathcal{R}$ ((a)–(c)) and of V^2, D^2 and $V^2 + D^2$ as a function of the EOM voltage (d). (a) Markers give the results for the normalized intensity N_0/N as a function of the phase shift ϕ, N_0 denoting the number of events registered at detector D_0. Squares (triangles, hardly visible because they overlap with the squares) represent the detection events generated by photons which followed path 0 (1). Open circles represent the total number of detection events. (b)–(c) Open (closed) circles give the results for the normalized intensities N_0/N (N_1/N) as a function of the phase shift ϕ, N_0 (N_1) denoting the number of events registered at detector D_0 (D_1), for (b) $\mathcal{R} = 0.05$ ($V \approx 0.45$) and (c) $\mathcal{R} = 0$ ($V = 0$). For each value of ϕ, the number of input events $N = 10\,000$. The number of detection events per data point is approximately the same as in experiment. Dashed lines represent the results of quantum theory. (d) Squares, circles and triangles present the simulation results for V^2, D^2 and $V^2 + D^2$, respectively. Lines represent the theoretical expectations obtained from Eqs. (2), (3) and (7) in Ref. 76 with $\beta = 24°$ and $V_\pi = 217\,\mathrm{V}$.

Hence, although the photons have full WPI for all ϕ they can build an interference pattern by arriving one-by-one at a detector. Next, we calculate for $\mathcal{R} = 0.05$ and $\mathcal{R} = 0$ and for each phase shift ϕ and configuration (open or closed) of the MZI the number of events registered by the two detectors behind the output BS, just like in the experiment. Figures 6(b) and 6(c) depict the normalized detection counts at D_0 (open circles) and D_1 (closed circles). The simulation data quantitatively agree with the averages calculated from quantum theory and qualitatively agree with experiment (see Fig. 3 in Ref. 76). Calculation of D as described in Ref. 76 gives the results

for D^2 and V^2 shown in Fig. 6(d). Comparison with Fig. 4 in Ref. 76 shows excellent qualitative agreement.

5.4. *Single neutron interferometry*

Now that we have demonstrated the event-based simulation approach for the event-by-event realization of an interference pattern in various single-photon interference experiments, we consider in this section one of the basic experiments in neutron interferometry, namely a Mach–Zehnder type of interferometer. In neutron optics there exist various realizations of the Mach–Zehnder type of interferometer, but we only consider a triple Laue diffraction type silicon perfect single crystal interferometer. [36,87,88]

Figure 7(left) shows the experimental configuration. The three crystal plates, named the splitter, mirror and analyzer plate, are assumed to be identical, which means that they have the same transmission and reflection properties.[36] The three crystal plates have to be parallel to high accuracy[87] and the whole device needs to be protected from vibrations in order to observe interference.[89] A monoenergetic neutron beam is split by the splitter plate (BS0). Neutrons refracted by beam splitters BS1 and BS2 (mirror plate) are directed to the analyzer plate (BS3), also acting as a BS, thereby first passing through a rotatable-plate phase shifter (e.g. aluminum foil[36]). Absorption of neutrons by the aluminum foil is assumed to be negligible.[36] Minute rotations of the foil about an axis perpendicular to the base plane of the

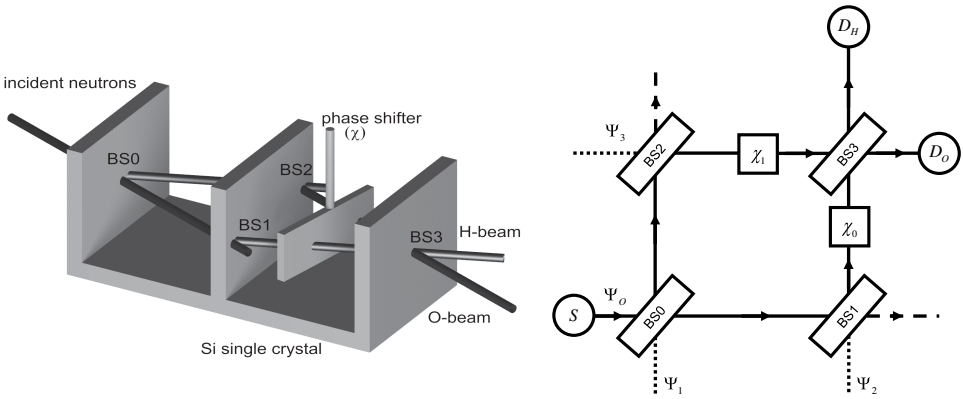

Fig. 7. Left: Schematic picture of the silicon-perfect-crystal neutron interferometer.[87] BS0, . . . , BS3: BSs; phase shifter χ: aluminum foil; neutrons that are transmitted by BS1 or BS2 leave the interferometer and do not contribute to the interference signal. Detectors count the number of neutrons in the O- and H-beams. Right: Event-based network of the interferometer shown on the left. S: single neutron source; BS0, . . . , BS3: BSs; χ_0, χ_1: phase shifters; D_O, D_H: detectors counting all neutrons that leave the interferometer via the O- and H-beams, respectively. In the experiment and in the event-based simulation, neutrons enter the interferometer via the path labeled by Ψ_0 only. The wave amplitudes labeled by Ψ_1, Ψ_2 and Ψ_3 (dotted lines) are used in the quantum theoretical treatment only (see text). Particles leaving the interferometer via the dashed lines are not counted.

interferometer induce large variations in the phase difference $\chi = \chi_0 - \chi_1$.[36,90] Finally, the neutrons are detected by one of the two detectors placed in the so-called H-beam or O-beam. In contrast to single-photon detectors, neutron detectors can have a very high, almost 100%, efficiency.[36] Neutrons which are not refracted by BS1 and BS2 leave the interferometer and are not counted. The intensities in the O- and H-beams, obtained by counting individual neutrons for a certain amount of time, exhibit sinusoidal variations as a function of the phase shift χ, a characteristic of interference.[36]

The experiment could be interpreted in different ways. In the quantum-corpuscular view a wave packet is associated with each individual neutron. At BS0 the wave packet splits in two components, one directed toward BS1 and other toward BS2. At BS1 and BS2, these two components each split in two. Two of the in total four components leave the interferometer and the other two components are redirected toward each other at BS3 where they recombine. At BS3 the recombined wave packet splits again in two components. Only one of these two components triggers a detector. It is a mystery how four components of a wave packet can conspire to do such things. Assuming that only a neutron, not merely a part of it can trigger the nuclear reaction that causes the detector to "click", on elementary logical grounds, the argument that was just given rules out a wave-packet picture for the individual neutron (invoking the wave function collapse only adds to the mystery). In the statistical interpretation of quantum mechanics there is no such conflict of interpretation.[2,66] As long as we consider descriptions of the statistics of the experiment with many neutrons, we may think of one single "probability" wave propagating through the interferometer and as the statistical interpretation of quantum theory is silent about single events, there is no conflict with logic either.[36]

In what follows we demonstrate that as in the case of the single-photon interference experiments, it is possible to construct a logically consistent, cause-and-effect description in terms of discrete-event, particle-like processes which produce results that agree with those of neutron interferometry experiments (individual detection events and an interference pattern after many single detection events have been collected) and the quantum theory thereof (interference pattern only).

5.4.1. *Event-based model*

We construct a model for the messengers representing the neutrons and for the processing units representing the various components in the experimental setup (see Fig. 7(right)).

— *Source and particles*: In analogy to the event-based model of a polarized photon (see Sec. 5.3.1), a neutron is regarded as a messenger carrying a message represented by the two-dimensional unit vector

$$\mathbf{u} = (e^{i\psi^{(1)}} \cos(\theta/2), e^{i\psi^{(2)}} \sin(\theta/2)), \tag{29}$$

where $\psi^{(i)} = \nu t + \delta_i$, for $i = 1, 2$. Here, t specifies the time of flight of the neutron and ν is an angular frequency which is characteristic for a neutron that moves with a fixed velocity v. A monochromatic beam of incident neutrons is assumed to consist of neutrons that all have the same value of ν, that is: they have the same velocity.[36] Both θ and $\delta = \delta_1 - \delta_2 = \psi^{(1)} - \psi^{(2)}$ determine the magnetic moment of the neutron, if the neutron is viewed as a tiny classical magnet spinning around the direction $\mathbf{m} = (\cos\delta\sin\theta, \sin\delta\sin\theta, \cos\theta)$, relative to a fixed frame of reference defined by a magnetic field. The third degree of freedom in Eq. (29) is used to account for the time of flight of the neutron. Within the present model, the state of the neutron is fully determined by the angles $\psi^{(1)}$, $\psi^{(2)}$ and θ and by rules (to be specified), by which these angles change as the neutron travels through the network.

A messenger with message $\mathbf{u}$ at time t and position $\mathbf{r}$ that travels with velocity v, along the direction $\mathbf{q}$ during a time interval $t' - t$, changes its message according to $\psi^{(i)} \to \psi^{(i)} + \phi$ for $i = 1, 2$, where $\phi = \nu(t' - t)$.

In the presence of a magnetic field $\mathbf{B} = (B_x, B_y, B_z)$, the magnetic moment rotates about the direction of $\mathbf{B}$ according to the classical equation of motion. Hence, in a magnetic field the message $\mathbf{u}$ is changed into the message $\mathbf{w} = e^{ig\mu_N T\sigma\cdot\mathbf{B}}\mathbf{u}$, where g denotes the neutron g-factor, μ_N the nuclear magneton, T the time during which the neutron experiences the magnetic field and σ denotes the Pauli vector (here we use the isomorphism between the algebra of Pauli matrices and rotations in three-dimensional space).

When the source creates a messenger, its message needs to be initialized. This means that the three angles $\psi^{(1)}$, $\psi^{(2)}$ and θ need to be specified. The specification depends on the type of source that has to be simulated. For a fully coherent spin-polarized beam of neutrons, the three angles are different but the same for all the messengers being created. Hence, three random numbers are used to specify $\psi^{(1)}$, $\psi^{(2)}$ and θ for all messengers.

— *Beam splitters* BS0, ..., BS3: Exploiting the similarity between the magnetic moment of the neutron and the polarization of a photon, we use a similar model for the BS as the one used in Sec. 5.3.1 for polarized photons. The only difference is that we assume that neutrons with spin up and spin down have the same reflection and transmission properties, while photons with horizontal and vertical polarization have different reflection and transmission properties.[42] Hence, what needs to be changed with respect to Sec. 5.3.1 are the complex numbers $h_{0,n}, \ldots, h_{3,n}$. For the neutrons, we have

$$\begin{pmatrix} h_{0,n} \\ h_{1,n} \\ h_{2,n} \\ h_{3,n} \end{pmatrix} = \begin{pmatrix} \sqrt{\mathcal{T}} & i\sqrt{\mathcal{R}} & 0 & 0 \\ i\sqrt{\mathcal{R}} & \sqrt{\mathcal{T}} & 0 & 0 \\ 0 & 0 & \sqrt{\mathcal{T}} & i\sqrt{\mathcal{R}} \\ 0 & 0 & i\sqrt{\mathcal{R}} & \sqrt{\mathcal{T}} \end{pmatrix}$$

$$\times \begin{pmatrix} \sqrt{v_{0,n}} & 0 & 0 & 0 \\ 0 & \sqrt{v_{1,n}} & 0 & 0 \\ 0 & 0 & \sqrt{v_{0,n}} & 0 \\ 0 & 0 & 0 & \sqrt{v_{1,n}} \end{pmatrix} \begin{pmatrix} R_{0,0,n} \\ R_{0,1,n} \\ R_{1,0,n} \\ R_{1,1,n} \end{pmatrix}$$

$$= \begin{pmatrix} \sqrt{v_{0,n}}\sqrt{\mathcal{T}}R_{0,0,n} + i\sqrt{v_{1,n}}\sqrt{\mathcal{R}}R_{0,1,n} \\ i\sqrt{v_{0,n}}\sqrt{\mathcal{R}}R_{0,0,n} + \sqrt{v_{1,n}}\sqrt{\mathcal{T}}R_{0,1,n} \\ \sqrt{v_{0,n}}\sqrt{\mathcal{T}}R_{1,0,n} + i\sqrt{v_{1,n}}\sqrt{\mathcal{R}}R_{1,1,n} \\ i\sqrt{v_{0,n}}\sqrt{\mathcal{R}}R_{1,0,n} + \sqrt{v_{0,n}}\sqrt{\mathcal{T}}R_{1,1,n} \end{pmatrix}, \tag{30}$$

where the reflectivity $\mathcal{R}$ and transmissivity $\mathcal{T} = 1 - \mathcal{R}$ are real numbers which are considered to be parameters to be determined from experiment.

— *Phase shifter* χ_0, χ_1: In the event-based model, a phase shifter is simulated without DLM. The device has only one input and one output port and transforms the nth input message $\mathbf{u}_n$ into an output message

$$\mathbf{w}_n = e^{i\chi_j}\mathbf{u}_n, \quad j = 0, 1. \tag{31}$$

— *Detector*: Detectors count all incoming particles. Hence, we assume that the neutron detectors have a detection efficiency of 100%. This is an idealization of real neutron detectors which can have a detection efficiency of 99% and more.[89]

5.4.2. *Simulation results*

In Fig. 8, we present a few simulation results for the neutron MZI and compare them to the quantum theoretical result ((a)–(c)) and to experiment (d). A quantum theoretical treatment of the neutron MZI depicted in Fig. 7 is given in Ref. 91. The quantum statistics of the neutron interferometry experiment is described in terms of the state vector

$$|\Psi\rangle = (\Psi_{0\uparrow}, \Psi_{0\downarrow}, \Psi_{1\uparrow}, \Psi_{1\downarrow}\Psi_{2\uparrow}, \Psi_{2\downarrow}, \Psi_{3\uparrow}, \Psi_{3\downarrow})^T, \tag{32}$$

where the components of this vector represent the complex-valued amplitudes of the wave function. The first subscript labels the pathway and the second subscript denotes the direction of the magnetic moment relative to some **B**-field. The latter is not relevant for the neutron MZI experiment since the outcome of this experiment does not depend on the magnetic moment of the neutron. As usual, the state vector is assumed to be normalized, meaning that $\langle\Psi|\Psi\rangle = 1$. In the abstract representation of the experiment (see Fig. 7(right)) we use the notation $\Psi_j = (\Psi_{j\uparrow}, \Psi_{j\downarrow})$ for $j = 0, \ldots, 3$.

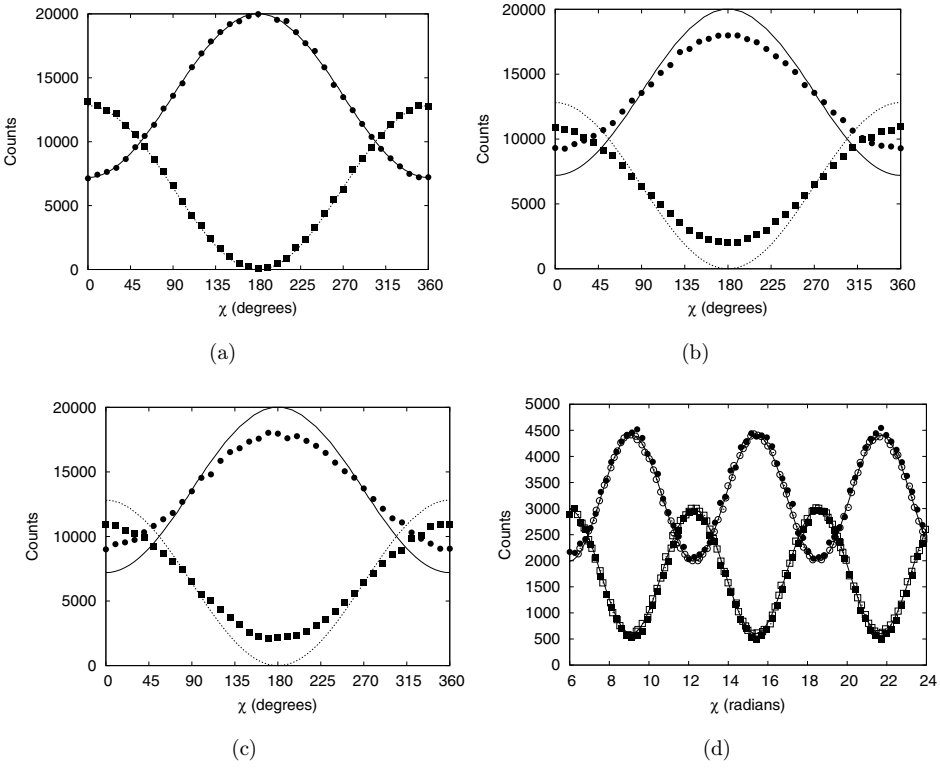

Fig. 8. (a)–(c) Event-by-event simulation results of the number of neutrons leaving the interferometer via the H-beam (circles) and O-beam (squares) as a function of the phase difference χ between the two paths inside the interferometer. For each value of χ, the number of particles generated in the simulation is $N = 100\,000$. The lines are the predictions of quantum theory. Solid line: p_H, see Eq. (34); dotted line: p_O, see Eq. (35). (a) Model parameters: $\mathcal{R} = 0.2, \gamma = 0.99, \delta_1 = \delta_2 = 0$. (b) Same as (a) except that $\gamma = 0.5$, reducing the accuracy and increasing the response time of the DLM. (c) Same as (a) except that to mimic the partial coherence of the incident neutron beam, the initial message carried by each particle has been modified by choosing δ_1 and δ_2 uniformly random from the interval $[-\pi/3, \pi/3]$, reducing the amplitude of the interference. (d) Comparison between the counts of neutrons per second and per square cm in the beams of a neutron interferometry experiment[89] (open symbols) and the number of neutrons per sample leaving the interferometer in an event-by-event simulation (solid symbols). Circles: counts in the H-beam; squares: counts in the O-beam. The experimental data has been extracted from Fig. 2 of Ref. 89. The simulation parameters $\mathcal{R} = 0.22$ and $\gamma = 0.5$ have been adjusted by hand to obtain a good fit and the number of incident particles in the simulation is $N = 22\,727$ per angle χ. Lines through the data points are guides to the eye.

As the state vector propagates through the interferometer, it changes according to

$$
\begin{aligned}
|\Psi'\rangle = &\begin{pmatrix} t^* & r \\ -r^* & t \end{pmatrix}_{5,7} \begin{pmatrix} t^* & r \\ -r^* & t \end{pmatrix}_{4,6} \begin{pmatrix} e^{i\phi_1} & 0 \\ 0 & e^{i\phi_1} \end{pmatrix}_{6,7} \begin{pmatrix} e^{i\phi_0} & 0 \\ 0 & e^{i\phi_0} \end{pmatrix}_{4,5} \\
&\times \begin{pmatrix} t^* & r \\ -r^* & t \end{pmatrix}_{3,7} \begin{pmatrix} t^* & r \\ -r^* & t \end{pmatrix}_{2,6} \begin{pmatrix} t & -r^* \\ r & t^* \end{pmatrix}_{1,5} \begin{pmatrix} t & -r^* \\ r & t^* \end{pmatrix}_{0,4} \\
&\times \begin{pmatrix} t & -r^* \\ r & t^* \end{pmatrix}_{1,3} \begin{pmatrix} t & -r^* \\ r & t^* \end{pmatrix}_{0,2} |\Psi\rangle, \qquad (33)
\end{aligned}
$$

where t and r denote the common transmission and reflection coefficients, respectively, and the subscripts i, j refer to the pair of elements of the eight-dimensional vector on which the matrix acts. Conservation of probability demands that $|t|^2 + |r|^2 = 1$.

In neutron interferometry experiments, particles enter the interferometer via the path corresponding to the amplitude Ψ_0 only (see Fig. 7(right)), meaning that $|\Psi\rangle = (1, 0, 0, 0, 0, 0, 0, 0)^T$. The probabilities to observe a particle leaving the interferometer in the H- and O-beams are then given by

$$p_H = |\Psi'_2|^2 = \mathcal{R}(\mathcal{T}^2 + \mathcal{R}^2 - 2\mathcal{R}\mathcal{T}\cos\chi), \tag{34}$$

$$p_O = |\Psi'_3|^2 = 2\mathcal{R}^2\mathcal{T}(1 + \cos\chi), \tag{35}$$

where $\chi = \chi_0 - \chi_1$ is the relative phase shift, $\mathcal{R} = |r|^2$ and $\mathcal{T} = |t|^2 = 1 - \mathcal{R}$. Note that p_H and p_O do not depend on the imaginary part of t or r, leaving only one free model parameter (for instance $\mathcal{R}$). In the case of a 50–50 BS ($\mathcal{T} = \mathcal{R} = 0.5$), Eqs. (34) and (35) reduce to the familiar expressions $p_H = (1/2)\sin^2\chi/2$ and $p_O = (1/2)\cos^2\chi/2$, respectively. The extra factor two is due to the fact that one half of all incoming neutrons, that is the neutrons that are transmitted by BS1 or BS2 (see Fig. 7), leave the interferometer without being counted.

The simulation results presented in Fig. 8(a) demonstrate that the event-by-event simulation reproduces the results of quantum theory if γ approaches one.[3,5,7,8] Indeed, there is excellent agreement with quantum theory. In this example, the reflectivity of the BSs is taken to be $\mathcal{R} = 0.2$. The parameter γ which controls the learning pace of the DLM-based processor can be used to account for imperfections of the neutron interferometer. This is illustrated in Fig. 8(b) which shows simulation results for $\gamma = 0.5$.

The quantum theoretical treatment assumes a fully coherent beam of neutrons. In the event-based approach, the case of a coherent beam may be simulated by assuming that the degree of freedom that accounts for the time of flight of the neutron takes the same initial value each time a message is created ($\delta_1 = \delta_2 = 0$). In the event-based approach, we can mimic a partially coherent beam by simply adding some noise to the message, that is when a message is created, δ_i for $i = 1, 2$ is chosen random in a specified range. In Fig. 8(c), we present simulation results for the case that δ_i is drawn randomly and uniformly from the interval $[-\pi/3, \pi/3]$, showing that reducing the coherence of the beam reduces the visibility, as expected on the basis of wave theory.[42] Comparing Figs. 8(b) and 8(c), we conclude that the same reduced visibility can be obtained by either reducing γ or by adding noise to the messages. On the basis of this interferometry experiment alone, it is difficult to exclusively attribute the cause of a reduced visibility to one of these mechanisms.

Conclusive evidence that the event-based model reproduces the results of a single-neutron interferometry experiment comes from comparing simulation data with experimental data. In Fig. 8(d), we present such a comparison using experimental

data extracted from Fig. 2 of Ref. 89. It was not necessary to try to make the best fit: the parameters $\mathcal{R}$ and γ and the offset of the phase χ were varied by hand. As shown in Fig. 8(d), the event-based simulation model reproduces, quantitatively, the experimental results reported in Fig. 2 of Ref. 89.

6. Entanglement

In quantum theory, entanglement is the property of a state of a two or many-body quantum system in which the states of the constituting bodies are correlated. The most prominent example is the singlet state of two spin-$\frac{1}{2}$ particles

$$|\Psi\rangle = \frac{1}{\sqrt{2}}(|\uparrow\downarrow\rangle - |\downarrow\uparrow\rangle), \tag{36}$$

which cannot be written as a product state. According to quantum theory, if the singlet state describes the correlation between the spins of the two particles and if we perform a measurement of both spins along the same direction, we observe that the particles have opposite but otherwise random values of their spins. Thus, in the quantum theoretical description, the state of the two spin-$\frac{1}{2}$ particles may be correlated even though the particles are spatially and temporally separated and do not necessarily interact. Note however that this is a statistical interpretation which does not support the assumption that this singlet state is a property of each pair of particles and does not support the idea that changing the state of one particle has a causal effect on the state of the other.

6.1. *EPRB thought experiment*

In 1935, Einstein, Podolsky and Rosen (EPR) designed a thought experiment demonstrating the "incompleteness" of quantum theory.[93] The thought experiment involves the measurement of the position and momentum of two particles which interacted in the past but not at the time of measurement. Since this experiment is not suited for designing a laboratory experiment, Bohm proposed in 1951 a more realistic experiment which measures the intrinsic angular momentum of a correlated pair of atoms one-by-one.[92] A schematic diagram of the experiment is shown in Fig. 9. A source emits charge-neutral pairs of particles with opposite magnetic moments $+\mathbf{S}$ and $-\mathbf{S}$. The two particles separate spatially and propagate in free space to an observation station in which they are detected. As the particle arrives at station $i = 1, 2$, it passes through a Stern–Gerlach magnet. The magnetic moment of a particle interacts with the inhomogeneous magnetic field of the Stern–Gerlach magnet. The Stern–Gerlach magnet deflects the particle, depending on the orientation of the magnet $\mathbf{a}_i$ and the magnetic moment of the particle. The Stern–Gerlach magnet divides the beam of particles in two, spatially well-separated parts. As the particle leaves the Stern–Gerlach magnet, it generates a signal in one of the two detectors $D_{\pm,i}$. The firing of a detector corresponds to a detection event.

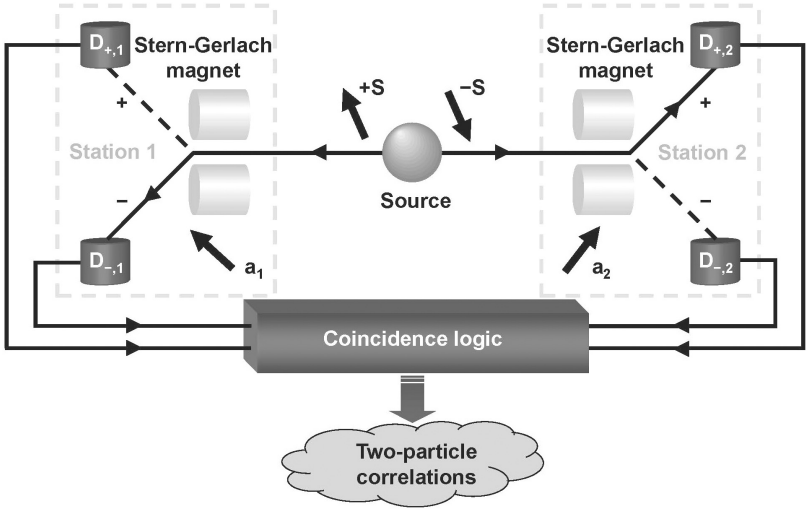

Fig. 9. Schematic diagram of the EPRB experiment with magnetic particles.[92] The source emits charge-neutral pairs of particles with opposite magnetic moments $+\mathbf{S}$ and $-\mathbf{S}$. One of the particles moves to station 1 and the other one to station 2. As the particle arrives at station $i = 1, 2$, it passes through a Stern–Gerlach magnet which deflects the particle, depending on the orientation of the magnet $\mathbf{a}_i$ and the magnetic moment of the particle. As the particle leaves the Stern–Gerlach magnet, it generates a signal in one of the two detectors $D_{\pm,i}$. Coincidence logic pairs the detection events of station 1 and station 2 so that they can be used to compute two-particle correlations.

According to quantum theory of the EPRB thought experiment, the results of repeated measurements of the system of two spin-$\frac{1}{2}$ particles in the spin state $|\Psi\rangle = \alpha_0|\uparrow\uparrow\rangle + \alpha_1|\downarrow\uparrow\rangle + \alpha_2|\uparrow\downarrow\rangle + \alpha_3|\downarrow\downarrow\rangle$ with $\sum_{j=0}^{3} |\alpha_j|^2 = 1$ are given by the single-spin expectation values

$$\begin{aligned} \hat{E}_1(\mathbf{a}_1) &= \langle\Psi|\sigma_1 \cdot \mathbf{a}_1|\Psi\rangle = \langle\Psi|\sigma_1|\Psi\rangle \cdot \mathbf{a}_1, \\ \hat{E}_2(\mathbf{a}_2) &= \langle\Psi|\sigma_2 \cdot \mathbf{a}_2|\Psi\rangle = \langle\Psi|\sigma_2|\Psi\rangle \cdot \mathbf{a}_2 \end{aligned} \tag{37}$$

and the two-particle correlations $\hat{E}(\mathbf{a}_1, \mathbf{a}_2) = \langle\Psi|\sigma_1 \cdot \mathbf{a}_1 \sigma_2 \cdot \mathbf{a}_2|\Psi\rangle = \mathbf{a}_1 \cdot \langle\Psi|\sigma_1 \cdot \sigma_2|\Psi\rangle \cdot \mathbf{a}_2$, where $\mathbf{a}_1$ and $\mathbf{a}_2$ are unit vectors specifying the directions of the analyzers, σ_i denote the Pauli vectors describing the spin of the particles $i = 1, 2$, and $\langle X\rangle = \mathrm{Tr}\rho X$ with ρ being the 4×4 density matrix describing the two spin-$\frac{1}{2}$ particle system. We have introduced the notation $\hat{E}$ to make a distinction between the quantum theoretical results and the results obtained by analysis of data sets from a laboratory experiment and from an event-based simulation (see Sec. 6.3). Quantum theory of the EPRB thought experiment assumes that $|\Psi\rangle$ does not depend on $\mathbf{a}_1$ or $\mathbf{a}_2$. Therefore, from Eq. (37) it follows immediately that $\hat{E}_1(\mathbf{a}_1)$ does not depend on $\mathbf{a}_2$ and that $\hat{E}_2(\mathbf{a}_2)$ does not depend on $\mathbf{a}_1$. Note that this holds for any state $|\Psi\rangle$. For later use, it is expedient to introduce the function

$$S \equiv S(\mathbf{a}_1, \mathbf{a}_2, \mathbf{a}_1', \mathbf{a}_2') = E(\mathbf{a}_1, \mathbf{a}_2) - E(\mathbf{a}_1, \mathbf{a}_2') + E(\mathbf{a}_1', \mathbf{a}_2) + E(\mathbf{a}_1', \mathbf{a}_2'), \tag{38}$$

for which it can be shown that $|S| \leq 2\sqrt{2}$, independent of the choice of ρ.[94]

The quantum theoretical description of the EPRB experiment assumes that the state of the two spin-$\frac{1}{2}$ particles is described by the singlet state Eq. (36). For the singlet state, $\hat{E}_1(\mathbf{a}_1) = \hat{E}_2(\mathbf{a}_2) = 0$, $\hat{E}(\mathbf{a}_1, \mathbf{a}_2) = -\mathbf{a}_1 \cdot \mathbf{a}_2$ and the maximum value of $|S|$ is $2\sqrt{2}$. Note that the singlet state is fully characterized by the three quantities $\hat{E}_1(\mathbf{a}_1)$, $\hat{E}_2(\mathbf{a}_2) = 0$ and $\hat{E}(\mathbf{a}_1, \mathbf{a}_2)$. Hence, in any laboratory experiment, thought experiment or computer simulation of such an experiment, which has the goal to measure effects of the system being represented by a singlet state, these three quantities have to be measured and computed.

6.2. *Bell and Boole inequalities*

Quantum theory yields statistical estimates for $\hat{E}_1$, $\hat{E}_2$ and $\hat{E}_{12}$ and cannot say anything about individual measurements.[1] Nevertheless, for the singlet state quantum theory predicts that, if measurement of the component $\sigma_1 \cdot \mathbf{a}_1$ with $\mathbf{a}_1$ being a unit vector, yields the value $+1$, then measurement of $\sigma_2 \cdot \mathbf{a}_1$ must yield the value -1 and vice versa. The fundamental question is how to relate the statistical results of quantum theory and the individual measurements.

6.2.1. *Bell's model and inequality*

Bell made the following assumptions in constructing his model and deriving his inequality[95]:

(1) $A(\mathbf{a_1}, \lambda) = \pm 1$ and $B(\mathbf{a_2}, \lambda) = \pm 1$, where A (B) denotes the result of measuring $\sigma_1 \cdot \mathbf{a_1}$ ($\sigma_2 \cdot \mathbf{a}_2$) and λ denotes a variable or a set of variables which only depend on the preparation (source) and not on the measurement (magnet settings) of the spin components. Note that this assumption already includes the hypothesis that the orientation of one magnet does not influence the measurement result obtained with the other magnet (often referred to as the locality condition). In other words, A (B) does not depend on $\mathbf{a}_2$ ($\mathbf{a}_1$).

(2) If $\rho(\lambda)$ is the probability distribution of λ ($\int \rho(\lambda) d\lambda = 1$) then the expectation value of the product of the two components $\sigma_1 \cdot \mathbf{a}_1$ and $\sigma_2 \cdot \mathbf{a}_2$ can be written as $P(\mathbf{a}_1, \mathbf{a}_2) = \int d\lambda \rho(\lambda) A(\mathbf{a}_1, \lambda) B(\mathbf{a}_2, \lambda)$. Note that one could also introduce variables λ' and λ'' depending on the characteristics of the instruments on both sides. Averaging over these instrument dependent variables would result in new variables having values between -1 and $+1$. However, this is only the case if λ' and λ'' are completely independent. For example, if λ' and λ'' are sets of variables including the detection times, used for coincidence measurements in a laboratory experiment, then assumption 2 does not hold.[96]

(3) $A(\mathbf{a}_1, \lambda) = -B(\mathbf{a}_1, \lambda)$ so that $P(\mathbf{a}_1, \mathbf{a}_2) = -\int d\lambda \rho(\lambda) A(\mathbf{a}_1, \lambda) A(\mathbf{a}_2, \lambda)$. This assumption follows from the observation that $P(\mathbf{a}_1, \mathbf{a}_2) = \int d\lambda \rho(\lambda) A(\mathbf{a}_1, \lambda) B(\mathbf{a}_2, \lambda)$ reaches -1 at $\mathbf{a}_1 = \mathbf{a}_2$ only if $A(\mathbf{a}_1, \lambda) = -B(\mathbf{a}_1, \lambda)$. Note that $P(\mathbf{a}_1, \mathbf{a}_1) = -1$ if and only if $A(\mathbf{a}_1, \lambda) = -B(\mathbf{a}_1, \lambda)$, making both these assumptions equivalent. Hence, what Bell assumed is that the results of the measurements at both sides of

the source can be represented by one and the same symbol "A" that depends only on the respective magnet setting and on λ. Moreover, also the measurement outcomes of an experiment with another setting of (only one of) the magnets, can be represented by the same symbol "A".

Using the above hypotheses and considering a third unit vector $\mathbf{a}_3$, Bell derived the inequality[95]

$$|P(\mathbf{a}_1, \mathbf{a}_2) - P(\mathbf{a}_1, \mathbf{a}_3)| \leq 1 + P(\mathbf{a}_2, \mathbf{a}_3), \tag{39}$$

which is violated for certain magnet settings $\mathbf{a}_1, \mathbf{a}_2, \mathbf{a}_3$ if $P(\mathbf{a}_1, \mathbf{a}_2)$ is replaced by $\hat{E}(\mathbf{a}_1, \mathbf{a}_2) = -\mathbf{a}_1 \cdot \mathbf{a}_2$, the quantum theoretical two-particle expectation value describing the averaged two-particle correlations obtained in EPRB experiments. Note that 1, 2 and 3 are sufficient conditions for the Bell inequality to be obeyed. Hence, if the Bell inequality is obeyed then one cannot say anything about the validity of the assumptions, but if it is violated then one can say that at least one of the assumptions must be false, thereby refuting Bell's model. It is worth mentioning that Bell analyzed a very restricted class of classical models, namely models which do not account for (i) the physics of the detection process and/or (ii) the use of time-coincidences to define particle pairs (see below). Although the above conclusion is the only logical conclusion that can be drawn, it is common but erroneous practice to take a violation of a Bell inequality as a "proof" of the quantum nature of the system under study. Far reaching conclusions drawn from Bell's results, such as violations of Bell-like inequalities having implications for action-on-a-distance, locality, realism, etc. have all been shown to be logical fallacies.[29,97–112]

6.2.2. *Boole inequality for the correlations of two-valued variables*

We consider two-valued variables $S(x, n) = \pm 1$ where x can be considered to represent the orientations $\mathbf{a}_1, \mathbf{a}_2, \mathbf{a}_3$ of the magnets in an EPRB experiment and $n = 1, \ldots N$ simply numbers the measurements in an experimental run. From the variables $S(x, n)$ with $x = \mathbf{a}_1, \mathbf{a}_2, \mathbf{a}_3$ we compute the averages $F_{\mathbf{a}_1,\mathbf{a}_2} = \sum_{n=1}^{N} S(\mathbf{a}_1, n) S(\mathbf{a}_2, n)/N$, $F_{\mathbf{a}_1,\mathbf{a}_3} = \sum_{n=1}^{N} S(\mathbf{a}_1, n) S(\mathbf{a}_3, n)/N$ and $F_{\mathbf{a}_2,\mathbf{a}_3} = \sum_{n=1}^{N} S(\mathbf{a}_2, n) S(\mathbf{a}_3, n)/N$. According to Boole[113] it is impossible to violate

$$|F_{\mathbf{a}_1,\mathbf{a}_2} \pm F_{\mathbf{a}_1,\mathbf{a}_3}| \leq 1 \pm F_{\mathbf{a}_2,\mathbf{a}_3}, \tag{40}$$

if there is a one-to-one correspondence between the two-valued variables $S(\mathbf{a}_1, n)$, $S(\mathbf{a}_2, n)$, $S(\mathbf{a}_3, n)$ of the mathematical description and each triple $\{X(\mathbf{a}_1, n), X(\mathbf{a}_2, n), X(\mathbf{a}_3, n)\}$ of binary data collected in the experimental run denoted by n. This one-to-one correspondence is a necessary and sufficient condition for the inequality to be obeyed. Note that inequalities Eqs. (39) and (40) have the same structure. We emphasize that it is essential that the correlations $F_{\mathbf{a}_1,\mathbf{a}_2}$, $F_{\mathbf{a}_1,\mathbf{a}_3}$ and $F_{\mathbf{a}_2,\mathbf{a}_3}$ have been calculated from one data set that contains triples instead of from three sets in which the data has been collected in pairs.[111]

6.2.3. *An inequality within quantum theory*

From the algebraic identity $(1 \pm xy)^2 = (x \pm y)^2 + (1 - x^2)(1 - y^2)$ it follows that $|x \pm y| \leq 1 \pm xy$ for real numbers x and y with $|x| \leq 1$ and $|y| \leq 1$. From this inequality, it immediately follows that

$$|xz \pm yz| \leq 1 \pm xy, \tag{41}$$

for real numbers x, y, z such that $|x| \leq 1$, $|y| \leq 1$ and $|z| \leq 1$.

If we now assume that the two spin-$\frac{1}{2}$ particle system is in a product state $|\Psi\rangle = |\Psi\rangle_1|\Psi\rangle_2$ with $|\Psi\rangle_j = \alpha_{0,j}|\uparrow\rangle_j + \alpha_{1,j}|\uparrow\rangle_j$ with $|\alpha_{0,j}|^2 + |\alpha_{1,j}|^2 = 1$ for $j = 1, 2$, then

$$\begin{aligned} \hat{E}_1(\mathbf{a}_1) &= \langle\Psi|\sigma_1|\Psi\rangle_1 \cdot \mathbf{a}_1, \\ \hat{E}_2(\mathbf{a}_2) &= \langle\Psi|\sigma_2|\Psi\rangle_2 \cdot \mathbf{a}_2, \\ \hat{E}(\mathbf{a}_1, \mathbf{a}_2) &= \langle\Psi|\sigma_1|\Psi\rangle_1 \cdot \mathbf{a}_1 \langle\Psi|\sigma_2|\Psi\rangle_2 \cdot \mathbf{a}_2 = \hat{E}_1(\mathbf{a}_1)\hat{E}_2(\mathbf{a}_2) \end{aligned} \tag{42}$$

and the correlation $\hat{E}(\mathbf{a}_1, \mathbf{a}_2) - \hat{E}_1(\mathbf{a}_1)\hat{E}_2(\mathbf{a}_2) = 0$. Using Eq. (41) and unit vectors $\mathbf{a}_1$, $\mathbf{a}_2$, $\mathbf{a}_3$, we obtain a Bell-type inequality

$$|\hat{E}(\mathbf{a}_1, \mathbf{a}_2) - \hat{E}(\mathbf{a}_1, \mathbf{a}_3)| \leq 1 + \hat{E}(\mathbf{a}_2, \mathbf{a}_3) \tag{43}$$

and similarly the Bell-CHSH inequality[114]

$$|S| = |\hat{E}(\mathbf{a}_1, \mathbf{a}_2) - \hat{E}(\mathbf{a}_1, \mathbf{a}_2') + \hat{E}(\mathbf{a}_1', \mathbf{a}_2) + \hat{E}(\mathbf{a}_1', \mathbf{a}_2')| \leq 2, \tag{44}$$

for unit vectors $\mathbf{a}_1$, $\mathbf{a}_1'$, $\mathbf{a}_2$ and $\mathbf{a}_2'$.

Hence, if the state of the two spin-$\frac{1}{2}$ particle system is a product state, then the Bell and Bell-CHSH inequality hold. On the other hand, if the Bell or Bell-CHSH inequality is violated then the two-particle quantum system is not in a product state. Note that these logical statements are made entirely within the framework of quantum theory.

6.2.4. *Bell inequality tests*

In a typical ideal EPRB experiment three runs are performed in which N detection events are collected on both sides (referred to by 1 and 2) of the source. The outcomes of the detection events take the values $+1$ or -1 and are represented by the symbol X. This results in the three data sets

$$\begin{aligned} \Gamma_{\mathbf{a},\mathbf{b}} &= \{X(\mathbf{a}, n, 1), X(\mathbf{b}, n, 2) \,|\, n = 1, \ldots, N\}, \\ \tilde{\Gamma}_{\mathbf{a},\mathbf{c}} &= \{\tilde{X}(\mathbf{a}, \tilde{n}, 1), \tilde{X}(\mathbf{c}, \tilde{n}, 2) \,|\, \tilde{n} = 1, \ldots, N\}, \\ \hat{\Gamma}_{\mathbf{b},\mathbf{c}} &= \{\hat{X}(\mathbf{b}, \hat{n}, 1), \hat{X}(\mathbf{c}, \hat{n}, 2) \,|\, \hat{n} = 1, \ldots, N\}. \end{aligned} \tag{45}$$

Note that in real experiments the measurement outcomes are also labeled by the time of measurement but for simplicity we omit this label here. Using these data sets

for testing the validity of Bell's inequality Eq. (39) and of the structurally equivalent Boole inequality Eq. (40), requires making the following assumptions:

(1) The same symbol X can be used for all the data collected in the three runs. This results in the data set $\Upsilon = \{X(\mathbf{a}, n, 1), X(\mathbf{a}, \tilde{n}, 1), X(\mathbf{b}, n, 2), X(\mathbf{b}, \tilde{n}, 1), X(\mathbf{c}, \tilde{n}, 2),\ X(\mathbf{c}, \hat{n}, 2) \,|\, n, \tilde{n}, \hat{n} = 1, \ldots, N\}$.
(2) The data can be rearranged such that $X(\mathbf{a}, n, 1) = X(\mathbf{a}, \tilde{n}, 1),\ X(\mathbf{b}, \hat{n}, 1) = X(\mathbf{b}, n, 1)$ and $X(\mathbf{c}, \tilde{n}, 2) = X(\mathbf{c}, \hat{n}, 2) = X(\mathbf{c}, n, 2)$. This results in the data set $\Upsilon' = \{X(\mathbf{a}, n, 1), X(\mathbf{b}, n, 2), X(\mathbf{b}, n, 1), X(\mathbf{c}, n, 2) \,|\, n = 1, \ldots, N\}$, a data set containing quadruples, not yet triples, as used in the derivation of Bell's inequality and as required by Boole for his inequality to be obeyed. Reduction to a set of triples requires the extra assumption:
(3) $X(\mathbf{b}, n, 1) = X(\mathbf{b}, n, 2)$

Since the data in EPRB laboratory experiments are not collected as one set of triples but as three sets of pairs, in case a violation of Boole's inequality Eq. (40) is found, at least one of the assumptions 1, 2 or 3 is false. In other words, if the data sets collected in an EPRB experiment satisfy these three conditions, the one-to-one correspondence between the two-valued variables in the mathematical description and the observed two-valued experimental data is guaranteed, and hence Boole's and thus also Bell's inequality are satisfied. If the Bell inequality is violated then at least one of the sufficient conditions 1, 2 or 3 to derive the Bell inequality is false, but then also at least one of the assumptions listed above is false.

6.2.5. *Summary*

One could ask the question how to translate the inequality Eq. (43) together with its accompanying assumptions, derived within the context of quantum theory, into an experimental test. The answer is one simply cannot. It is not legitimate to replace the quantum theoretical expectations that appear in Eq. (43) by certain empirical data, simply because Eq. (43) has been derived within the mathematical framework of quantum theory, not for sets of data collected, grouped and characterized by experimenters. Since the collected data have values $+1$ or -1 they can be tested against the Boole inequalities only and the conclusions that follow from their violation (see Sec. 6.2.4) have no bearing on the quantum theoretical model, without making additional assumptions which are not self-evident.

In conclusion, an inequality cannot be blindly applied to any set of experimental data, a model or theory. The inequality should be derived in the proper context and conditions and conclusions belonging to the respective derivations cannot simply be mixed.

6.3. *EPRB experiment with single photons*

In this experiment, the polarization of each photon plays the role of the spin-$\frac{1}{2}$ degree-of-freedom in Bohm's version[92] of the EPR thought experiment.[93] Using the fact that

the two-dimensional vector space with basis vectors $\{|H\rangle, |V\rangle\}$, where H and V denote the horizontal and vertical polarization of the photon, respectively, is isomorphic to the vector space with basis vectors $\{|\uparrow\rangle, |\downarrow\rangle\}$ of spin-$\frac{1}{2}$ particles, we may use the quantum theory of the latter to describe the EPRB experiments with photons. The expressions for the single-photon expectation values and the two-photon correlations are similar to those of the genuine spin-$\frac{1}{2}$ particle problem except for the restriction of $\mathbf{a}_1$ and $\mathbf{a}_2$ to lie in planes orthogonal to the direction of propagation of the photons and that the polarization is defined modulo π, not modulo 2π as in the case of the spin-$\frac{1}{2}$ particles. The latter results in a multiplication of the angles by a factor of two. For simplicity, it is often assumed that $\mathbf{a}_i = (\cos a_i, \sin a_i, 0)$ for $i = 1, 2$. For the singlet state we then have $\hat{E}_1(\mathbf{a}_1) = \hat{E}_2(\mathbf{a}_2) = 0$ and $\hat{E}(\mathbf{a}_1, \mathbf{a}_2) = -\cos 2(a_1 - a_2)$.

We take the EPRB experiment with single photons, carried out by Weihs *et al.*[25,115] as a concrete example. We first describe the data collection and analysis procedure of the experiment and present results demonstrating that the conclusion that the experimental results can be described by quantum theory is premature. Next we illustrate how to construct an event-based model of an idealized version of this EPRB experiment which reproduces the predictions of quantum theory for the single and two-particle averages for a quantum system of two spin-$\frac{1}{2}$ particles in the singlet state and a product state,[3,31] without making reference to concepts of quantum theory.

— *Data collection*: Figure 10 shows a schematic diagram of the EPRB experiment with single photons carried out by Weihs *et al.*[25,115] The source emits pairs of photons. The photon pair splits and each photon travels in free space to an observation station, labeled by $i = 1$ or $i = 2$, in which it is manipulated and detected. The two stations are assumed to be identical and are separated spatially and temporally. Hence, the observation at station 1 (2) cannot have a causal effect on the data registered at station 2 (1).[25] As the photon arrives at station $i = 1, 2$ it first passes through an EOM which rotates the polarization of the photon by an angle θ_i depending on the voltage applied to the EOM.[25,115] This voltage is controlled by a binary variable A_i, which is chosen at random.[25,115] Optionally, a bias voltage is added to the randomly varying voltage.[25,115] The relation between the voltage applied to the EOM and the resulting rotation of the polarization is determined experimentally, hence there is some uncertainty in relating the applied voltage to the rotation angle.[25,115] As the photon leaves the EOM, a PBS directs it to one of the two detectors. The detector produces a signal $x_{n,i} = \pm 1$ where the subscript n labels the nth detection event. Each station has its own clock which assigns a time-tag $t_{n,i}$ to each signal generated by one of the two detectors.[25,115] Effectively, this procedure discretizes time in intervals, the width of which is determined by the time-tag resolution τ. In the experiment, the time-tag generators are synchronized before each run.[25,115]

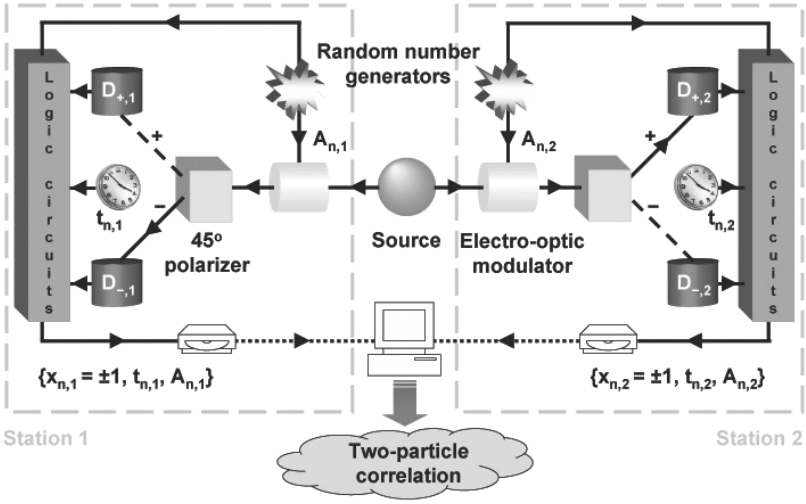

Fig. 10. Schematic diagram of the EPRB experiment with single photons.[25,115] The source emits pairs of photons. The photon pair splits and one of the photons moves to station 1 and the other one to station 2. As the photon arrives at station $i = 1, 2$ it first passes through an EOM which rotates the polarization of the photon by an angle θ_i depending on the voltage applied to the EOM. This voltage is controlled by a binary variable A_i, which is chosen at random. As the photon leaves the EOM, a PBS directs it to one of the two detectors $D_{\pm,i}$. The detector produces a signal $x_{n,i} = \pm 1$ where the subscript n labels the nth detection event. Each station has its own clock which assigns a time-tag $t_{n,i}$ to each detection signal. A data set $\{x_{n,i}, t_{n,i}, A_{n,i} \,|\, n = 1, \ldots, N_i\}$ is stored on a hard disk for each station. Long after the experiment is finished both data sets can be analyzed and among other things, two-particle correlations can be computed.

The firing of a detector is regarded as an event. At the nth event at station i, the dichotomic variable $A_{n,i}$, controlling the rotation angle $\theta_{n,i}$, the dichotomic variable $x_{n,i}$ designating which detector fires, and the time-tag $t_{n,i}$ of the detection event are written to a file on a hard disk, allowing the data to be analyzed long after the experiment has terminated.[25,115] The set of data collected at station i may be written as

$$\Upsilon_i = \{x_{n,i}, t_{n,i}, \theta_{n,i} \,|\, n = 1, \ldots, N_i\}, \tag{46}$$

where we allow for the possibility that the number of detected events N_i at stations $i = 1, 2$ need not (and in practice is not) to be the same and we have used the rotation angle $\theta_{n,i}$ instead of the corresponding experimentally relevant dichotomic variable $A_{n,i}$ to facilitate the comparison with the quantum theoretical description.

— *Data analysis procedure*: A laboratory EPRB experiment requires some criterion to decide which detection events are to be considered as stemming from a single or two-particle system. In EPRB experiments with photons, this decision is taken on the basis of coincidence in time.[25,116] Here, we adopt the procedure employed by Weihs *et al.*[25,115] Coincidences are identified by comparing the

time differences $t_{n,1} - t_{m,2}$ with a window W,[25,115,116] where $n = 1, \ldots, N_1$ and $m = 1, \ldots, N_2$. By definition, for each pair of rotation angles a_1 and a_2, the number of coincidences between detectors $D_{x,1}$ ($x = \pm 1$) at station 1 and detectors $D_{y,2}$ ($y = \pm 1$) at station 2 is given by

$$\begin{aligned} C_{xy} &= C_{xy}(a_1, a_2) \\ &= \sum_{n=1}^{N_1} \sum_{m=1}^{N_2} \delta_{x,x_{n,1}} \delta_{y,x_{m,2}} \delta_{a_1,\theta_{n,1}} \delta_{a_2,\theta_{m,2}} \Theta(W - |t_{n,1} - t_{m,2}|), \end{aligned} \tag{47}$$

where $\Theta(t)$ denotes the unit step function. In Eq. (47), the sum over all events has to be carried out such that each event (= one detected photon) contributes only once. Clearly, this constraint introduces some ambiguity in the counting procedure as there is *a priori*, no clear-cut criterion to decide which events at stations $i = 1$ and $i = 2$ should be paired. One obvious criterion might be to choose the pairs such that C_{xy} is maximum, but such a criterion renders the data analysis procedure (not the data production) acausal. It is trivial though to analyze the data generated by the experiment of Weihs *et al.* such that conclusions do not suffer from this artifact.[80] In general, the values for the coincidences $C_{xy}(a_1, a_2)$ depend on the time-tag resolution τ and the window W used to identify the coincidences.

The single-particle averages and correlation between the coincidence counts are defined by

$$\begin{aligned} E_1(a_1, a_2) &= \frac{\sum_{x,y=\pm 1} x C_{xy}}{\sum_{x,y=\pm 1} C_{xy}} = \frac{C_{++} - C_{--} + C_{+-} - C_{-+}}{C_{++} + C_{--} + C_{+-} + C_{-+}}, \\ E_2(a_1, a_2) &= \frac{\sum_{x,y=\pm 1} y C_{xy}}{\sum_{x,y=\pm 1} C_{xy}} = \frac{C_{++} - C_{--} - C_{+-} + C_{-+}}{C_{++} + C_{--} + C_{+-} + C_{-+}}, \\ E(a_1, a_2) &= \frac{\sum_{x,y=\pm 1} xy C_{xy}}{\sum_{x,y=\pm 1} C_{xy}} = \frac{C_{++} + C_{--} - C_{+-} - C_{-+}}{C_{++} + C_{--} + C_{+-} + C_{-+}}, \end{aligned} \tag{48}$$

where the denominator $N_c = N_c(a_1, a_2) = C_{++} + C_{--} + C_{+-} + C_{-+}$ in Eq. (48) is the sum of all coincidences.

In practice, coincidences are determined by a four-step procedure[115]:

(1) Compute a histogram of time-tag differences $t_{n,1} - t_{m,2}$ of pairs of detection events.
(2) Determine the time difference Δ_G for which this histogram shows a maximum.
(3) Add Δ_G to the time-tag data $t_{n,1}$, thereby moving the position of the maximum of the histogram to zero.
(4) Determine the coincidences using the new time-tag differences, each photon contributing to the coincidence count at most once.

The global offset, denoted by Δ_G, may be attributed to the loss of synchronization of the clocks used in the stations 1 and 2.[115]
Local-realistic treatments of the EPRB experiment assume that the correlation, as measured in the experiment, is given by[117]

$$C_{xy}^{(\infty)}(a_1, a_2) = \sum_{n=1}^{N} \delta_{x,x_{n,1}} \delta_{y,x_{n,2}} \delta_{a_1,\theta_{n,1}} \delta_{a_2,\theta_{m,2}}, \tag{49}$$

which is obtained from Eq. (47) (in which each photon contributes only once) by assuming that $N = N_1 = N_2$, pairs are defined by $n = m$ and by taking the limit $W \to \infty$. However, the working hypothesis that the value of W should not matter because the time window only serves to identify pairs may not apply to real experiments. The analysis of the data of the experiment of Weihs *et al.* shows that the average time between pairs of photons is of the order of 30 μs or more, much larger than the typical values (of the order of a few nanoseconds) of the time-window W used in the experiments.[115] In other words, in practice, the identification of photon pairs does not require the use of W's of the order of a few nanoseconds.

— *Data analysis results*: Here, we present only a very limited set of results of our analysis of the experimental data of Weihs *et al.* This data has already been analyzed in Refs. 29, 31, 80, 118–124.
In order to test whether the experimental results are compatible with the predictions of quantum theory for a system of two spin-$\frac{1}{2}$ particles we first check whether $E_1(a_1, a_2)$ is independent of a_2 and $E_2(a_1, a_2)$ is independent of a_1 because quantum theory predicts that this is the case independent of the state of the two-particle system (see Eq. (37)). Since we are dealing with real data we need a criterion to decide whether the data complies with this quantum theoretical prediction. We consider the data $E_1(a_1, a_2)$ ($E_2(a_1, a_2)$) to be in conflict with the quantum theoretical prediction if the data show a dependency on a_1 (a_2) that exceeds five times the upper bound $1/\sqrt{N_C(a_1, a_2)}$ to the standard deviation σ_{N_c}. We analyze a selection of single-particle expectations as a function of W for the dataset newlongtime2 (see Fig. 11(a)). For small W, the total number of coincidences is too small to yield statistically meaningful results. For $W > 20$ ns, it is clear that the curves for $E_1(a_1 = 0, a_2 = \pi/8)$ and $E_1(a_1, a_2' = 3\pi/8)$ (open symbols), and for $E_2(a_1 = 0, a_2 = \pi/8)$ and $E_2(a_1' = \pi/4 = 0, a_2 = \pi/8)$ (closed symbols) are not independent of the settings a_2 and a_1, respectively. The change of these single-spin averages observed in station 1 (station 2) when the settings are changed in station 2 (station 1), systematically exceeds five standard deviations, clearly violating our criterion for the data to be compatible with the prediction of quantum theory of the EPRB model. According to standard practice of hypothesis testing, the likelihood that this data set can be described by the quantum theory of the EPRB experiment should be considered as extremely small. An analysis of in total 23 data sets produced by the experiment of Weihs *et al.* shows that none of

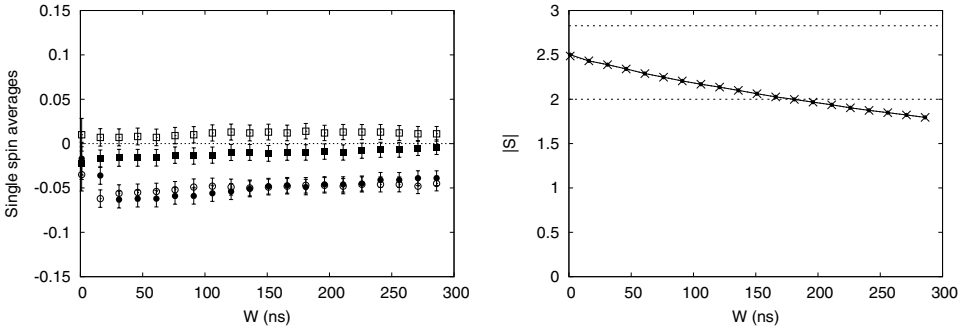

(a) (b)

Fig. 11. Analysis of the data set newlongtime2. (a) Selected single-particle averages as a function of W for $\Delta_G = 0$ and $a_1 = 0$, $a'_1 = \pi/4$, $a_2 = \pi/8$ and $a'_2 = 3\pi/8$. Open squares: $E_1(a_1, a_2)$; open circles: $E_1(a_1, a'_2)$; solid squares: $E_2(a_1, a_2)$; solid circles: $E_2(a'_1, a_2)$. The error bars correspond to 2.5 standard deviations. (b) $|S| = |E(a_1, a_2) - E(a_1, a'_2) + E(a'_1, a_2) + E(a'_1, a'_2)|$ as a function of the time window W. The dashed lines represent the maximum value for a quantum system of two $\mathrm{S} = 1/2$ particles in a separable (product) state ($|S| = 2$) and in a singlet state ($|S| = \sqrt{2}/2$), respectively. Crosses: $\Delta_G = 0$; solid circles connected by the solid line: $\Delta_G = 0.5\,\mathrm{ns}$.

these data sets satisfies our hypothesis test for being compatible with the predictions of quantum theory of the EPRB model. Based on the observation of dependency of $E_1(a_1, a_2)$ on a_2 and $E_2(a_1, a_2)$ on a_1 one could conclude that the data exhibits a spurious kind of "nonlocality" which cannot be described by the quantum theory of the EPRB experiment. In trying to find an explanation for this "nonlocality" we demonstrated elsewhere[80,125] that including a model for the detection efficiencies of the detectors cannot resolve the conflict between the experimental data of Weihs *et al.* and the quantum theoretical description of the EPRB experiment.

Although the results for the single particle expectations demonstrate that the experimental data cannot be described by a quantum theoretical model of two spin-$\frac{1}{2}$ particles (independent of the state which the two photons are in), in what follows we nevertheless investigate the function S (see Eq. (38)) as a function of the time window W. Our motivation to do this is two-fold. First, the goal of the experiment of Weihs *et al.* was to demonstrate a violation of the Bell-CHSH inequality. We show that the amount of violation depends on W, a parameter absent in the data collection procedure but chosen in the data analysis procedure. Second, in Sec. 6.3.1, we demonstrate that the Bell-CHSH inequality can also be violated in an event-based model, a classical dynamical system outside the realm of classical Hamiltonian dynamics, of the type of EPRB experiment performed by Weihs *et al.*

Figure 11(b) shows results of the function S as a function of W for the dataset newlongtime2. For $W < 150\,\mathrm{ns}$, the Bell-CHSH inequality $|S| \leq 2$ is clearly violated. For $W > 200\,\mathrm{ns}$, much less than the average time ($> 30\,\mu\mathrm{s}$) between two

coincidences, the inequality $|S| \leq 2$ is satisfied, demonstrating that the "nature" of the emitted pairs is not an intrinsic property of the pairs themselves but also depends on the choice of W made by the experimenter. For $W > 20$ ns, there is no significant statistical evidence that the "noise" on the data depends on W but if the only goal is to maximize $|S|$, it is expedient to consider $W < 20$ ns.

In other words, depending on the value of W, chosen by the experimenter when analyzing the data, the inequality $|S| \leq 2$ may or may not be violated. Hence, also the conclusion about the state of the system depends on the value of W. Analysis of the data of the experiment by Weihs *et al.* shows that W can be as large as 150 ns for the Bell-CHSH inequality to be violated and in the time-stamping EPRB experiment of Agüero *et al.*[122] $|S| \leq 2$ is clearly violated for $W < 9\,\mu$s. Hence, the use of a time-coincidence window does not create a "loophole". Nevertheless, very often it is mentioned that these single-photon Bell test experiments suffer from the fair sampling loophole, being the result of the usage of a time window W to filter out coincident photons or being the result of the usage of inefficient detectors.[120] The detection loophole was first closed in an experiment with two entangled trapped ions[126] and later in a single-neutron interferometry experiment[127] and in an experiment with two entangled qubits.[128] However, the latter three experiments are not Bell test experiments performed according to the CHSH protocol[114] because the two degrees of freedom are not manipulated and measured independently.

The narrow time window W in the experiment by Weihs *et al.* mainly acts as a filter that selects pairs of which the individual photons differ in their time tags by the order of nanoseconds. The possibility that such a filtering mechanism can lead to correlations that are often thought to be a characteristic of quantum systems only was, to our knowledge, first pointed out by Pearle[129] and later by Fine,[99] opening the route to a description in terms of locally causal, classical models. A concrete model of this kind was proposed by Pascazio who showed that his model approximately reproduces the correlation of the singlet state[130] with an accuracy that seems beyond what is experimentally achievable to date. Larson and Gill showed that Bell-like inequalities need to be modified in the case that the coincidences are determined by a time-window filter.[96] We found models that exactly reproduce the results of quantum theory for the singlet and uncorrelated state.[3,26,28,31] Here, we closely follow Refs. 4, 28 and 31.

6.3.1. *Event-based simulation*

A minimal, discrete-event simulation model of the EPRB experiment by Weihs *et al.* (see Fig. 10) requires a specification of the information carried by the particles, of the algorithm that simulates the source and the observation stations, and of the procedure to analyze the data. Since in the description of the experiment the orientation of the polarization vectors and the orientations of the optical axis of the polarizers $\mathbf{a}_i = (\cos a_i, \sin a_i, 0)$ for $i = 1, 2$ is limited to the xy-plane we omit the z-component in the simulation.

— *Source and particles*: Each time, the source emits two particles which carry a vector $\mathbf{u}_{n,i} = (\cos(\xi_n + (i-1)\pi/2), \sin(\xi_n + (i-1)\pi/2))$, representing the polarization of the photons. This polarization is completely characterized by the angle ξ_n and the direction $i = 1, 2$ to which the particle moves. A uniform pseudo-random number generator is used to pick the angle $0 \leq \xi_n < 2\pi$. Clearly, the source emits two particles with a mutually orthogonal, hence correlated but otherwise random polarization. Note that for the simulation of this experiment it is not necessary that the particles carry information about the phase $2\pi f t_{i,n}$, although it would be possible. In this case the time of flight $t_{i,n}$ is determined by the time-tag model (see below).

— EOM: The EOM in station $i = 1, 2$ rotates the polarization of the incoming particle by an angle θ_i, that is its polarization angle becomes $\xi'_{n,i} \equiv \mathrm{EOM}_i(\xi_n + (i-1)\pi/2, \theta_i) = \xi_n + (i-1)\pi/2 - \theta_i$ symbolically. Mimicking the experiment of Weihs *et al.* in which θ_1 can take the values a_1, a'_1 and θ_2 can take the values a_2, a'_2, we generate two binary uniform pseudo-random numbers $A_i = 0, 1$ and use them to choose the value of the angles θ_i, that is $\theta_1 = a_1(1 - A_1) + a'_1 A_1$ and $\theta_2 = a_2(1 - A_2) + a'_2 A_2$.

— PBS: The simulation model for a PBS is defined by the rule

$$x_{n,i} = \begin{cases} +1 & \text{if } r_n \leq \cos^2 \xi'_{n,i}, \\ -1 & \text{if } r_n > \cos^2 \xi'_{n,i}, \end{cases} \tag{50}$$

where $0 < r_n < 1$ are uniform pseudo-random numbers. It is easy to see that for fixed $\xi'_{n,i} = \xi'_i$, this rule generates events such that

$$\lim_{N \to \infty} \frac{1}{N} \sum_{n=1}^{N} x_{n,i} = \cos^2 \theta_{n,i}, \tag{51}$$

with probability one, showing that the distribution of events complies with Malus law. Note that this model for the PBS does not make use of a DLM and is therefore much more simple than the event-based model of the PBS described in Sec. 5.3.1. This simplified mathematical model suffices to simulate the EPRB experiment but cannot be used to simulate other optics experiments (for instance Wheeler's delayed choice experiment). However, the PBS described in Sec. 5.3.1 can be used to simulate the EPRB experiment.[3]

— *Time-tag model*: As is well-known, as light passes through an EOM (which is essentially a tunable wave plate), it experiences a retardation depending on its initial polarization and the rotation by the EOM. However, to our knowledge, time delays caused by retardation properties of waveplates, being components of various optical apparatuses, have not yet been explicitly measured for single photons. Therefore, in the case of single-particle experiments, we hypothesize that for each particle this delay is represented by the time tag[28,31]

$$t_{n,i} = \lambda(\xi'_{n,i}) r'_n, \tag{52}$$

that is, the time tag is distributed uniformly ($0 < r'_n < 1$ is a uniform pseudo-random number) over the interval $[0, \lambda(\xi'_{n,i})]$. For $\lambda(\xi'_{n,i}) = T_0 \sin^4 2\xi'_{n,i}$ this time-tag model, in combination with the model of the PBS, rigorously reproduces the results of quantum theory of the EPRB experiments in the limit $W \to 0$.[28,31] We therefore adopt the expression $\lambda(\xi'_{n,i}) = T_0 \sin^4 2\xi'_{n,i}$ leaving only T_0 as an adjustable parameter.

— *Detector*: The detectors are ideal particle counters, meaning that they produce a click for each incoming particle. Hence, we assume that the detectors have 100% detection efficiency. Note that adaptive threshold detectors can be used (see Sec. 5.1.1) equally well.[3]

— *Simulation procedure*: The simulation algorithm generates the data sets Υ_i, similar to the ones obtained in the experiment (see Eq. (46)). In the simulation, it is easy to generate the events such that $N_1 = N_2$. We analyze these data sets in exactly the same manner as the experimental data are analyzed, implying that we include the post-selection procedure to select photon pairs by a time-coincidence window W. The latter is crucial for our simulation method to give results that are very similar to those observed in a laboratory experiment. Although in the simulation the ratio of detected to emitted photons is equal to one, the final detection efficiency is reduced due to the time-coincidence post-selection procedure.

6.3.2. *Simulation results*

In Fig. 12(a), we present simulation results for the distribution of time-tag differences, as obtained by using time-tag model Eq. (52). The distribution is sharply peaked and displays long tails, in qualitative agreement with experiment.[115] The single-particle averages $E_1(a_1, a_2)$ and $E_2(a_1, a_2)$ (results not shown) are zero up to the usual statistical fluctuations and do not show any statistically relevant dependence on a_2 or a_1, respectively, in concert with a rigorous probabilistic treatment of this simulation model.[31]

Some typical simulation results for the two-particle correlations are depicted in Fig. 12(b) for $W = 50\,\text{ns}$. For this value of the time-window W, the minimum and maximum value of the two-particle correlations is not -1 and $+1$, respectively, as would be expected from the quantum theoretical description. Moreover, the two-particle correlations look more like flattened cosine functions. For $W = 50\,\text{ns}$ we find $|S| = 2.62$ which compares very well with the values between 2 and 2.57 extracted from different sets of experimental data of Weihs *et al.* However, for $W = 2\,\text{ns}$ (results not shown), the results for the two-particle correlations fit very well to the prediction of quantum theory for the EPRB experiment. From these data, we extract $|S| = 2.82$.

Figure 13(a) depicts $S(\theta)$ for $W = 2\,\text{ns}$ and shows that the event-based model reproduces the result predicted by quantum theory for the singlet state (solid line), namely $S = -2\sqrt{2}\cos\theta$. Note that the comparison between the simulation results

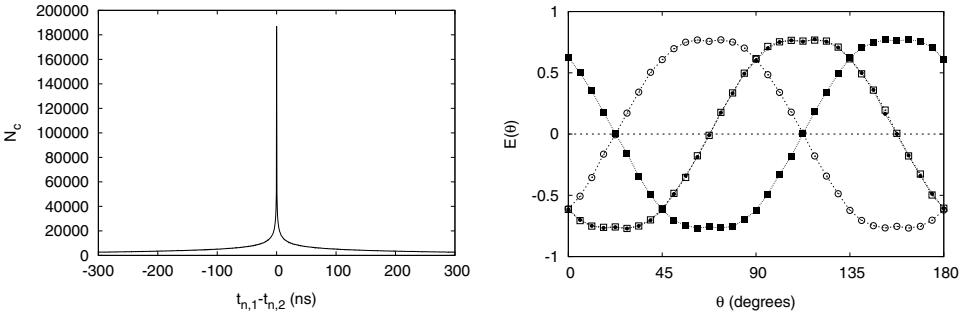

(a) (b)

Fig. 12. Simulation results using the time-tag model Eq. (52) with $T_0 = 1000\,\text{ns}$. The total number of pairs generated by the source is 3×10^5, roughly the same as in experiment.[25] (a) Coincidence count N_c as a function of the time-tag difference $t_{n,1} - t_{n,2}$. (b) Two-particle correlations as a function of θ for $W = 50\,\text{ns}$. Open squares: $E(\theta) = E(a_1 = \theta, a_2 = \pi/8)$; open circles: $E(\theta) = E(a_1' = \theta + \pi/4, a_2 = \pi/8)$; solid squares: $E(\theta) = E(a_1 = \theta, a_2' = 3\pi/8)$; solid circles: $E(\theta) = E(a_1' = \theta + \pi/4, a_2' = 3\pi/8)$.

and quantum theory becomes perfect if more pairs are generated by the source (10^6 pairs is sufficient for most purposes).

From Fig. 13(b), it follows that a violation of the Bell-CHSH inequality $|S| \leq 2$ depends on the choice of W, a parameter which is absent in the quantum theoretical description of the EPRB thought experiment. There are two limiting cases for which S become independent of W. If $W \to \infty$, it is impossible to let a digital computer violate the inequality $|S| \leq 2$ without abandoning the rules of Boolean logic or arithmetic.[111] For relatively small W ($W < 150\,\text{ns}$), the inequality $|S| \leq 2$ may be

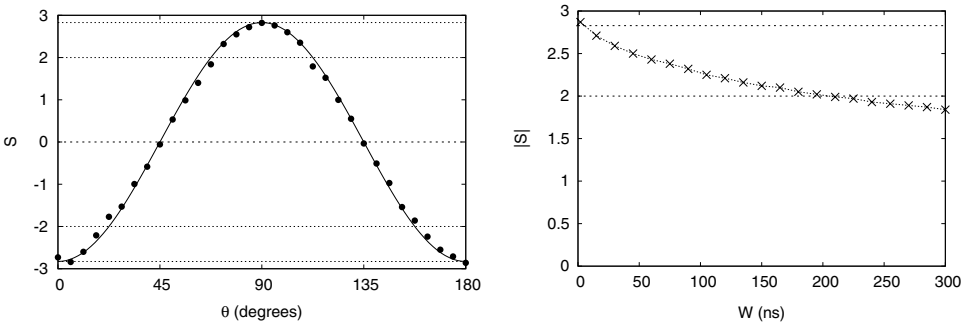

(a) (b)

Fig. 13. Simulation results for the function $S = E(a_1, a_2) - E(a_1, a_2') + E(a_1', a_2) + E(a_1', a_2')$ using the time-tag model Eq. (52) with $T_0 = 1000\,\text{ns}$. The total number of pairs generated by the source is 3×10^5, roughly the same as in experiment.[25] (a) S as a function of θ with $a_1 = \theta$, $a_1' = \pi/4 + \theta$, $a_2 = \pi/8$ and $a_2' = 3\pi/8$ for a time window $W = 2\,\text{ns}$. The line connecting the solid circles is the result $-2\sqrt{2}\cos\theta$ predicted by quantum theory. (b) $|S|$ as a function of W for $a_1 = 0$, $a_1' = \pi/4$, $a_2 = \pi/8$ and $a_2' = 3\pi/8$. The line connecting the crosses is a guide to the eye only. The dashed horizontal lines indicate the maximum value for a quantum system of two spin-$\frac{1}{2}$ particles in a product state ($|S| = 2$) and in a singlet state ($|S| = 2\sqrt{2}$).

violated. When $W \to 0$ the discrete-event models which generate the same type of data as real EPRB experiments, reproduce exactly the single- and two-spin averages of the singlet state and therefore also violate the inequality $|S| \leq 2$. Obviously, as the discrete-event model does not rely on any concept of quantum theory, a violation of the inequality $|S| \leq 2$ does not say anything about the "quantumness" of the system under observation.[109,111,131] Similarly, a violation of this inequality cannot say anything about locality and realism.[109–111,131] Clearly, the event-based model is contextual, literally meaning "being dependent of the (experimental) measurement arrangement". The fact that the event-based model reproduces, for instance, the correlations of the singlet state without violating Einstein's local causality criterion suggests that the data $\{x_{n,1}, x_{n,2}\}$ generated by the event-based model cannot be represented by a single Kolmogorov probability space. This complies with the idea that contextual, non-Kolmogorov models can lead to violations of Bell's inequality without appealing to nonlocality or nonobjectivism.[110,132,133]

In conclusion, event-based simulation models provide a cause-and-effect description of real EPRB experiments at a level of detail which is not covered by quantum theory, such as the effect of the choice of the time-window. Some of these simulation models exactly reproduce the results of quantum theory of the EPRB experiment, indicating that there is no fundamental obstacle for an EPRB experiment to produce data that can be described by quantum theory. However, as we have shown, it is highly unlikely that quantum theory describes the data of the EPRB experiment by Weihs *et al.* This suggests that in the real experiment, there may be processes at work which have not been identified yet.

6.3.3. *Why is Bell's inequality violated?*

In Ref. 31, we have presented a probabilistic description of our simulation model that (i) rigorously proves that for up to first-order in W it exactly reproduces the single particle averages and the two-particle correlations of quantum theory for the system under consideration; (ii) illustrates how the presence of the time-window W introduces correlations that cannot be described by the original Bell-like "hidden-variable" models.[117] Here, we repeat the discussion presented in Ref. 4.

The time-coincidence post-selection procedure with the time-window W filters out the "coincident" photons based on the time-tags $t_{n,i}$ thereby reducing the final detection efficiency to less than 100%, although in the simulation a measurement always returns a $+1$ or -1 for both photons in a pair (100% detection efficiency of the detectors). Hence, even in case of a perfect detection process the data set that is finally retained consists only of a subset of the entire ensemble of correlated photons that was emitted by the source, exactly as in the laboratory experiments.

We briefly elaborate on point (ii) (see Ref. 31 for a more extensive discussion). Let us assume that there exists a probability $P(x_1, x_2, t_1, t_2 \,|\, \theta_1, \theta_2)$ to observe the data $\{x_i, t_i\}$ conditional on the settings θ_i at stations i for $i = 1, 2$. The probability $P(x_1, x_2, t_1, t_2 \,|\, \theta_1, \theta_2)$ can always be expressed as an integral over the mutually

exclusive events ξ_1, ξ_2, representing the polarization of the photons

$$P(x_1, x_2, t_1, t_2 \,|\, \theta_1, \theta_2) = \frac{1}{4\pi^2} \int_0^{2\pi}\!\!\int_0^{2\pi} P(x_1, x_2, t_1, t_2 \,|\, \theta_1, \theta_2, \xi_1, \xi_2) \times P(\xi_1, \xi_2 \,|\, \theta_1, \theta_2) d\xi_1 d\xi_2. \tag{53}$$

We now assume that in the probabilistic version of our simulation model, for each event, (i) the values of $\{x_1, x_2, t_1, t_2\}$ are independent of each other, (ii) the values of $\{x_1, t_1\}$ ($\{x_2, t_2\}$) are independent of θ_2 and ξ_2 (θ_1 and ξ_1), (iii) ξ_1 and ξ_2 are independent of θ_1 or θ_2. With these assumptions Eq. (53) becomes

$$\begin{aligned} P(x_1, x_2, t_1, t_2 \,|\, \theta_1, \theta_2) &\overset{\text{(i)}}{=} \frac{1}{4\pi^2} \int_0^{2\pi}\!\!\int_0^{2\pi} P(x_1, t_1 \,|\, \theta_1, \theta_2, \xi_1, \xi_2) \\ &\quad \times P(x_2, t_2 \,|\, \theta_1, \theta_2, \xi_1, \xi_2) P(\xi_1, \xi_2 \,|\, \theta_1, \theta_2) d\xi_1 d\xi_2 \\ &\overset{\text{(ii)}}{=} \frac{1}{4\pi^2} \int_0^{2\pi}\!\!\int_0^{2\pi} P(x_1, t_1 \,|\, \theta_1, \xi_1) P(x_2, t_2 \,|\, \theta_2, \xi_2) \\ &\quad \times P(\xi_1, \xi_2 \,|\, \theta_1, \theta_2) d\xi_1 d\xi_2 \\ &\overset{\text{(i)}}{=} \frac{1}{4\pi^2} \int_0^{2\pi}\!\!\int_0^{2\pi} P(x_1 \,|\, \theta_1, \xi_1) P(t_1 \,|\, \theta_1, \xi_1) P(x_2 \,|\, \theta_2, \xi_2) \\ &\quad \times P(t_2 \,|\, \theta_2, \xi_2) P(\xi_1, \xi_2 \,|\, \theta_1, \theta_2) d\xi_1 d\xi_2 \\ &\overset{\text{(iii)}}{=} \frac{1}{4\pi^2} \int_0^{2\pi}\!\!\int_0^{2\pi} P(x_1 \,|\, \theta_1, \xi_1) P(t_1 \,|\, \theta_1, \xi_1) P(x_2 \,|\, \theta_2, \xi_2) \\ &\quad \times P(t_2 \,|\, \theta_2, \xi_2) P(\xi_1, \xi_2) d\xi_1 d\xi_2, \end{aligned} \tag{54}$$

which is the probabilistic description of our simulation model. According to our simulation model, the probability distributions that describe the polarizers are given by $P(x_i|\theta_i, \xi_i) = [1 + x_i \cos 2(\theta_i - \xi_i)]/2$ and those for the time-delays t_i that are distributed randomly over the interval $[0, \lambda(\xi_i + (i-1)\pi/2 - \theta_i)]$ are given by $P(t_i \,|\, \theta_i, \xi_i) = \Theta(t_i)\Theta(\lambda(\xi_i + (i-1)\pi/2 - \theta_i) - t_i)/\lambda(\xi_i + (i-1)\pi/2 - \theta_i)$, where $\Theta(\cdot)$ denotes the unit step function. In the experiment[25] and therefore also in our simulation model, the events are selected using a time window W that the experimenters try to make as small as possible.[115] Accounting for the time window, that is multiplying Eq. (54) by a step function and integrating over all t_1 and t_2, the expression for the probability for observing the event (x_1, x_2) reads

$$P(x_1, x_2 \,|\, \theta_1, \theta_2) = \int_0^{2\pi}\!\!\int_0^{2\pi} P(x_1 \,|\, \theta_1, \xi_1) P(x_2 \,|\, \theta_2, \xi_2) \rho(\xi_1, \xi_2 \,|\, \theta_1, \theta_2) d\xi_1 d\xi_2, \tag{55}$$

where the probability density $\rho(\xi_1, \xi_2 \,|\, \theta_1, \theta_2)$ is given by

$$\rho(\xi_1, \xi_2 \,|\, \theta_1, \theta_2) = \frac{\int_{-\infty}^{+\infty}\!\!\int_{-\infty}^{+\infty} P(t_1 \,|\, \theta_1, \xi_1) P(t_2 \,|\, \theta_2, \xi_2) \Theta \times (W - |t_1 - t_2|) P(\xi_1, \xi_2) dt_1 dt_2}{\int_0^{2\pi}\!\!\int_0^{2\pi}\!\!\int_{-\infty}^{+\infty}\!\!\int_{-\infty}^{+\infty} P(t_1 \,|\, \theta_1, \xi_1) P(t_2 \,|\, \theta_2, \xi_2) \Theta \times (W - |t_1 - t_2|) P(\xi_1, \xi_2) d\xi_1 d\xi_2 dt_1 dt_2}. \tag{56}$$

The simple fact that $\rho(\xi_1, \xi_2 \,|\, \theta_1, \theta_2) \neq \rho(\xi_1, \xi_2)$ brings the derivation of the original Bell (CHSH) inequality to a halt. Indeed, in these derivations it is assumed that the probability distribution for ξ_1 and ξ_2 does not depend on the settings θ_1 or θ_2.[2,117]

By making explicit use of the time-tag model (see Eq. (52)) it can be shown that[31] (i) if we ignore the time-tag information ($W > T_0$), the two-particle probability takes the form of the hidden variable models considered by Bell,[117] and we cannot reproduce the results of quantum theory,[117] (ii) if we focus on the case $W \to 0$ the single-particle averages are zero and the two-particle average $E(\theta_1, \theta_2) = -\cos 2(\theta_1 - \theta_2)$.

Although our simulation model and its probabilistic version Eq. (54) involve local processes only, the filtering of the detection events by means of the time-coincidence window W can produce correlations which violate Bell-type inequalities.[96,99,130] Moreover, for $W \to 0$ our classical, local and causal simulation model can produce single-particle and two-particle averages that correspond with those of a singlet state in quantum theory.

6.4. *Bell-test experiment with single neutrons*

The single-neutron interferometry experiment of Hasegawa *et al.*[127] demonstrates that the correlation between the spatial and spin degree of freedom of neutrons violates a Bell-CHSH inequality. In this section, we construct an event-based model that reproduces this correlation by using detectors that count every neutron and without using any post-selection procedure. We show that the event-based model reproduces the exact results of quantum theory if $\gamma \to 1^-$ and that by changing γ it can also reproduce the numerical values of the correlations, as measured in experiments.[127,134] Note that this Bell-test experiment involves two degrees of freedom of one particle, while the EPRB thought experiment[92] and EPRB experiments with single photons[25,115,118,122] involve two degrees of freedom of two particles. Hence, the Bell-test experiment with single neutrons is not performed according to the CHSH protocol[114] because the two degrees of freedom of one particle are not manipulated and measured independently.

Figure 14 shows a schematic picture of the single-neutron interferometry experiment. Incident neutrons pass through a magnetic-prism polarizer (not shown) which produces two spatially separated beams of neutrons with their magnetic moments aligned parallel (spin up), respectively anti-parallel (spin down) with respect to the magnetic axis of the polarizer which is parallel to the guiding field $\mathbf{B}$. The spin-up neutrons impinge on a silicon-perfect-crystal interferometer.[36] On leaving the first beam splitter BS0, neutrons are transmitted or refracted. A mu-metal spin-turner changes the orientation of the magnetic moment of the neutron from parallel to perpendicular to the guiding field $\mathbf{B}$. Hence, the magnetic moment of the neutrons following path H (O) is rotated by $\pi/2$ ($-\pi/2$) about the y-axis. Before the two paths join at the entrance plane of beam splitter BS3, a difference between the time of flights along the two paths can be manipulated by a phase shifter. The neutrons

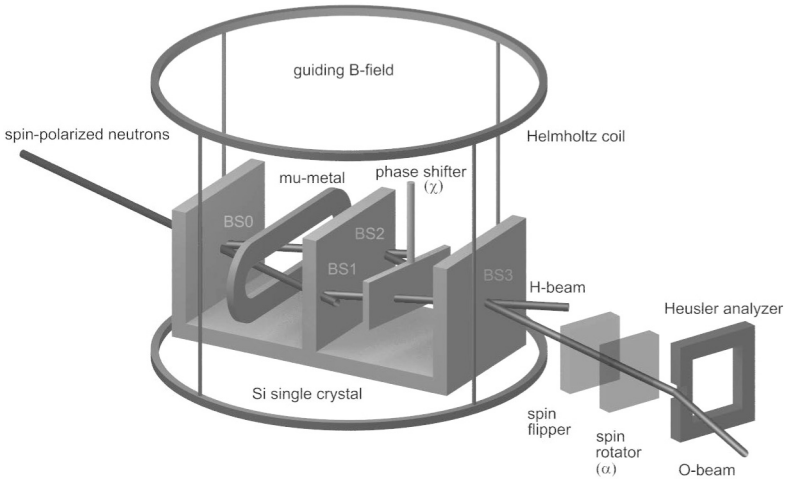

Fig. 14. Top: Schematic picture of the single-neutron interferometry experiment to test a Bell inequality violation (see also Fig. 1 in Ref. 127). BS0, ..., BS3: beam splitters; phase shifter χ: aluminum foil; neutrons that are transmitted by BS1 or BS2 leave the interferometer and do not contribute to the interference signal. Detectors count the number of neutrons in the O- and H-beams.

which experience two refraction events when passing through the interferometer form the O-beam and are analyzed by sending them through a spin rotator and a Heusler spin analyzer. If necessary, to induce an extra spin rotation of π, a spin flipper is placed between the interferometer and the spin rotator. The neutrons that are selected by the Heusler spin analyzer are counted with a neutron detector (not shown) that has a very high efficiency ($\approx 99\%$). Note that neutrons which are not refracted by the mirror plate leave the interferometer without being detected.

The single-neutron interferometry experiment yields the count rate $N(\alpha, \chi)$ for the spin-rotation angle α and the difference χ of the phase shifts of the two different paths in the interferometer.[127] The correlation $E(\alpha, \chi)$ is defined by[127]

$$E(\alpha, \chi) = \frac{N(\alpha, \chi) + N(\alpha + \pi, \chi + \pi) - N(\alpha + \pi, \chi) - N(\alpha, \chi + \pi)}{N(\alpha, \chi) + N(\alpha + \pi, \chi + \pi) + N(\alpha + \pi, \chi) + N(\alpha, \chi + \pi)}. \tag{57}$$

6.4.1. *Event-based model*

A minimal, discrete event simulation model of the single-neutron interferometry experiment requires a specification of the information carried by the particles, of the algorithm that simulates the source and the interferometer components (see Fig. 15), and of the procedure to analyze the data. Various ingredients of the simulation model have been described in Sec. 5.4.1. In the following, we specify the action of the remaining components, namely the magnetic-prism polarizer (not shown), the mu-metal spin-turner, the spin-rotator and spin analyzer.

— *Magnetic-prism polarizer*: This component takes as input a neutron with an unknown magnetic moment and produces a neutron with a magnetic moment that is

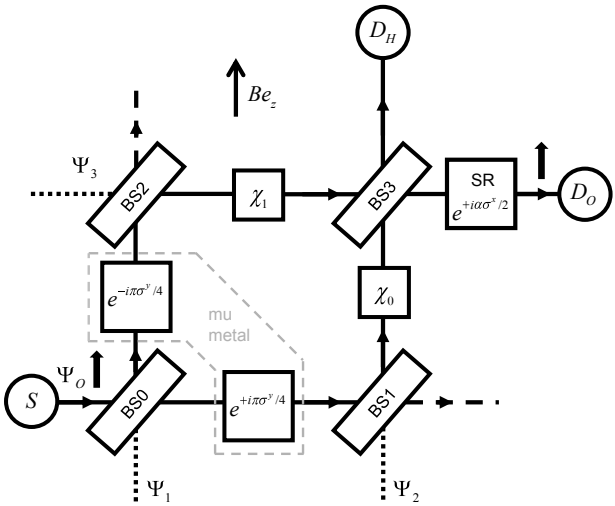

Fig. 15. Event-based network of the experimental setup shown in Fig. 14. S: single neutron source; BS0, ..., BS3: BSs; $e^{+i\pi\sigma^y/4}$, $e^{-i\pi\sigma^y/4}$: spin rotators modeling the action of a mu-metal; χ_0, χ_1: phase shifters; SR $e^{i\alpha\sigma^x/2}$: spin rotator; D_O, D_H: detectors counting all neutrons that leave the interferometer via the O- and H-beams, respectively. In the experiment and in the event-based simulation, neutrons with spin up (magnetic moment aligned parallel with respect to the guiding magnetic field $\mathbf{B}$) enter the interferometer via the path labeled by Ψ_0 only. The wave amplitudes labeled by Ψ_1, Ψ_2 and Ψ_3 (dotted lines) are used in the quantum theoretical treatment only (see text). Particles leaving the interferometer via the dashed lines are not counted.

either parallel (spin up) or antiparallel (spin down) with respect to the z-axis (which by definition is parallel to the guiding field $\mathbf{B}$). In the experiment, only a neutron with spin up is injected into the interferometer. Therefore, as a matter of simplification, we assume that the source S only creates messengers with spin up. Hence, we assume that $\theta = 0$ in Eq. (29).

— *Mu-metal spin turner*: This component rotates the magnetic moment of a neutron that follows the H-beam (O-beam) by $\pi/2$ ($-\pi/2$) about the y-axis. The processor that accomplishes this takes as input the direction of the magnetic moment, represented by the message $\mathbf{u}$ and performs the rotation $\mathbf{u} \to e^{i\pm\pi\sigma^y/4}\mathbf{u}$. We emphasize that we use Pauli matrices as a convenient tool to express rotations in three-dimensional space, not because in quantum theory the magnetic moment of the neutron is represented by spin-$\frac{1}{2}$ operators.

— *Spin-rotator and spin-flipper*: The spin-rotator rotates the magnetic moment of a neutron by an angle α about the x-axis. The spin-flipper is a spin-rotator with $\alpha = \pi$.

— *Spin analyzer*: This component selects neutrons with spin up, after which they are counted by a detector. The model of this component projects the magnetic moment of the particle on the z-axis and sends the particle to the detector if the projected value exceeds a pseudo-random number r.

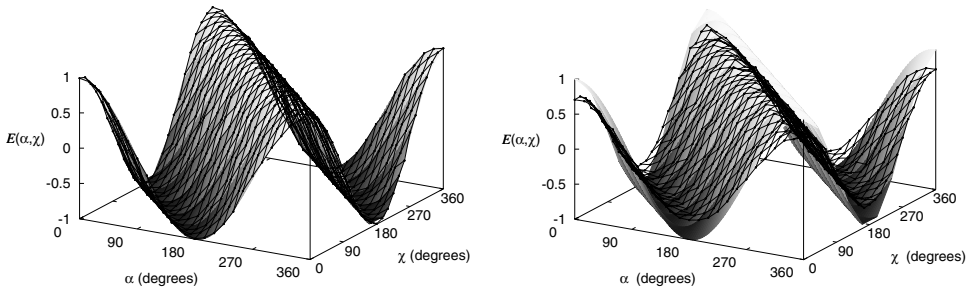

(a) (b)

Fig. 16. (a) Correlation $E(\alpha,\chi)$ between spin and path degree of freedom as obtained from an event-based simulation of the experiment depicted in Fig. 14. Solid surface: $E(\alpha,\chi) = \cos(\alpha+\chi)$ predicted by quantum theory; circles: simulation data. The lines connecting the markers are guides to the eye only. Model parameters: reflection percentage of BS0, ..., BS3 is 20% and $\gamma = 0.99$. For each pair (α,χ), four times 10 000 particles were used to determine the four counts $N(\alpha,\chi)$, $N(\alpha+\pi,\chi+\pi)$, $N(\alpha,\chi+\pi)$ and $N(\alpha+\pi,\chi+\pi)$. (b) Same as figure (a) but $\gamma = 0.55$.

6.4.2. *Simulation results*

In Fig. 16(a), we present simulation results for the correlation $E(\alpha,\chi)$, assuming that the experimental conditions are very close to ideal and compare them to the quantum theoretical result.

The quantum theoretical description of the experiment[127] requires a four-state system for the path and another two-state system to account for the spin-$\frac{1}{2}$ degree-of-freedom. Thus, the statistics of the experimental data is described by the state vector Eq. (32). In the experiment,[127] the neutrons that enter the interferometer all have spin up, relative to the direction of the guiding field $\mathbf{B}$ (see Fig. 14). Thus, the state describing the incident neutrons is $|\Psi\rangle = (1,0,0,0,0,0,0,0)^T$, omitting irrelevant phase factors. As the state vector propagates through the interferometer and the spin-rotator (see Fig. 15), it changes according to

$$\begin{aligned}
|\Psi'\rangle = &\begin{pmatrix} \cos(\alpha/2) & i\sin(\alpha/2) \\ i\sin(\alpha/2) & \cos(\alpha/2) \end{pmatrix}_{6,7} \begin{pmatrix} t^* & r \\ -r^* & t \end{pmatrix}_{5,7} \begin{pmatrix} t^* & r \\ -r^* & t \end{pmatrix}_{4,6} \\
&\times \begin{pmatrix} e^{i\phi_1} & 0 \\ 0 & e^{i\phi_1} \end{pmatrix}_{6,7} \begin{pmatrix} e^{i\phi_0} & 0 \\ 0 & e^{i\phi_0} \end{pmatrix}_{4,5} \begin{pmatrix} t^* & r \\ -r^* & t \end{pmatrix}_{3,7} \begin{pmatrix} t^* & r \\ -r^* & t \end{pmatrix}_{2,6} \\
&\times \begin{pmatrix} t & -r^* \\ r & t^* \end{pmatrix}_{1,5} \begin{pmatrix} t & -r^* \\ r & t^* \end{pmatrix}_{0,4} \begin{pmatrix} 1/\sqrt{2} & 1/\sqrt{2} \\ -1/\sqrt{2} & 1/\sqrt{2} \end{pmatrix}_{2,3} \begin{pmatrix} 1/\sqrt{2} & -1/\sqrt{2} \\ 1/\sqrt{2} & 1/\sqrt{2} \end{pmatrix}_{0,1} \\
&\times \begin{pmatrix} t & -r^* \\ r & t^* \end{pmatrix}_{1,3} \begin{pmatrix} t & -r^* \\ r & t^* \end{pmatrix}_{0,2} |\Psi\rangle, \qquad (58)
\end{aligned}$$

where the subscripts i,j refer to the pair of elements of the eight-dimensional vector on which the matrix acts. Reading backwards, the first pair of matrices in Eq. (58)

represents beam splitter BS0, the second pair the mu-metal (a spin rotation about the y-axis by $\pi/4$ and $-\pi/4$, respectively), the third and fourth pair beam splitters BS1 and BS2, respectively, the fifth pair the phase shifters, the sixth pair beam splitter BS3 and the last matrix represents the spin-rotator SR.

From Eq. (58), it follows that the probability to detect a neutron with spin up in the O-beam is given by

$$p_O(\alpha,\chi) = |\Psi'_{3,\uparrow}|^2 = \mathcal{T}\mathcal{R}^2[1+\cos(\alpha+\chi)], \tag{59}$$

where $\chi = \chi_0 - \chi_1$. From Eq. (59) it follows that the correlation $E_O(\alpha,\chi)$ is given by[127]

$$\begin{aligned} E_O(\alpha,\chi) &\equiv \frac{p_O(\alpha,\chi)+p_O(\alpha+\pi,\chi+\pi)-p_O(\alpha+\pi,\chi)-p_O(\alpha,\chi+\pi)}{p_O(\alpha,\chi)+p_O(\alpha+\pi,\chi+\pi)+p_O(\alpha+\pi,\chi)+p_O(\alpha,\chi+\pi)} \\ &= \cos(\alpha+\chi), \end{aligned} \tag{60}$$

independent of the reflectivity $\mathcal{R} = |r|^2 = 1-\mathcal{T}$ of the BSs (which have been assumed to be identical). The fact that $E_O(\alpha,\chi) = \cos(\alpha+\chi)$ implies that the state of the neutron cannot be written as a product of the state of the spin and the phase. In other words, in quantum language, the spin- and phase-degree-of-freedom are entangled.[127,135] Repeating the calculation for the probability of detecting a neutron in the H-beam shows that $E_H(\alpha,\chi) = 0$, independent of the direction of the spin. If the mu-metal would rotate the spin about the x-axis instead of about the y-axis, then we would find $E_O(\alpha,\chi) = \cos\alpha\cos\chi$, a typical expression for a quantum system in a product state.

As shown by the markers in Fig. 16(a), disregarding the small statistical fluctuations, there is close-to-perfect agreement between the event-based simulation data for nearly ideal experimental conditions ($\gamma = 0.99$ and $\mathcal{R} = 0.2$) and quantum theory. However, the laboratory experiment suffers from unavoidable imperfections, leading to a reduction and distortion of the interference fringes.[127] In the event-based approach it is trivial to incorporate mechanisms for different sources of imperfections by modifying or adding update rules. However, to reproduce the available data it is sufficient to use the parameter γ to control the deviation from the quantum theoretical result. For instance, for $\gamma = 0.55$, $\mathcal{R} = 0.2$ the simulation results for $E(\alpha,\chi)$ are shown in Fig. 16(b).

In order to quantify the difference between the simulation results, the experimental results and quantum theory it is customary to form the Bell-CHSH function[114,117]

$$S = S(\alpha,\chi,\alpha',\chi') = E_O(\alpha,\chi) + E_O(\alpha,\chi') - E_O(\alpha',\chi) + E_O(\alpha',\chi'), \tag{61}$$

for some set of experimental settings α, χ, α', and χ'. If the quantum system can be described by a product state, then $|S| \le 2$. If $\alpha = 0$, $\chi = \pi/4$, $\alpha' = \pi/2$, and $\chi' = \pi/4$, then $S \equiv S_{\max} = 2\sqrt{2}$, the maximum value allowed by quantum theory.[94]

For $\gamma = 0.55$, $\mathcal{R} = 0.2$ the simulation results yield $S_{\max} = 2.05$, in excellent agreement with the value 2.052 ± 0.010 obtained in experiment.[127] For $\gamma = 0.67$,

$\mathcal{R} = 0.2$ the simulation yields $S_{\max} = 2.30$, in excellent agreement with the value 2.291 ± 0.008 obtained in a similar, more recent experiment.[136]

In conclusion, since experiment shows that $|S| > 2$, according to quantum theory it is impossible to interpret the experimental result in terms of a quantum system in the product state.[2] The system must be described by an entangled state. However, the event-based simulation which makes use of classical, Einstein-local and causal event-by-event processes can reproduce all features of this entangled state.

6.4.3. *Why are results from quantum theory produced?*

From Ref. 3, we know that the event-based model for the BS produces results corresponding to those of classical wave or quantum theory when applied in interferometry experiments. Important for this outcome is that the phase difference χ between the two paths in the interferometer is constant for a relatively large number of incoming particles. If, for each incoming neutron, we pick the angle χ randomly from the same set of predetermined values to produce Fig. 16, an event-based simulation with $\gamma = 0.99$ yields (within the usual statistical fluctuations) the correlation $E(\alpha, \chi) \approx [\cos(\alpha + \chi)]/2$, which does not lead to a violation of the Bell-CHSH inequality (results not shown). Thus, if the neutron interferometry experiment could be repeated with random choices for the phase shifter χ for each incident neutron, and the experimental results would show a significant violation of the Bell-CHSH inequality, then the event-based model that we have presented here would be ruled out.

7. Discussion

We have presented an event-based simulation method which allows for a mystery-free, particle-only description of interference and entanglement phenomena observed in various single-photon experiments and single-neutron interferometry experiments. The statistical distributions which are observed in these single-particle experiments and which are usually thought to be of quantum mechanical origin, are shown to emerge from a time series of discrete events generated by causal adaptive systems, which in principle could be build using macroscopic mechanical parts.

As shown in the examples, in the stationary state (after processing many events), the event-based model reproduces the statistical distributions of quantum theory. This might raise questions about the efficiency of the method. Although the event-based simulation method can be used to simulate a universal quantum computer,[21,22] the so-called "quantum speed-up" cannot be obtained. This by itself is no surprise because the quantum speed-up is the result of a mathematical construct in which each unitary operation on the state of the quantum computer is counted as one operation and in which preparation and read-out of the quantum computer are excluded. Whether or not this mathematical construct is realized in Nature is an open question.

We hope that our simulation results will stimulate the design of new dedicated single-photon and neutron interferometry experiments which help extending and refining our event-based approach.

Acknowledgment

We would like to thank K. De Raedt, K. Keimpema, F. Jin, S. Miyashita, S. Yuan, and S. Zhao for many thoughtful comments and contributions to the work on which this review is based.

References

1. D. Home, *Conceptual Foundations of Quantum Physics* (Plenum Press, New York, 1997).
2. L. E. Ballentine, *Quantum Mechanics: A Modern Development* (World Scientific, Singapore, 2003).
3. K. Michielsen, F. Jin and H. De Raedt, *J. Comput. Theor. Nanosci.* **8**, 1052 (2011).
4. H. De Raedt and K. Michielsen, *Ann. Phys.* (*Berlin*) **524**, 393 (2012).
5. H. De Raedt, F. Jin and K. Michielsen, *Quantum Matter* **1**, 1 (2012).
6. P. Grangier, G. Roger and A. Aspect, *Europhys. Lett.* **1**, 173 (1986).
7. H. De Raedt, K. De Raedt and K. Michielsen, *Europhys. Lett.* **69**, 861 (2005).
8. K. De Raedt, H. De Raedt and K. Michielsen, *Comput. Phys. Comm.* **171**, 19 (2005).
9. V. Jacques, E. Wu, F. Grosshans, F. Treussart, P. Grangier, A. Aspect and J.-F. Roch, *Science* **315**, 966 (2007).
10. S. Zhao, S. Yuan, H. De Raedt and K. Michielsen, *Europhys. Lett.* **82**, 40004 (2008).
11. K. Michielsen, S. Yuan, S. Zhao, F. Jin and H. De Raedt, *Physica E* **42**, 348 (2010).
12. P. D. D. Schwindt, P. G. Kwiat and B.-G. Englert, *Phys. Rev. A* **60**, 4285 (1999).
13. F. Jin, S. Zhao, S. Yuan, H. De Raedt and K. Michielsen, *J. Comput. Theor. Nanosci.* **7**, 1771 (2010).
14. H. De Raedt, M. Delina, F. Jin and K. Michielsen, *Phys. Scr.* **T151**, 014004 (2012).
15. V. Jacques, E. Wu, T. Toury, F. Treussart, A. Aspect, P. Grangier and J.-F. Roch, *Eur. Phys. J. D* **35**, 561 (2005).
16. F. Jin, S. Yuan, H. De Raedt, K. Michielsen and S. Miyashita, *J. Phys. Soc. Jpn.* **79**, 074401 (2010).
17. S. Zhao and H. De Raedt, *J. Comput. Theor. Nanosci.* **5**, 490 (2008).
18. I. N. Agafonov, M. V. Chekhova, T. S. Iskhakov and A. N. Penin, *Phys. Rev. A* **77**, 053801 (2008).
19. F. Jin, H. De Raedt and K. Michielsen, *Commun. Comput. Phys.* **7**, 813 (2010).
20. K. Michielsen, F. Jin, M. Delina and H. De Raedt, *Phys. Scr.* **T151**, 014005 (2012).
21. H. De Raedt, K. De Raedt and K. Michielsen, *J. Phys. Soc. Jpn. Suppl.* **76**, 16 (2005).
22. K. Michielsen, K. De Raedt and H. De Raedt, *J. Comput. Theor. Nanosci.* **2**, 227 (2005).
23. A. Aspect, P. Grangier and G. Roger, *Phys. Rev. Lett.* **49**, 91 (1982).
24. A. Aspect, J. Dalibard and G. Roger, *Phys. Rev. Lett.* **49**, 1804 (1982).
25. G. Weihs, T. Jennewein, C. Simon, H. Weinfurther and A. Zeilinger, *Phys. Rev. Lett.* **81**, 5039 (1998).
26. K. De Raedt, K. Keimpema, H. De Raedt, K. Michielsen and S. Miyashita, *Eur. Phys. J. B* **53**, 139 (2006).
27. H. De Raedt, K. De Raedt, K. Michielsen, K. Keimpema and S. Miyashita, *J. Phys. Soc. Jpn.* **76**, 104005 (2007).

28. K. De Raedt, H. De Raedt and K. Michielsen, *Comput. Phys. Commun.* **176**, 642 (2007).
29. H. De Raedt, K. De Raedt, K. Michielsen, K. Keimpema and S. Miyashita, *J. Comput. Theor. Nanosci.* **4**, 957 (2007).
30. H. De Raedt, K. Michielsen, S. Miyashita and K. Keimpema, *Eur. Phys. J. B* **58**, 55 (2007).
31. S. Zhao, H. De Raedt and K. Michielsen, *Found. Phys.* **38**, 322 (2008).
32. B. Trieu, K. Michielsen and H. De Raedt, *Comput. Phys. Comm.* **182**, 726 (2011).
33. R. P. Feynman, R. B. Leighton and M. Sands, *The Feynman Lectures on Physics*, Vol. 3 (Addison-Wesley, Reading MA, 1965).
34. T. Young, *Philos. Trans. R. Soc. Lond.* **92**, 12 (1802).
35. A. Zeilinger, R. Gähler, C. G. Shull, W. Treimer and W. Mampe, *Rev. Mod. Phys.* **60**, 1067 (1988).
36. H. Rauch and S. A. Werner, *Neutron Interferometry: Lessons in Experimental Quantum Mechanics* (Clarendon, London, 2000).
37. D. W. Keith, C. R. Ekstrom, Q. A. Turchette and D. E. Pritchard, *Phys. Rev. Lett.* **66**, 2693 (1991).
38. O. Carnal and J. Mlynek, *Phys. Rev. Lett.* **66**, 2689 (1991).
39. M. Arndt, O. Nairz, J. Vos-Andreae, C. Keller, G. van der Zouw and A. Zeilinger, *Nature* **401**, 680 (1999).
40. B. Brezger, L. Hackermüller, S. Uttenthaler, J. Petschinka, M. Arndt and A. Zeilinger, *Phys. Rev. Lett.* **88**, 100404 (2002).
41. T. Juffmann, A. Milic, M. Müllneritsch, P. Asenbaum, A. Tsukernik, J. Tüxen, M. Mayor, O. Cheshnovsky and M. Arndt, *Nature Nanotechnol.* **7**, 297 (2012).
42. M. Born and E. Wolf, *Principles of Optics* (Pergamon, Oxford, 1964).
43. R. Feynman, *Lectures in Physics*, Vol. 1 (Addison Wesley Publishing Company Reading, Mass, 1963).
44. G. Möllenstedt and H. Düker, *Naturwissenschaften* **42**, 41 (1955).
45. G. Möllenstedt and H. Düker, *Z. Phys.* **145**, 377 (1956).
46. C. Jönsson, *Z. Phys.* **161**, 454 (1961).
47. F. Hasselbach, *Rep. Prog. Phys.* **73**, 016101 (2010).
48. R. Rosa, *Phys. Perspect.* **14**, 178 (2012).
49. O. Donati, G. P. Missiroli and G. Pozzi, *Am. J. Phys.* **41**, 639 (1973).
50. P. G. Merli, G. F. Missiroli and G. Pozzi, *Am. J. Phys.* **44**, 306 (1976).
51. A. Tonomura, J. Endo, T. Matsuda, T. Kawasaki and H. Ezawa, *Am. J. Phys.* **57**, 117 (1989).
52. S. Frabboni, G. C. Gazzadi and G. Pozzi, *Appl. Phys. Lett.* **93**, 073108 (2008).
53. S. Frabboni, C. Frigeri, G. C. Gazzadi and G. Pozzi, *Ultramicroscopy* **110**, 483 (2010).
54. S. Frabboni, C. Frigeri, G. C. Gazzadi and G. Pozzi, *Am. J. Phys.* **79**, 615 (2011).
55. S. Frabboni, A. Gabrielli, G. C. Gazzadi, F. Giorgi, G. Matteucci, G. Pozzi, N. S. Cesari, M. Villa and A. Zoccoli, *Ultramicroscopy* **116**, 73 (2012).
56. R. Bach, D. Pope, S. Liu and H. Batelaan, *New J. Phys.* **15**, 033018 (2013).
57. J. J. Thomson, *Proc. Camb. Philos. Soc.* **14**, 417 (1908).
58. G. I. Taylor, *Proc. Camb. Philos. Soc.* **15**, 114 (1909).
59. Y. Tsuchiya, E. Inuzuka, T. Kurono and M. Hosoda, *Adv. Electron. Electron Phys.* **64A**, 21 (1985).
60. S. Parker, *Am. J. Phys.* **39**, 420 (1971).
61. A. Weis and R. Wynands, *PhyDid.* **1 / 2**, S67 (2003).
62. T. L. Dimitrova and A. Weis, *Am. J. Phys.* **76**, 137 (2008).
63. I. G. Saveliev, M. Sanz and N. Garcia, *J. Opt. B: Quantum Semiclassical Opt.* **4**, S477 (2002).

64. N. Garcia, I. G. Saveliev and M. Sharonov, *Philos. Trans. R. Soc. Lond. A.* **360**, 1039 (2002).
65. P. Kolenderski, C. Scarcella, K. Johnsen, D. Hamel, C. Holloway, L. Shalm, S. Tisa, A. Tosi, K. Resch and T. Jennewein, Time-resolved double-slit experiment with entangled photons, arXiv:1304.4943.
66. A. E. Allahverdyan, R. Balian and T. M. Nieuwenhuizen, *Phys. Rep.* **525**, 1 (2013).
67. S. Wolfram, *A New Kind of Science* (Wolfram Media, 2002).
68. A. Petersen, *Bull. Atom. Sci.* **19**, 8 (1963).
69. A. Plotnitsky, *AIP Conf. Proc.* **1232**, 128 (2010).
70. W. Gerlach and O. Stern, *Z. Phys.* **9**, 349 (1922).
71. W. Gerlach and O. Stern, *Ann. Phys.* **74**, 673 (1924).
72. H. De Raedt, K. De Raedt, K. Michielsen and S. Miyashita, *Comput. Phys. Commun.* **174**, 803 (2006).
73. H. De Raedt and K. Michielsen, Computational Methods for Simulating Quantum Computers, in *Handbook of Theoretical and Computational Nanotechnology*, eds. M. Rieth and W. Schommers (American Scientific Publishers, Los Angeles, 2006), pp. 2–48.
74. L. de Broglie, *Ann. Phys.* **3**, 22 (1925).
75. J. A. Wheeler, *Mathematical Foundations of Quantum Theory*, ed. A. R. Marlow (Academic, New York, 1978), [reprinted in *Quantum Theory and Measurements*, eds. J. A. Wheeler and W. H. Zurek (Princeton University Press, Princeton, NJ, 1983), pp. 182–213].
76. V. Jacques, E. Wu, F. Grosshans, F. Treussart, P. Grangier, A. Aspect and J.-F. Roch, *Phys. Rev. Lett.* **100**, 220402 (2008).
77. R. L. Pfleegor and L. Mandel, *Phys. Rev.* **159**, 1084 (1967).
78. T. de Jong, http://demonstrations.wolfram.com/EventByEventSimulationOfDoubleSlitExperimentsWithSinglePhoto/.
79. R. P. Feynman, *QED — The Strange Theory of Light and Matter* (Princeton University Press, 1985).
80. H. De Raedt, K. Michielsen and F. Jin, *AIP Conf. Proc.* **1424**, 55 (2012).
81. A. Taflove and S. Hagness, *Computational Electrodynamics: The Finite-Difference Time-Domain Method* (Artech House, Boston, 2005).
82. R. H. Hadfield, *Nature Photon.* **3**, 696 (2009).
83. D. L. Alkon, *Biophys. J.* **80**, 2056 (2001).
84. T. de Jong and H. De Raedt, http://demonstrations.wolfram.com/EventByEventSimulationOfTheMachZehnderInterferometer/.
85. G. Baym, *Lectures on Quantum Mechanics* (W.A. Benjamin, Reading MA, 1974).
86. T. Hellmuth, H. Walther, A. Zajonc and W. Schleich, *Phys. Rev. A* **72**, 2532 (1987).
87. H. Rauch, W. Treimer and U. Bonse, *Phys. Lett. A* **47**, 369 (1974).
88. Y. Hasegawa and H. Rauch, *New J. Phys.* **13**, 115010 (2011).
89. G. Kroupa, G. Bruckner, O. Bolik, M. Zawisky, M. Hainbuchner, G. Badurek, R. J. Buchelt, A. Schricker and H. Rauch, *Nucl. Instrum. Methods Phys. Res. A* **440**, 604 (2000).
90. H. Lemmel and A. G. Wagh, *Phys. Rev. A* **82**, 033626 (2010).
91. H. Rauch and M. Suda, *Phys. Stat. Sol. A* **25**, 495 (1974).
92. D. Bohm, *Quantum Theory* (Prentice-Hall, New York, 1951).
93. A. Einstein, A. Podolsky and N. Rosen, *Phys. Rev.* **47**, 777 (1935).
94. B. S. Cirel'son, *Lett. Math. Phys.* **4**, 93 (1980).
95. J. S. Bell, *Physics* **1**, 195 (1964).

96. J.-Å. Larsson and R. D. Gill, *Europhys. Lett.* **67**, 707 (2004).
97. L. de la Peña, A. M. Cetto and T. A. Brody, *Lett. Nuovo Cimento* **5**, 177 (1972).
98. A. Fine, *Synthese.* **29**, 257 (1974).
99. A. Fine, *Synthese.* **50**, 279 (1982).
100. T. Brody, *The Philosphy Behind Physics* (Springer, Berlin, 1993).
101. M. Kupczyński, *Phys. Lett. A* **116**, 417 (1986).
102. E. T. Jaynes, Clearing up mysteries — The original goal, in *Maximum Entropy and Bayesian Methods*, ed. J. Skilling, Vol. 36 (Kluwer Academic Publishers, Dordrecht, 1989), pp. 1–27.
103. L. Sica, *Opt. Comm.* **170**, 55 (1999).
104. K. Hess and W. Philipp, *Proc. Natl. Acad. Sci. USA* **98**, 14228 (2001).
105. K. Hess and W. Philipp, *AIP Conf. Proc.* **750**, 150 (2005).
106. A. F. Kracklauer, *AIP Conf. Proc.* **750**, 219 (2005).
107. E. Santos, *Philos. Mod. Phys.* **36**, 544 (2005).
108. T. M. Nieuwenhuizen, *AIP Conf. Proc.* **1101**, 127 (2009).
109. K. Hess, K. Michielsen and H. De Raedt, *Europhys. Lett.* **87**, 60007 (2009).
110. T. M. Nieuwenhuizen, *Found. Phys.* **41**, 580 (2011).
111. H. De Raedt, K. Hess and K. Michielsen, *J. Comput. Theor. Nanosci.* **8**, 1011 (2011).
112. K. Hess, H. De Raedt and K. Michielsen, *Phys. Scr.* **T151**, 014002 (2012).
113. G. Boole, *Philos. Trans. R. Soc. Lond.* **152**, 225 (1862).
114. J. F. Clauser, M. A. Horne, A. Shimony and R. A. Holt, *Phys. Rev. Lett.* **23**, 880 (1969).
115. G. Weihs, Ein Experiment zum Test der Bellschen Ungleichung unter Einsteinscher Lokalität, PhD thesis, University of Vienna (2000), http://www.uibk.ac.at/exphys/photonik/people/gwdiss.pdf.
116. J. F. Clauser and M. A. Horne, *Phys. Rev. D* **10**, 526 (1974).
117. J. S. Bell, *Speakable and Unspeakable in Quantum Mechanics* (Cambridge University Press, Cambridge, 1993).
118. A. Hnilo, A. Peuriot and G. Santiago, *Found. Phys. Lett.* **15**, 359 (2002).
119. A. A. Hnilo, M. D. Kovalsky and G. Santiago, *Found. Phys.* **37**, 80 (2007).
120. G. Adenier and A. Y. Khrennikov, *J. Phys. B: At. Mol. Opt. Phys.* **40**, 131 (2007).
121. J. H. Bigelow, A close look at the EPR data of Weihs *et al.*, arXiv: 0906.5093v1.
122. M. B. Agüero, A. A. Hnilo, M. G. Kovalsksy and M. A. Larotonda, *Eur. Phys. J. D* **55**, 705 (2009).
123. H. De Raedt, S. Zhao, S. Yuan, F. Jin, K. Michielsen and S. Miyashita, *Physica E* **42**, 298 (2010).
124. J. H. Bigelow, Explaining counts from EPRB experiments: Are they consistent with quantum theory?, arXiv: 1112.3399.
125. H. De Raedt, F. Jin and K. Michielsen, *Proc. SPIE* **8832**, 88321N1–11 (2013).
126. M. A. Rowe, D. Kielpinski, V. Meyer, C. A. Sackett, W. M. Itano, C. Monroe and D. J. Wineland, *Nature* **401**, 791 (2001).
127. Y. Hasegawa, R. Loidl, G. Badurek, M. Baron and H. Rauch, *Nature* **425**, 45 (2003).
128. M. Ansmann, H. Wang, R. C. Bialczak, M. Hofheinz, E. Lucero, M. Neeley, A. D. O'Connell, D. Sank, M. Weides, J. Wenner, A. N. Cleland and J. M. Martinis, *Nature* **461**, 504 (2009).
129. P. M. Pearle, *Phys. Rev. D* **2**, 1418 (1970).
130. S. Pascazio, *Phys. Lett. A* **118**, 47 (1986).
131. K. Hess, K. Michielsen and H. De Raedt, *Europhys. Lett.* **91**, 40002 (2010).
132. A. Y. Khrennikov, *Contextual Approach to Quantum Formalism* (Springer, Berlin, 2009).

133. A. Y. Khrennikov, *J. Comput. Theor. Nanosci.* **8**, 1006 (2011).
134. C. Bartsch and J. Gemmer, *Phys. Rev. Lett.* **102**, 110403 (2009).
135. S. Basu, S. Bandyopadhyay, G. Kar and D. Home, *Phys. Lett. A* **279**, 281 (2001).
136. H. Bartosik, J. Klepp, C. Schmitzer, S. Sponar, A. Cabello, H. Rauch and Y. Hasegawa, *Phys. Rev. Lett.* **103**, 040403 (2009).